Université des Sciences et Technologies de Lille

Laboratoire de Mécanique de Lille (UMR CNRS 8107)

Année 2007 **N°4040**

THESE

Pour obtenir le grade de

Docteur de L'Université des Sciences et Technologies de Lille

Discipline: Génie Civil

Présentée et soutenue publiquement par

Hanbing BIAN

2007

Modèle numérique pour les sols sableux non saturés en zone sismique: application à la liquéfaction

Sous la direction de

Professeur Isam SHAHROUR

Soutenance le 21 Novembre, 2007 à LML
Devant le Jury Composé de :

GATMIRI Behrouz, Professeur, ENPC de Marne La Vallée, France	**Rapporteur**
LIU Han-Long, Professeur, HOHAI Université, Chine	**Rapporteur**
CUI Yu-Jun, Professeur, ENPC de Marne La Vallée, France	**Examinateur**
SHAO Jian-Fu, Professeur, Université de Lille I, France	**Examinateur**
ROUAINIA Mohamed, Professeur, Newcastle Université, UK	**Examinateur**
NISHIMURA Tomoyoshi, Professeur, Ashikaga Institue de Technologie, Japon	**Examinateur**
SHAHROUR Isam, Professeur, Université de Lille I, France	**Directeur de Thèse**

Université des Sciences et Technologies de Lille

Laboratoire de Mécanique de Lille (UMR CNRS 8107)

Année 2007 **N° 4040**

THESE

Pour obtenir le grade de

Docteur de L'Université des Sciences et Technologies de Lille

Discipline: Génie Civil

Présentée et soutenue publiquement par

Hanbing BIAN

2007

Numerical model for unsaturated sandy soils in seismic area: Application to liquefaction

Under the direction of:

Professor Isam SHAHROUR

Defence on November 21, 2007 at LML
Before the JURY of:

GATMIRI Behrouz, Professeur, ENPC de Marne La Vallée, France	**Rapporteur**
LIU Han-Long, Professeur, HOHAI Université, Chine	**Rapporteur**
CUI Yu-Jun, Professeur, ENPC de Marne La Vallée, France	**Examinateur**
SHAO Jian-Fu, Professeur, Université de Lille I, France	**Examinateur**
ROUAINIA Mohamed, Professeur, Newcastle Université, UK	**Examinateur**
NISHIMURA Tomoyoshi, Professeur, Ashikaga Institue de Technologie, Japon	**Examinateur**
SHAHROUR Isam, Professeur, Université de Lille I, France	**Directeur de Thèse**

Table of Content

Table of Content

Résumé

Ce travail comporte la formulation d'un modèle numérique pour les sols sableux partiellement saturés et son application à l'analyse de la liquéfaction de ces sols. La liquéfaction est un phénomène important qui se peut se produire sous sollicitation sismique. Depuis le séisme de Niigata en 1964, des recherches importantes ont été menées sur ce phénomène. La plupart de ces recherches ont été consacrée aux sols saturés. Cependant, les observations montrent qu'une légère diminution de la saturation en eau engendre une augmentation significative de la résistance des sols à liquéfaction. A noter que dans le domaine de la géotechnique, les sols sont souvent en condition partiellement saturée. Les couches des sols liquéfiables qui sont situées au-dessous de la nappe sont dans un état quasi-saturé. Il est donc nécessaire d'étudier la liquéfaction des sols sableux en condition partiellement saturée.

A partir des observations expérimentales, des hypothèses sont proposées dans ce travail pour la construction d'un modèle numérique: égalité de la pression de l'air et celle de l'eau dans l'espace poreux; absence d'interaction entre ces deux phases; absence du flux d'air. Un modèle est formulé pour les sols partiellement saturés dans le cadre de la théorie de la poromécanique fondée par Coussy. Le modèle proposé est adapté aux problèmes des sols en condition saturée ou partiellement saturée. Les sols saturés sont considérés comme un cas particulier. Les analyses du module de compressibilité et du coefficient de Skempton confirment les fondements théoriques du modèle proposé. Enfin, le modèle est validé sur des observations expérimentales.

Dans la dernière partie, un modèle élastoplastique cyclique est utilisé dans le cadre du modèle proposé pour étudier l'influence de la saturation sur la liquéfaction des sables. Les résultats montrent que la diminution de la saturation en eau conduit à une augmentation de la résistance des sables à la liquéfaction. L'étude de la réponse en champ libre montre que la saturation initiale influence d'une manière significative la liquéfaction de sols. Elle conduit à réduire le risque de liquéfaction de ces sols. Le tassement pendant la phase de chargement (avant la dissipation de la surpression) augmente avec la diminution de la saturation en eau. L'influence de la perméabilité des sols partiellement saturés est moins significative que celle en condition saturée.

Mots clés : liquéfaction, sols, sables, partiellement saturé, dynamique, sismique, champ libre, poreux.

Abstract

This work presents a framework for partially saturated sandy soils and its application to liquefaction. Liquefaction constitutes a major cause of damage induced by moderate or large earthquakes. Since the 1964 Niigata earthquake, intensive efforts have been made on the liquefaction researches. However, most liquefaction researches were based on fully saturated conditions. The experimental observations indicated that a little decrease in water saturation results a significant increase in liquefaction resistance. On the other hand, the soils frequently encountered in the geotechnical engineering are unsaturated soils. The liquefiable soil layers located below the phreatic surface are not, as usual assumed, fully saturated but in near-fully saturated states. So it is necessary to study the liquefaction under partially saturated conditions.

Based on experimental observations, reasonable assumptions are taken: the pore-air pressure is equal to the pore-water pressure; the interaction between pore-air and pore-water is neglected; the pore-air flux is negligible. Within the formulation of Coussy, a numerical model for partially saturated sandy soil is established. The proposed model has a similar form as that for fully saturated cases. The main difference lies in the Biot modulus, which is constant in saturated case. In partially saturated case it depends on the pore-water pressure, the water saturation and the porosity. In fact, the proposed model can deal with both saturated and unsaturated problems. The analyses on the bulk modulus and the Skempton coefficient confirm and verify the proposed model. The laboratory observations also confirm the results of this model.

An effective stress elasto-plastic constitutive equation for granular material (MODSOL) is implanted into the proposed model to study the influence of water saturation on liquefaction. The decrease in water saturation leads to an increase in the liquefaction resistance. The free-field response of liquefiable sandy soil layer under dynamic loading shows that the initial water saturation has significant influence on liquefaction resistance. With the decrease in water saturation, the liquefaction will be delayed and the liquefaction risk will be reduced. The settlement at the top of layer before the dissipation of the excess pore pressure will increase with the decrease in water saturation. The influence of permeability in partially saturated sandy soils is less significant than that for fully saturated cases.

Key words: liquefaction, unsaturated, dynamic, sandy soils, earthquake, free field, poro-Mechanics

Introduction

Soil liquefaction constitutes a major cause of damage induced by earthquakes. It has been observed in moderate and large earthquake, for example, Loma 1989, Luzon 1990, Manjil 1990, Kobe 1995, Manzanillo 1995, Chi-Chi 1999, Kocaeli 1999, Bhuj 2001 (Bird et al., 2004). During the past several decades, intensive efforts have been made by the geotechnical research community to understand the mechanism of liquefaction, and to develop methods for evaluating liquefaction potential at a site during a given seismic event.

Most researches on liquefaction supposed that the soil were fully saturated with constant compressibility for the pore-water. Research results (for example: Martin et al., 1975; Yoshimi et al., 1989; Yang et al., 2003) showed that a small reduction in the degree of water saturation of sand could result in a significant increase in strength against liquefaction. It is worth to indicate that the researches aimed to demonstrate the importance of achieving full saturation in laboratory sand specimen to avoid overestimating the strength of the specimen against liquefaction. However, Sheng (1999) indicated that even in unsaturated zone, the liquefaction was observed. The soils frequently encountered in geotechnical engineering are unsaturated. The liquefiable soil layer under the phreatic surface is not, as usual assumed fully saturated, but in a partially saturated sates (Tsukamoto and Ishihara, 2002 and 2006).

New developments in the area of unsaturated soils (Fredlund, 1993, 2006; Coussy, 1991, 2004) together with the generalization of the concept of effective stress to unsaturated soils (Bishop, 1959 and 1963) could help the research of soil liquefaction under partially saturated conditions. The definition of liquefaction has also been extended from the failure to the excess pore pressure generation process. Experimental researches in Northeastern University, Boston (USA) by Yegian et al. (2007) indicated that the induced partial saturation could prevent the liquefaction in sandy soils and the partial saturation could sustain long term with little variations. The site observation reported by Okamura et al. (2006) indicated that the partial saturation in sandy soils could maintain for 26 years and more. Nagao et al. (2007) have tested a new method called micro-bubble-injection which can reduce the full saturated specimen to a partial saturation as low as $S_w = 75\%$. Several series liquefaction resistance tests on partially saturated specimens have been executed in Japan (Yoshimi et al., 1989; Tsukamoto et al., 2004; Okamura et al., 2006; etc.).

Remediation methods against liquefaction have been developed and applied to structures since the Niigata earthquake in 1964. However, only a few remediation methods which can be applied to existing structures have been developed. A huge number of old structures have not

been treated to resist liquefaction. Remediation of old structures is quite important, for example oil storage tanks, river dikes (Yasuda, 2007). Induced partial saturation as a potential cost-effective liquefaction mitigation method is very attractive. It could be applied to both new and existed constructions.

In this thesis, a numerical model is developed for describing the behaviour of unsaturated soils under seismic loading. It is used to study the liquefaction of partially saturated sandy soils. The dissertation includes three chapters.

The first chapter concerns the literature analysis. The behaviour of unsaturated soils is firstly reviewed and discussed. For the case of partially saturated sandy soils, some in-situ and experimental observations are presented and discussed. Then the state of arts of liquefaction researches is discussed.

In the second chapter, based on the laboratory and in-situ observations, three reasonable assumptions are taken for partially saturated sandy soils; the soil suction, the effect of air dissolved into water and the air flux are neglected. Based on Coussy's formulation, a numerical model is established for unsaturated sandy soils. This model can deal with both saturated and unsaturated conditions. The implementation of this model in a finite element code is presented. Finally some numerical applications are presented.

In the third chapter, a cyclic constitutive equation based on the concept of effective stress for granular material is presented. After implementation of this constitutive equation in the numerical model, some applications are illustrated. Firstly, the simulations of triaxial experiments for both monotonic and cyclic loadings are presented. The influence of water saturation on the liquefaction resistance is analyzed. Then, the influence of water saturation on the free-field response is analyzed. Some key factors, namely the permeability and relative density are studied. At last the tests conducted by Yegian et al. (2007) are reviewed and discussed.

Chapter 1: Literature review: Response of unsaturated soils to seismic loading

1.1. Unsaturated soils

In classic soil mechanics, most soils (almost all the soils) studied are either dry or saturated. However, both of these soils do not exist in nature, they are just two simple models used by the geotechnical engineers. The researches on partially saturated soils began in the early of last century. Until last decades, the publication of "Soil mechanics for unsaturated soils" by Fredlund et al. (1993) indicates the beginning of the maturation of partially saturated soil mechanics (Sheng, 1999).

The profile of natural soils is illustrated in Figure 1.1. Generally the soil below the phreatic surface is considered as saturated, while those above the water table are unsaturated. The location of water table varies according to the region and the climate. The phreatic surface is influenced by precipitation and the evapotranspiration. Human activities will also influence the distribution of ground water; the irrigation will cause a variation of the phreatic surface.

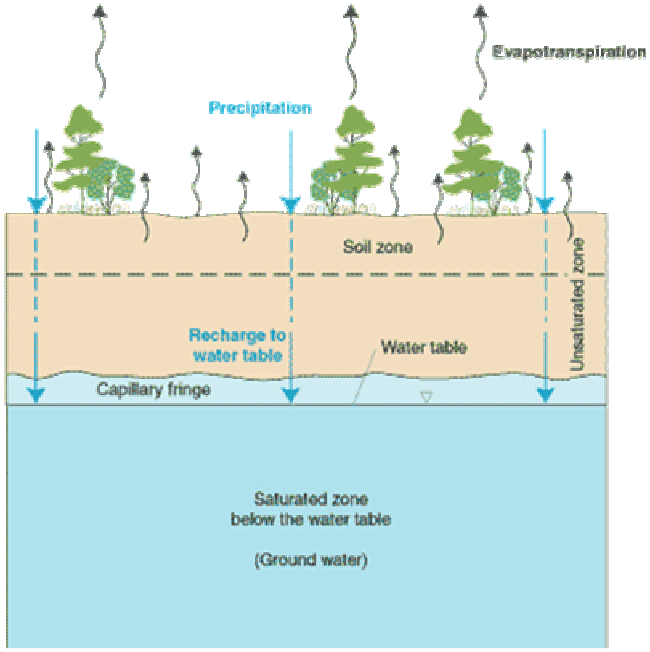

Figure 1.1: Illustration of profile of natural soils

It is thought that the dry soils have two phases: the solid and the pore-gas (void); and the saturated soils have two phases too, namely the solid and the pore-water (void). Partially saturated soils have three phases: the solid, pore-water and pore-gas. For the pore-gas, when the influence of temperature is important, it should be divided into two parts: dry air and water vapour (Yang et al., 1992; Loret et al., 2000; Khalili et al., 2001; Coussy, 2004; Jia, 2006). However, in our researches, the isothermal condition is assumed, there is no difference between

them. The translation between the liquid water and the water vapour is also neglected. The pore-air is considered as an ideal gas.

We consider a soil specimen with volume V in which the void occupies a volume V_V and the soil grain occupies a volume V_s (the subscript V indicates the void, s indicates the solid or soil grain), (Figure 1.2). The void is filled by both air with volume V_a and water with volume V_w (the subscript w indicates pore-water, a indicates the pore-air). If the void is occupied only by the air ($V_V = V_a, V_w = 0$), the soil is said dry, if the void is totally occupied by water ($V_V = V_w$, $V_a = 0$), the soil is said saturated. Between the two extreme cases ($V_V = V_w + V_a, V_a \neq 0, V_w \neq 0$), the soil is partially saturated, or unsaturated. The porosity and the water saturation are also shown in Figure 1.2. The water saturation or the water saturation degree, which is defined as the ratio of pore-water volume to total void, is an index which distinguishes the unsaturated soils from those saturated and dry soil. When the water saturation is less than unit and greater than zero, it is partially saturated. If the water saturation reaches zero (unit), the soil is dry (saturated). From mathematic viewpoint, the distribution of volumetric water saturation degree can be represented by a line with two ends of zero and unit. Consequently, all the soils could be considered as unsaturated soils, while dry and saturated soils are two special cases of partially saturated soils.

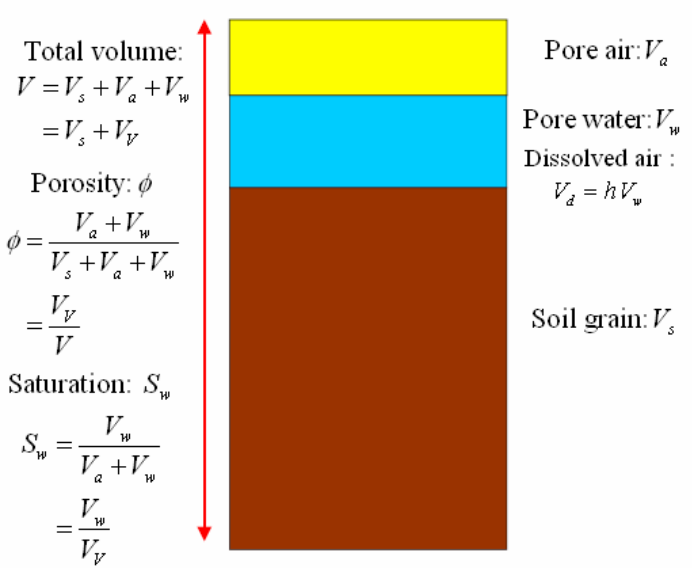

Figure 1.2: Unsaturated soil; volume of each phase, porosity and saturation

1.2. Induced partial saturation

Soils below the groundwater table are not, as usually assumed, fully saturated. The condition of partial saturation could be caused by, for example, fluctuating of the water table, due to the natural or manmade processes. If the soils are originally saturated or dry, while after a perturbation, the saturation is changed, and the soil becomes partially saturated. It is said

induced partial saturation. Kokusho (2000) revealed that the soil deposit several meters below the ground water table is not fully saturated but in a near fully saturated state. Yang et al. (2001) also indicated that in certain situation, soils below the water table may not be fully saturated. Incomplete water saturation could be caused by fluctuating water table, flooding or recharge of groundwater.

Okamura et al. (2006) investigated the in-situ water saturation of the foundation soil, which was improved by the sand compaction piles, shortly after the sand compaction pile installation at three sites in Japan. Samples were obtained by ground freezing method which is capable of obtaining high-quality undisturbed sand samples. The typical sand compaction pile construction procedure is illustrated in Figure 1.3. It includes the following steps: A casing pipe with a diameter of 0.4 m is penetrated by either a hydraulic jack or a vibro-hammer into the ground and sand is placed in the casing pipe from the top. Then, the casing pipe is withdrawn 0.5m and the sand is discharged into the bored hole with the aid of pressurized air of the order of 500 kPa supplied from the top. The sand pile is compressed vertically to increase its diameter to about 0.7m by penetrating the casing pipe 0.3m. The withdrawing and repenetrating procedure is repeated until a complete compacted sand pile is formed. It is observed during the sand pile construction in these sites that large amount of air which is exhausted with sand into the ground from the tip of the casing pipe continuously spouted from everywhere of the ground surface within the area about several meters from the casing.

Frozen samples were cut out and trimmed from sand layers and a few from clay and silt layers. The water content of each frozen specimen was measured and the degree of water saturation was determined. The water saturation of specimens was plotted against depth in Figure 1.4. It is apparent that the improved soils in sand layers as well as the sand piles contained a considerable amount of air. The degree of water saturation is lower than 77% for the sand piles and 91% for the improved soils in the sand layers under water table. It is also suggested that the air injected from the casing tip during ground improvement with sand compaction pile in coarse sand and gravel is subjected to splitting continuously into bubbles until limiting size is reached.

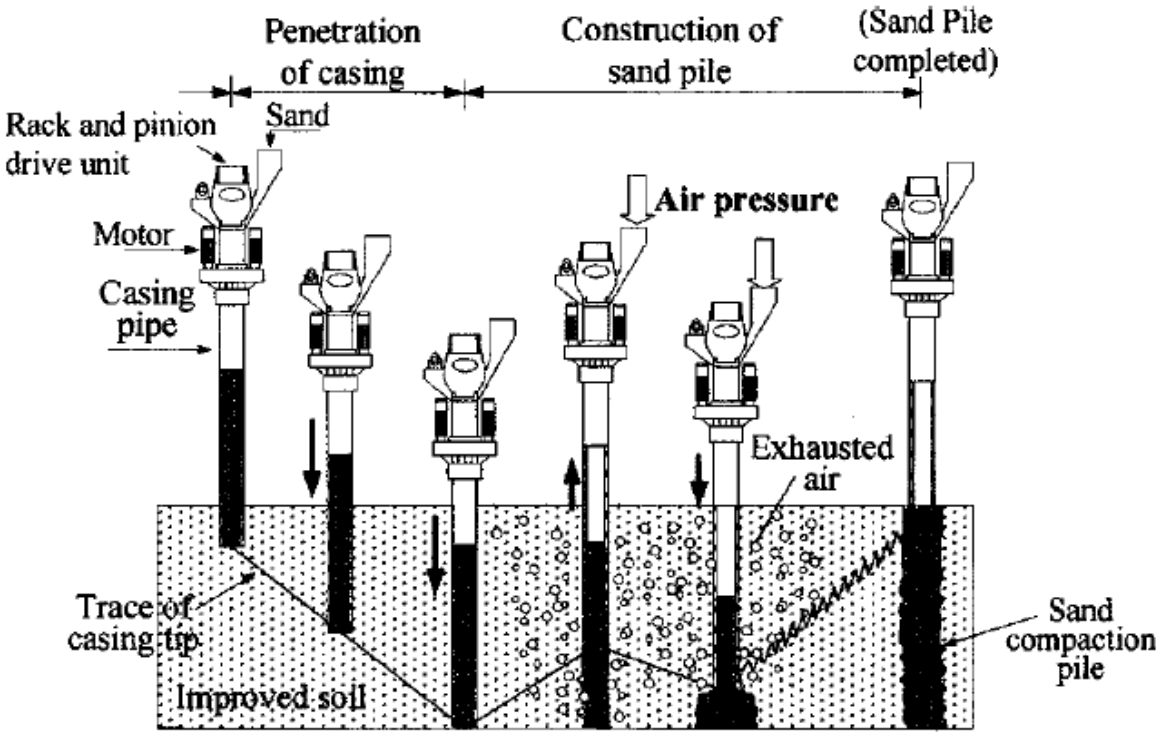

Figure 1.3: Sand Compaction Pile installation procedure (Okamura et al., 2006)

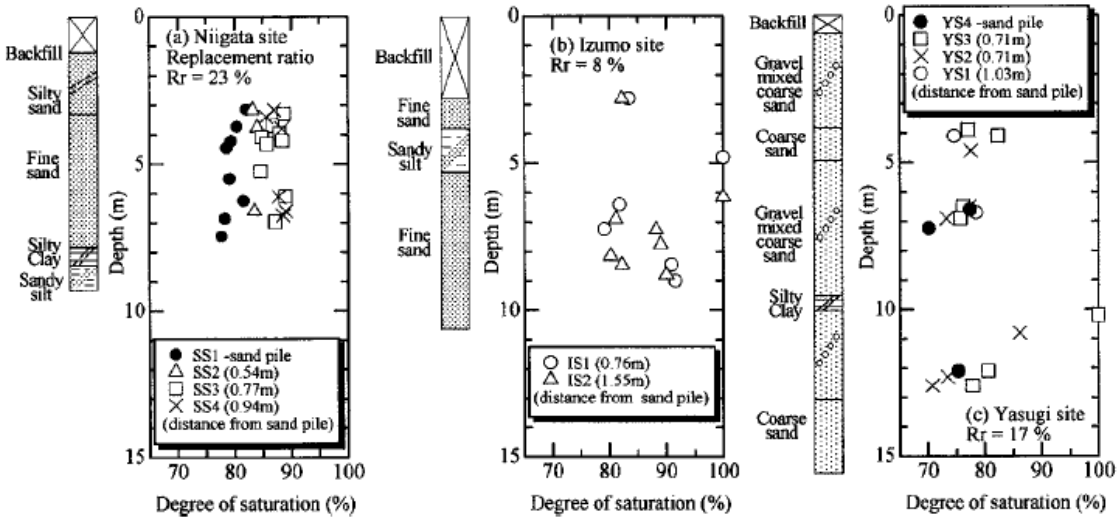

Figure 1.4: Degree of water saturation shortly after ground improvement (Okamura et al., 2006)

At Sekiya site (Okamura et al., 2006) the foundation soils had been improved with sand compaction pile about 26 years ago. Samples were obtained by the in-situ ground freezing method. The degree of water saturation under the water table was as low as 92%. In this site, the primary wave velocity was measured by PS loggings both inside and outside the improved area one month before the sampling. The measured primary wave velocities at the two locations suggest that the soil contained a considerable amount of air under the phreatic surface. On the

other hand, an apparently higher velocity was observed in the soil about 50m away from the improved area, corresponding roughly to water saturation $S_w = 99.9\%$ or higher. This fact confirms that soils in the improved area had been desaturated by the sand compaction pile and air bubbles in the soils have survived for about 26 years.

Yegian et al. (2007) have conducted a test referred as "long term air diffusion test" to investigate whether air bubbles would remain entrapped for a long time or have the tendency to quickly diffuse out of liquefaction susceptible sands. In a deep soil layer the water pressure will be higher and may force the air out of the voids. On the other hand, one can argue that it would be more difficult for the air molecules to find a path and escape through a deep soil layer. To evaluate the potential long-term tendency of air diffusion from a thick soil layer, the water saturation of a 151cm column of partially saturated sand was monitored in Northeastern University (USA). Figure 1.5(a) shows the test setup. A 184cm plastic tube with an outer diameter of 10.12cm was rigidly fixed to a concrete column in the basement of a building to minimize the effect of ambient vibrations. A 151cm column of loose fully saturated Ottawa sand specimen was prepared in the tube by the wet pluviation method. The void ratio and the initial water saturation of the specimen were calculated as 0.80 and $S_w = 96.7\%$, respectively. Partial saturation was then induced in the specimen using the drainage-recharge method. From daily measurement of the volume of water above the sand, and the sand height, the degree of water saturation of the specimen was computed by the phase relations. Figure 1.5(b) shows the variation of the water saturation. It indicates that the initial degree of water saturation $S_w = 82.1$ % slightly increased to $S_w = 83.9$ %, after 442 days' monitoring. It is noted that this small increase in the degree of water saturation was recorded within the first few days after the partial saturation was induced. Visual observations showed rearrangement of air bubbles in isolated regions within the specimen until equilibrium was achieved. This test shows that under hydrostatic conditions, small well-distributed air bubbles could remain trapped for long time.

Form the two evidences above we can see that, even under the water table, the soils could be partially saturated. The air entrapped in the soil under water table may hold for long time. The air diffusion is very slow. The fluctuation of the water table associated with the natural or manmade processes will entrapper some air. As indicated by Tsukamoto (2007), that down to about 5meters below the groundwater table, the soil layer could contain air bubbles. Ishihara et al. (2004) indicated that in gravely soils, the partial saturation could reach as deep as 10meters below the water table.

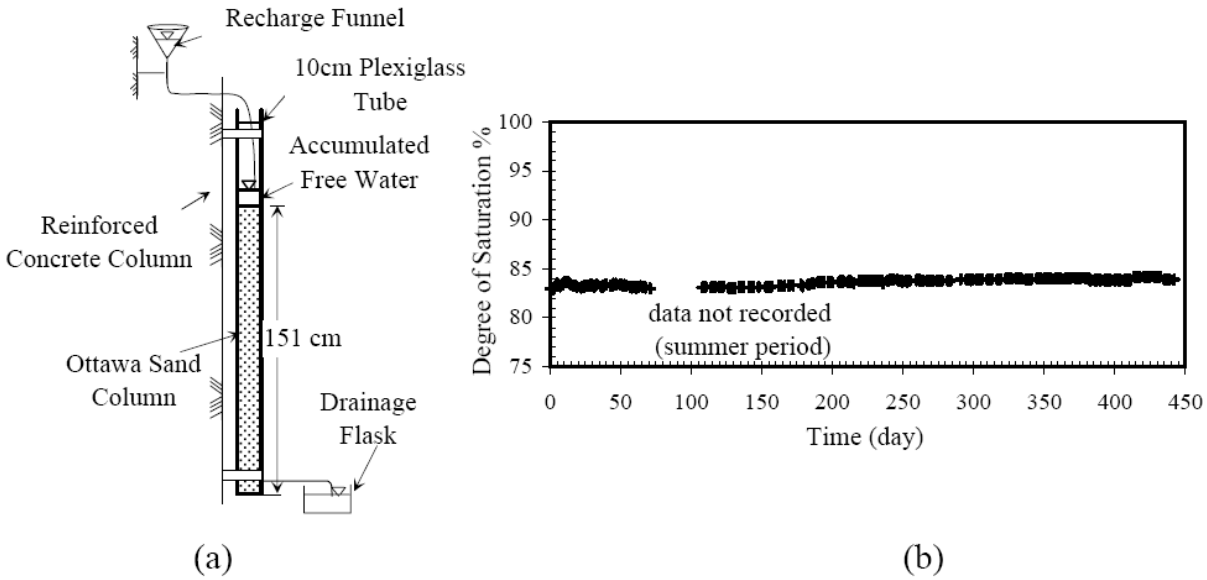

Figure 1.5: (a) The test setup used to investigate the long-term sustainability of air bubbles in a partially saturated sand column (b) Long-term monitoring of the degree of water saturation (Yegian et al., 2007)

1.3. Pore-water and pore-air interaction

As discussed in the two precedent sections, partially saturated soils are more popular than dry and saturated soils. More attention should be paid to it. For unsaturated soil, as illustrated in Figure 1.2, it includes three phases: the solid (soil grains or soil skeleton), fluid (pore-water) and pore-air (dry air and water vapour). Pore-air and pore-water can be combined as immiscible or miscible mixtures. The immiscible mixture is a combination of free air and pore-water without any interaction. The immiscible mixture is characterized by the separation produced by the contractile skin. A miscible pore-air and water mixture can have two forms. Firstly, the water vapour is one part of the air. Secondly, the air could dissolve into water and can occupy approximately 2% of water volume. In this section, the properties and behaviour of both pore-water and pore-air will be presented firstly. The interactions between them will be discussed later.

1.3.1. Pore-water

Naturally, water can be found in one of three states: the solid state as ice, the liquid state as water and the gaseous state as water vapor, which depend on the applied temperature and pressure as illustrated in Figure 1.6. At certain temperature and pressure, the water can coexist in three states; which is called the triple point of water (point A in Figure 1.6). The rate of condensation depends on the water vapour pressure. On the other hand, the evaporation rate

depends on the temperature. The line AC, which shows the combination of temperature and pressure for which the liquid and vapor states of water can coexist in equilibrium, is called the vapor pressure curve of water. This line also distinguishes the liquid state from gaseous state. Throughout this dissertation, the words "water" or "water phase", "pore-water" refers to the liquid state of water. The ice, which associates the frozen soil, will not be discussed in this dissertation, only the gaseous and liquid states will be discussed here.

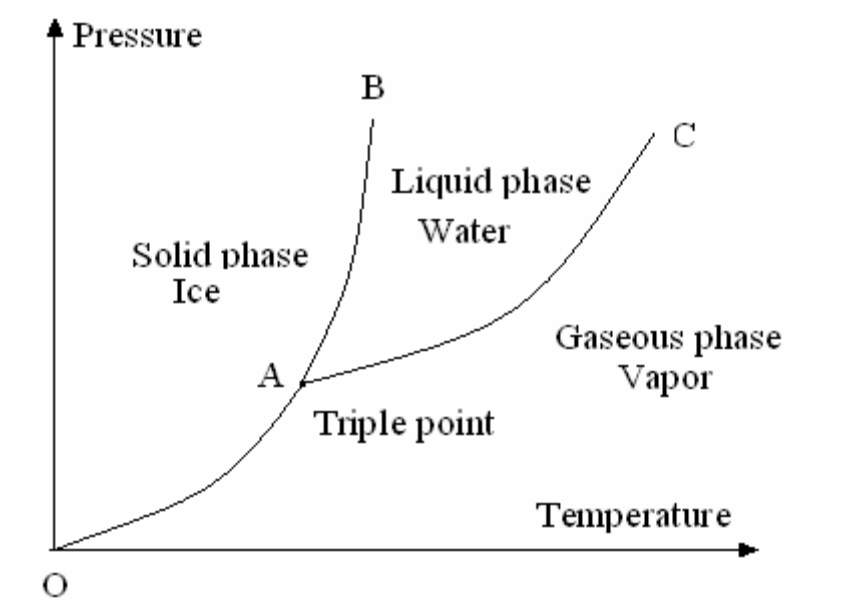

Figure 1.6: Three states of water in function of pressure and temperature (Fredlund et al., 1993)

Distilled water under the pressure of its saturated vapor is called pure, saturated water. The density of pure, saturated water depends on the applied pressure and temperature. In soil mechanics, the variation of water density due to temperature variation is more significant than its variation caused by applied pressure. Under isothermal conditions, the density of water is commonly taken as $1000 kg/m^3$.

The water compressibility, which is a measure of the relative volume change of water as a response to a pressure change, is a function of pressure and temperature. In soil mechanics, when coupled problem is considered, the bulk modulus of water is generally used. The bulk modulus of pure, saturated water can be as higher as $2.23\times10^9 Pa$, so the water is always considered as incompressible by comparing with the compressibility of the soil skeleton.

1.3.2. Pore-air

In the natural state, the air behaves as a mixture of several gases (including water vapor). The mixture is called dry air when no water vapor is presented, and is moist air when the water vapor is presented. Both dry and moist air can be considered to behave as an ideal gas under pressure and temperature commonly encountered in geotechnical engineering.

Unlike the water, the air is not "homogeneous"; it varies with the compositions of the mixture of dry air and water vapor. The density of air is not only the function of pressure and temperature, but also the function of its compositions. At 20°C, under the atmospheric pressure, when the relative humidity is 50%, the density of air is $1.2 kg/m^3$. This value is very small by comparing with that of water density.

The air is more compressible. Its bulk modulus is the function of applied temperature and pressure. According to the ideal gas law, the absolute air pressure can be taken as the bulk modulus. So the mechanical behaviour of air is highly nonlinear.

1.3.3. Water vapor in the air

In the atmosphere, the water vapour is mixed with air. However, the presence of air has no effect on the behavior of water vapour. The concentration of water vapour in the air is commonly expressed in term of relative humidity. The molecular mass of air depends on the compositions of the mixture of dry air and water vapour. The dry air has a molecular mass of about $28.966 kg/kmol$, and the molecular mass of water vapour is $18.016 kg/kmol$. The percentage in volume may range as little as $2.0 \times 10^{-6}\%$ to as high as $4-5\%$; this consequently affects the density of the air. Under isothermal condition, the process of evaporation and condensation are considered as equilibrium. So the variation of water and water vapour due to evaporation and condensation can be neglected. The air in the soils is considered as "saturated with water vapour". As discussed above, when the mass of air is neglected, the interaction in this direction then is very weak.

1.3.4. Air dissolved in water

On the other hand, air can dissolve in water. Water molecules form a lattice structure with openings referred to as a "cage" that can be occupied by the air. Air dissolves into water and fills the "cages" which have approximately 2% of total volume. The water lattice is relatively rigid and stable, so the density of water slightly changes due to the presence of the dissolved air. The process of air dissolving into water can be described by Henry's law, which states that the amount of a given air dissolved in a given type and volume liquid, at constant temperature, is

directly proportional to the absolute pressure of air in equilibrium with that solution. The air mass going into or coming out of water is time dependent. This dependency can either be ignored or taken into consideration, depending upon the engineering problems. The amount of air that can be dissolved in water is referred to its solubility, and the rate of solution is referred to its diffusivity.

The volume of dissolved air in water is essentially independent of the air or water pressure (Fredlund, 1993). At constant temperature, the volume of dissolved air in water is a constant for different pressures. This can be demonstrated by the ideal gas law and Henry's law. The ratio of the volume of dissolved air in a liquid to the volume of liquid is called the volumetric coefficient of solubility, h, which varies slightly with temperature. Figure 1.7 illustrates the volumetric solubility of air in water under different temperatures. At 20°C, the volumetric coefficient of solubility is about 2%.

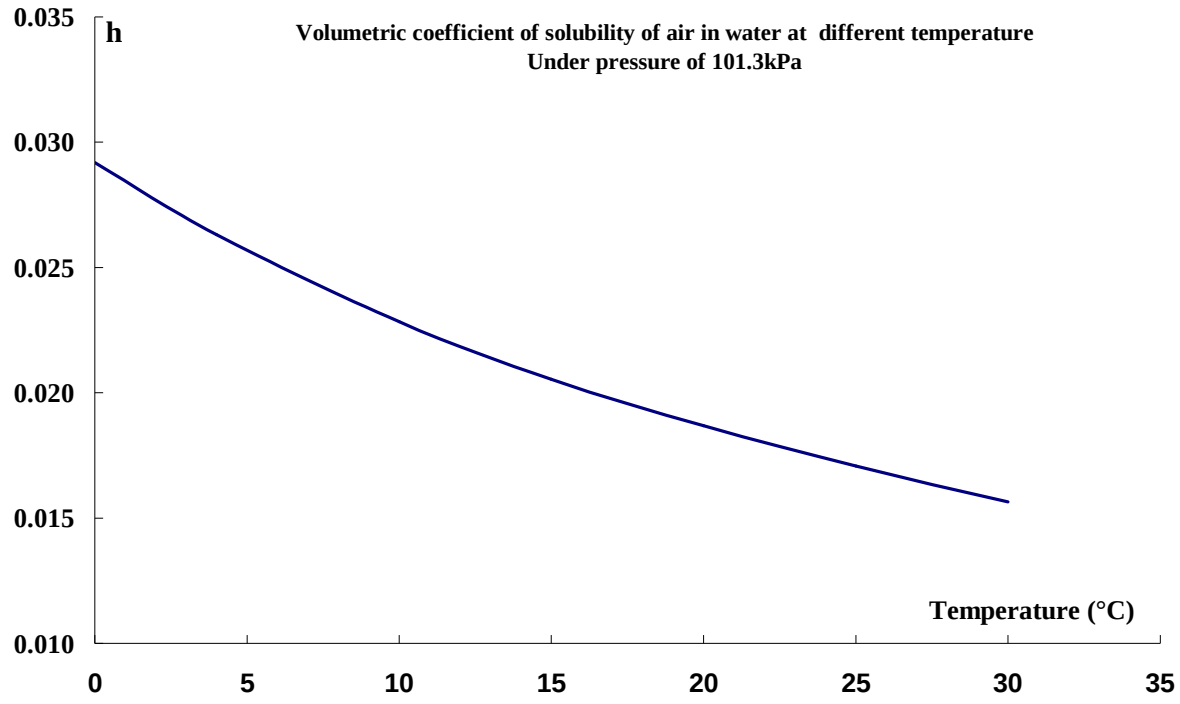

Figure 1.7: Volumetric coefficient of solubility of air in water at different temperature (Fredlund et al., 1993)

The rate at which the air can pass through water is described by Fick's law of diffusion. The rate at which mass is transferred across a unit area is equal to the product of the coefficient of diffusion, D, and the concentration gradient. In case of the diffusion of gas through water, the concentration difference is equal to the difference in the density between the free gas and the dissolved gas in the water. Under constant temperature conditions, the density of air is a function of the air pressure. An increase in the pressure of the air will develop a pressure difference between the free air and the dissolved air. This pressure difference becomes the

driving potential for the free air to diffuse into the water. The coefficient of diffusion D for natural air through free water is about $2.2\times10^{-9}\,\mathrm{m^2/s}$. However the diffusion coefficient of air through the water in soil appears to differ by several orders of magnitude from the coefficient of diffusion for air through free water.

However, whether the effect of air dissolved into water is taken into consideration will greatly influence the response. The following example will illustrate the importance of this effect. We suppose that in the equilibrium condition, the pore-air pressure and the pore-water pressure are equal, which implies that the contractile skin effect is neglect. A soil specimen with a porosity $n=0.4$ is considered, the total volume of the specimen is unit, and the initial volumetric water saturation is supposed as $S_w=80\%$. The initial pore-pressure is supposed equal to 101.3kPa (absolute pressure). The unsaturated specimen is submitted to isotropic compression loading under undrained condition. The soil is under the process of consolidation. It is supposed that the soil grain is incompressible. The bulk modulus of the pure water is $2.23\times10^{9}\,\mathrm{Pa}$; the volumetric solubility of the water at current temperature is 2%. The ideal gas law is used to study the response of the pore-pressure.

Figure 1.8 presents the relationship between the pore-pressure and the volumetric water saturation for both cases (taken the dissolution effect into consideration in square pink, no dissolution effect consideration in triangle bleu). It can be seen, when the dissolution effect is taken into consideration, the initial unsaturated soil becomes saturated soil when the pore-pressure arrives to 1370kPa. After that, there is no free air presented in the soil void, all the free air in the initial configuration is dissolved in the pore-water. While the air dissolution effect is not taken into consideration, the increase in the pore-pressure is more rapid, and the saturation will never arrive to unit. That means the soil is always unsaturated. It can be concluded that, the dissolution of the air in water will greatly influence the results, especially in the high saturation zone. However, the confining pressure of liquefiable soil layer generally is less than 400kPa. As indicated by Nagao et al. (2007), there is no need to take the air re-dissolved in water.

The procedure of air dissolution into water is time dependent. Taking it into consideration or not dependents on the problem considered. For dynamic problem, (for example earthquake) normally this effect is neglected. While for the long time diffusion problem, it should be taken into consideration.

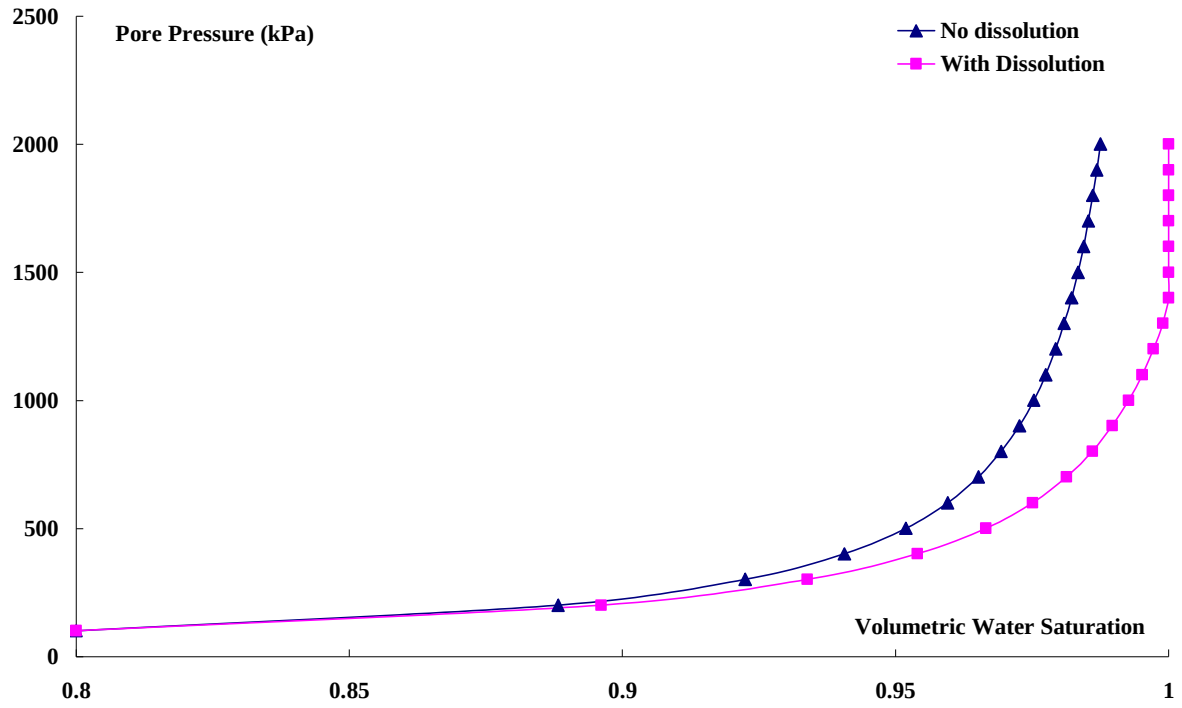

Figure 1.8: Influence of the dissolution of air into water
Pore-pressure Vs. Volumetric water saturation under isothermal undrained condition

1.4. Degree of water saturation

For the partially saturated soils, three different types of microstructure can be distinguished (Wroth et al., 1985):

a) At low degrees of water saturation, the gas phase is continuous and menisci of liquid adhere to most grain boundaries;
b) At higher degrees of water saturation, the liquid phase is continuous in part of the samples, whereas in the remaining part gas phase remains continuous;
c) As the degree of water saturation is further increased, the liquid phase maintains as continuum, while the gas phase becomes discontinuous in the form if bubbles embedded in the liquid phase.

Sheng (1999) indicated that when the water saturation varies between from about 50% to 90% for clay and from 30% to 80% for sand, both water and air are continua in the void. When the water saturation is greater than 80% for sand, the gas presents as air bubble in the void with different contact type as illustrated in Figure 1.9.

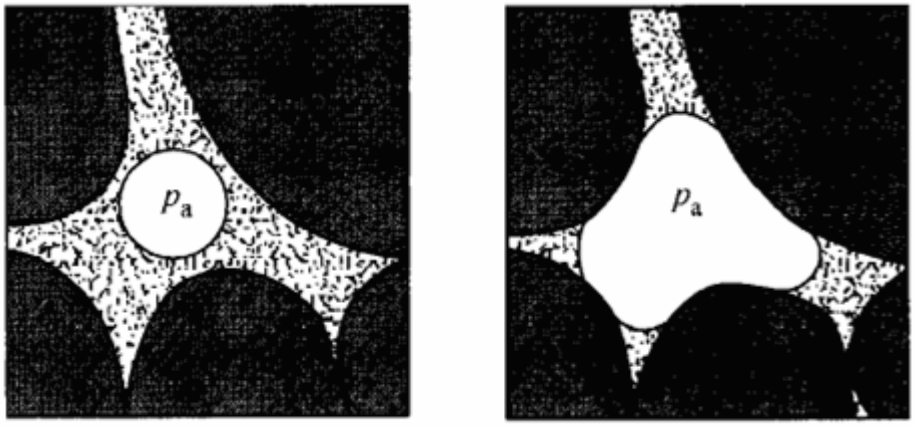

Figure 1.9: Air bubble in soil void
(a) air bubble not wetting solid surface; (b) both fluids in contact with solid surfaces (Zienkiewicz et al., 1999)

As indicated by Zienkiewicz et al. (1999), in the case (a) (Figure 1.9), the air bubble is not in contact with soil grains; the pore-water pressure is equal to the pore-air pressure, while for the case (b), the contractile skin effects may have some influence. The amplitude of the influence depends on the type of soil. Whether the fact should be taken into consideration depends on the grain size and pore distribution. It usually depicts by the soil suction and soil water characteristic curve (or alternatively water retention curve). This work will focus on partially saturated sandy soil with pore-air in discontinuous condition; the water saturation is in the range $S_w = 75\%$ to 100% .

1.5. Soil suction

The soil below the water table could be partially saturated as discussed above. The water is generally continuous with occluded air bubbles as illustrated in Figure 1.9. Pore-pressure in depths below the water table depends on the combination of the water weight lying above the given elevation and the drainage conditions below. The pore-pressure normally has a positive value and can be measured. If the water contained in the voids of soils is subjected to no other force than that due to gravity, the soil lying above the water table would be completely dry. However, powerful molecular forces acting at the boundary between the soil particles and water induce the water to be either drawn up into the other empty void spaces or held there without drainage following infiltration from the surface. The attraction that the soil exerts on the water is termed “soil suction” and manifests itself as a tensile hydraulic (b in Figure 1.9). The magnitude of the attractive force that soil above the water table exerts on water is governed by the size of the voids in manner similar to the way that the diameter of a small bore glass tube governs the height to which water will rise inside the tube when it is immersed in water. The smaller the void, the harder it is to remove the water from the void.

The meniscus formed between adjacent particles of soil by the soil suction creates a normal force between the particles, which bonds them in a temporary way. Thus soil suction, if it can be relied upon, can enhance the stability of earth structures. Soil suctions can be found in all ground that lies above the water table. For those lie below the phreatic surface, soil suction could exist too, if the soil is not fully saturated as illustrated in Figure 1.9(b).

The theoretical concept of the soil suction was developed in soil physics in the early 1900's (Fredlund, 1993). The soil suction theory was mainly developed in relation to the soil-water-plant system. The importance of soil suction in explaining the mechanical behavior of unsaturated soils relative to engineering problems was introduced at the Road Research Laboratory in England. Soil suction is commonly referred to as the free energy state of soil water and as quantified in terms of relative humidity. It has two components, namely, matric and osmotic suction. The matric suction is mainly arisen from the water content, while the osmotic suction is caused by the chemical forces which will be neglected in this study. Hereafter, the soil suction is referred as matric suction.

In geotechnical engineering, the soil suction is generally defined as the difference of pore-air pressure and the pore-water pressure:

$$s = p_a - p_w \tag{1.1}$$

In which s is soil suction, p_a is pore-air pressure, p_w is pore-water pressure.

Soil suction depends on the soil type, soil grain size and its distribution, void size and its distribution, and the water saturation degree. For the sandy soils, the soil suction is not significant. Goulding (2006) has conducted experimental researches on the suction of partially saturated Ottawa sand, the water saturation vary from 10% to 80%, the results indicates that soil suction in sandy soil is insignificant.

1.6. Soil water characteristic curve

The soil water characteristic curve (SWCC) or water retention curve (WRC) describes the relationship between the soil suction and the water saturation. This curve describes the thermodynamic potential of the pore-water related to free-water as a function of the water absorbed by the system. At relatively low water saturation, the pore-water potential is significantly reduced relative to free water, thus producing relatively high soil suction. At relatively high water saturation, the difference between the pore-water potential and the potential of free water decreases, thus the soil suction is low. When the potential of pore-water is equal to the potential of free water, the soil suction is equal to zero. This occurs when the

degree of water saturation is close to 100%. Figure 1.10 shows typical soil water characteristic curves for sand, silt, and clay. In general, for a given water saturation, soil suction is inversely proportional to particle size. Fine-grained materials are capable of sustaining significant suction over a wide range of water content. While for sandy soils, when the water saturation exceeds 40%, the matric suction is so small that it can be neglected.

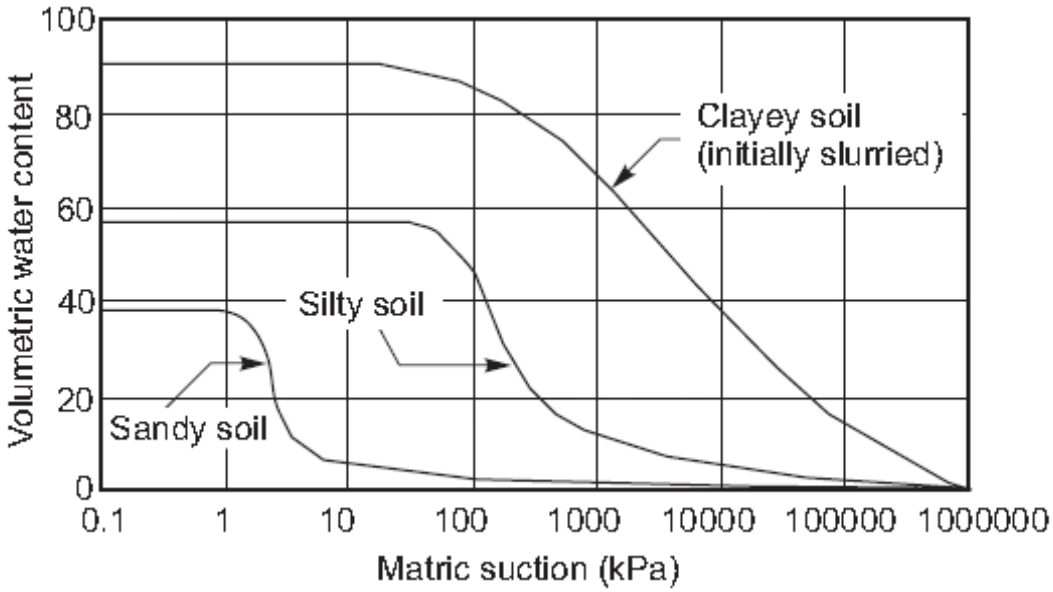

Figure 1.10: Soil water characteristic curve for sandy soil, silty soil and clayey soil (Fredlund and Xing, 1994)

The soil water characteristic curve for Hostun sand has been measured in Soil Mechanics Laboratory of Ashikaga Technologic Institute by the author, as illustrated in Figure 1.11 (triangle bleu). It is compared to that of Toyoura sand measured by Kamata et al. (2007) (cube red) and that of residual sand suggested by Matsushi et al. (2006) (line pink). It can be observed that the soil suction is very small over a very wide range of the water saturation degree: suction remains lower than 5kPa when the degree of water saturation exceeds 40%. This value is so small that can be neglected. As a result, the assumption of equality of pore-water pressure and pore-air pressure are feasible. The measured data agree well with that of Fredlund et al. (Figure 1.10).

This also confirms the results presented in the precedent sections: when the water saturation increases, the contact surface between the soil grain and the air decreases (Figure 1.9, situation from b to a), and consequently the contractile effects decrease.

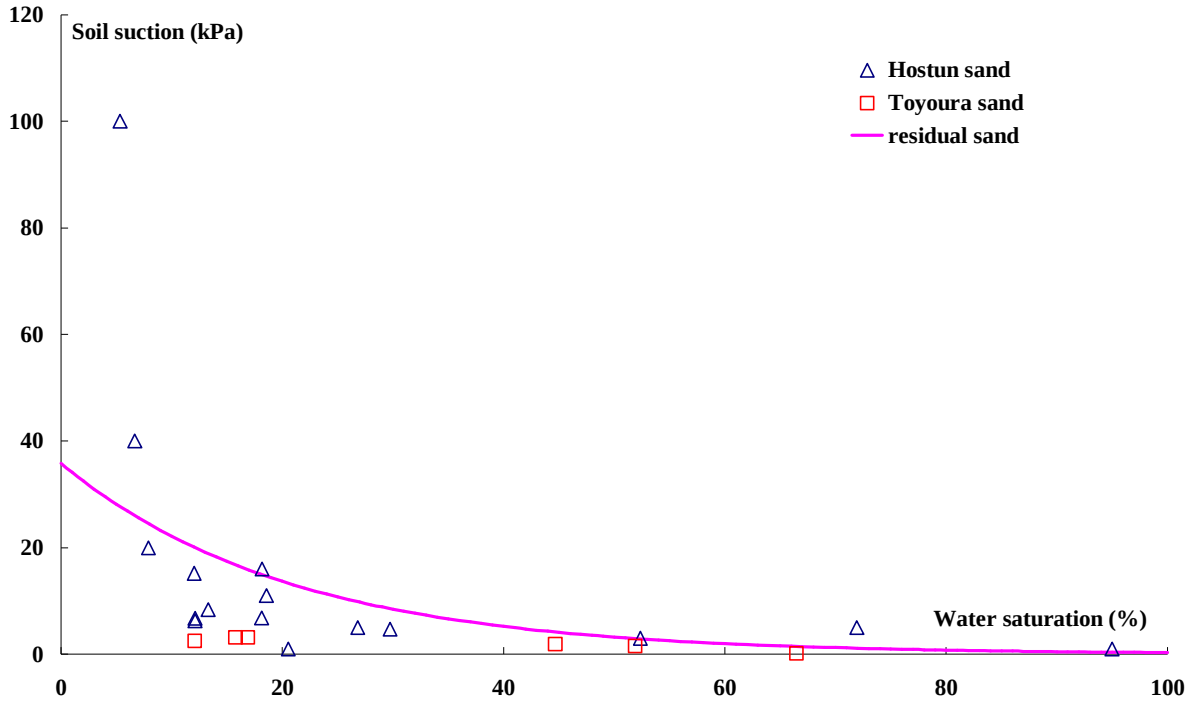

Figure 1.11: Soil water characteristic curve of sandy soils

1.7. Permeability and relative permeability

The coefficient of permeability with respect to the water phase, k_w, which is also referred as permeability, is a measure of the space available for water to flow through the soil. The coefficient of permeability depends upon the properties of the fluid and the properties of the porous medium. In a saturated soil, the coefficient of permeability is a function of the void ratio. The coefficient of permeability of a saturated soil is generally assumed to be constant. In an unsaturated soil, the coefficient of permeability is significantly affected by combined changes in the void ratio and the degree of water saturation. Water flows through the pore space filled with water; therefore, the percentage of voids filled with water is an important factor. As a soil becomes unsaturated, air replaces firstly some of the water in the large pores, and this causes the water to flow through the smaller pores with an increased tortuosity to the flow path. As a result, the coefficient of permeability with respect to the water phase decreases rapidly as the space available for water flow reduces. The change in the void ratio in an unsaturated soil may be small just like that in saturated case, and its effect on the coefficient of permeability may be secondary. However, the effect of a change in degree of water saturation may be highly significant. As a result, the coefficient of permeability is often described as a singular function of the degree of water saturation (Fredlund et al., 1993).

The coefficient of permeability for the air phase, k_a, similar to that of water, can be expressed as a function of the volume-mass properties of the soil. In this case, the volumetric percentage of air in the pores is an important factor, since air flows through the pore space filled with air. As the degree of water saturation decreases, the air coefficient of permeability increases. In a relative high water saturation, however, the air can exist in the state of air bubbles, just like the case in Figure 1.9, and the relative permeability is significantly reduced. The amplitude is close to zero. This is why in the section 1.2 the induced partial saturation can survive for a relative long term below the phreatic surface.

For a single fluid (i.e. saturated case), the permeability has a clear signification; however if there are two or more fluids, their interactions should be taken into consideration. The presence of a fluid will eventually has some impact on the other. The concept of relative permeability (Luckner et al., 1989) is used. It supposes that the permeability is an intrinsic property. The permeability of each fluid is just a frictional part of this property, as:

$$k_w^{rl} = \sqrt{S_w}\left(1-\left(1-S_w^{\frac{1}{m}}\right)^m\right)^2 \tag{1.2}$$

$$k_a^{rl} = \sqrt{1-S_w}\left(1-S_w^{\frac{1}{m}}\right)^{2m} \tag{1.3}$$

k_w^{rl} is the relative permeability of pore-water, and k_a^{rl} is the relative permeability of pore-air, m is a parameter which can be determined from experimental results. It can be seen that the relative permeability is defined as a function of the water saturation.

As illustrated in Figure 1.12, the relative permeability of pore-water k_w^{rl} and of pore-air k_a^{rl} of sandy soils are plotted as a function of the water saturation (Abaci et al. 1992). It can be seen that, when the water saturation is less than 10%, there is no water flux; when the saturation is greater than 80%, there relative permeability of the pore-air approaches to zero; that means that the pore-air has been entrapped in the soil and there is no air flux. This evidence confirms the conclusion in sections 1.5 and 1.6. This experimental result also confirms that the air entrapped in the void of this kind of soil will survive for a long time under hydrostatic condition.

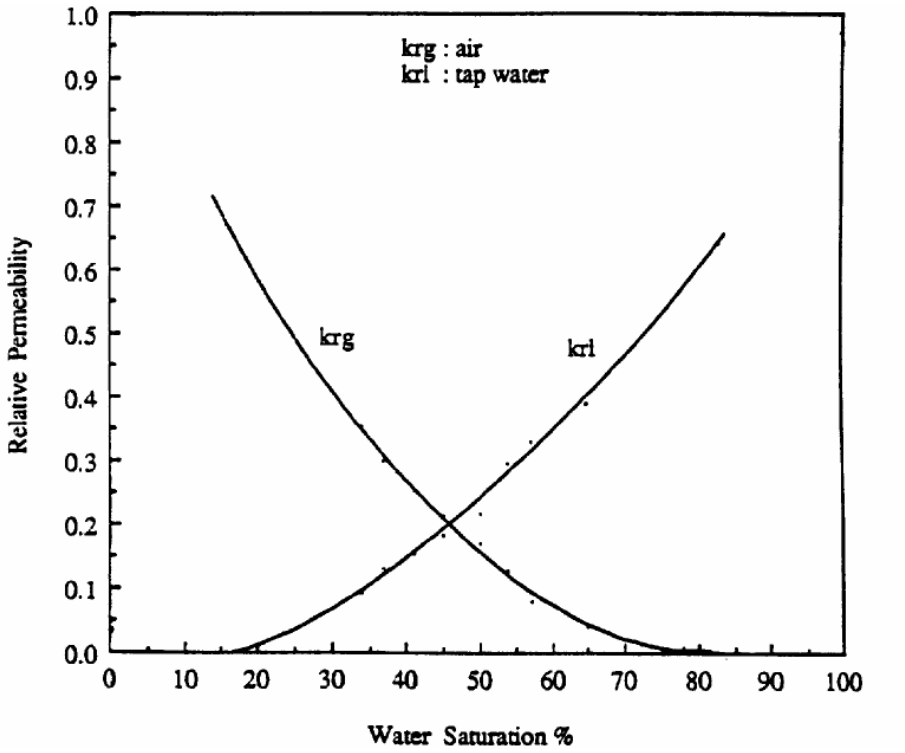

Figure 1.12: Laboratory measured relative permeability of 7-20Mesh sand (porosity 35%) (Abaci et al., 1992)

1.8. Poro-Mechanics

Poro-Mechanics (Lewis and Schrefler, 1998; Coussy, 1991 and 2004) could be used to study both the saturated and unsaturated soils. Porous materials are classified as those with an internal structure. They comprise a solid phase and pores filled with one or two fluids. The solid and the fluid usually have a relative velocity to each other, and because of their different material properties, there is an interaction between the constituents. Furthermore, the pore structure has, in general, an extremely complicated geometry which makes a mechanical description of the problem rather difficult. In geotechnical engineering, the proposition of a substitute model at the macroscopic scale is normally assumed that the interacting constituents are presumed to occupy the entire controlled space. This distribution is obtained by means of the volume fraction concept. Volume fractions are given by the ratio of the volume of the constituents to the volume of the controlled space. A consequence of the volume fraction concept is that the substitute constituents have reduced densities. These substitutes could then be treated via the method of continuum mechanics.

Two strategies are generally used to describe the behaviour of these substitute continua: one starts from a macromechanics viewpoint, while the other from a micromechanics viewpoint. Phenomenological and mixture theory approaches, integrated by the concept of volume fraction, belong to the first strategy. Averaging theories, sometimes called hybrid mixture theories,

belong to the second one. Modern mixture theories were developed rapidly. A macroscopic thermodynamic approach to Biot's theory was used by Coussy (1991 and 2004).

The unsaturated soil behavior is more complicated than that of saturated or dry soils. For these coupled problems (unsaturated hydro-mechanical), generally two approaches had been proposed. The first is the effective stress approach proposed by Terzaghi (1936) for saturated soil, then extended by Bishop (1959), Gatmiri et al. (1998) and Zienkiewicz et al. (1999), Loret et al. (2000 and 2002), Khalili et al. (2004) to unsaturated soils. The second is the independent stress variables approach, proposed by Fredlund et al. (1993) and Alonso et al. (1990).

Fredlund and Morgenstern (1977) proposed that the constitutive behavior of unsaturated soils could be described using two independent stress variables, namely $(\sigma_{ij} - p_a\delta_{ij})$ and $(p_a - p_w)$. They argued that the mechanical behavior of soils is controlled by the same stress variables which control the equilibrium of the soil. As noted by Alonso et al. (1987), the form of the equilibrium equations is not necessarily a proof of an effective stress statement for constitutive behavior. Fredlund and Morgenstern (1977) also argued that the expression of effective stress contains a material parameter χ and that the variables used for the description of a stress should be independent of the material properties. The theoretical basis for this argument is not clear. However, it is evident that it could only be applicable to single-phase homogeneous materials. In multiphase systems, such as saturated and unsaturated soils, the stress state within each phase will naturally be a function of the properties of that phase as well as the other phases within the system. It's necessary to ensure deformation compatibility between the phases.

To avoid the introduction of a material parameter in the effective stress equation, Fredlund and Morgenstern (1977) defined the state of stress in unsaturated soils in terms of two independent, no additive stresses, the first described at the macroscopic scale $(\sigma_{ij} - p_a\delta_{ij})$, while the other at the pore scale $(p_a - p_w)$. A separate set of material properties was then introduced for each of the stresses. This was in contrast with the usual approach in continuum mechanics, in which the state variables are averaged over the elemental volume (i.e., described at the macroscopic scale) and the macroscopic observations are described in terms of entities which are measured and/or defined at a macroscopic level. In general, mixing of scales can lead to complex constitutive equations with intractable stress-strain relationships.

However the effective stress concept is simpler than that of two independent stress variables and could be more easily applied. Most the constitutive equations used in geotechnical engineering are based on the concept of effective stress proposed by Terzaghi. They can be easily extended to partially saturated soils if the effective stress extended to unsaturated soil. In the case of sandy soils, the soil suction with a negligible magnitude, consequently the concept of effective stress can be used for partially saturated soils.

1.9. Effective stress concept

Soil mechanics as a science has been successfully applied to many geotechnical problems involving saturated soils. Its success is due to the concept of effective stress introduced by Terzaghi (1936) which related observed soil behavior to stress condition. The effective stress concept is commonly expressed as follows:

$$\sigma'_{ij} = \sigma_{ij} - p_w \delta_{ij} \tag{1.4}$$

Where σ'_{ij} is the effective stress, σ_{ij} is the total stress, p_w is pore pressure, δ_{ij} is Kronecker's delta.

The successes of the effective stress in saturated soils encourage researchers to extent this concept from saturated conditions to unsaturated conditions. Bishop (1959) suggested the following generalization:

$$\sigma'_{ij} = (\sigma_{ij} - p_a \delta_{ij}) + \chi (p_a - p_w) \delta_{ij} \tag{1.5}$$

Where χ is a parameter related to the degree of water saturation of the soil, the magnitude of χ is unity for a saturated soil and zero for a dry soil. The relationship between χ and the degree of water saturation could be obtained experimentally. Bishop and Blight (1963) provided experimental evidences supporting the validity of Equation (1.5) with $\chi = (1 - K / K_s) S_w$, K and K_s are the bulk moduli of the skeleton and of the solid matrix, respectively.

Zienkiewicz et al. (1999) suggested an average pore-pressure method to deal with the unsaturated problems. The average pressure is defined as:

$$p = \chi_w p_w + \chi_a p_a \tag{1.6}$$

p is the average pressure used to describe the effective stress by using Equation (1.4) instead of the pore-water pressure, χ_w and χ_a are two coefficients referring to pore-water and pore-air, respectively with $\chi_a + \chi_w = 1$. The two coefficients are functions of the water saturations, as $\chi_w = \chi_w(S_w)$, $\chi_a = \chi_a(S_a)$.

Khalili et al. (2001, 2004) proposed the following expression for the effective stress:

$$\sigma' = (\sigma - p_a) + \chi (p_a - p_w) \tag{1.7}$$

with $\chi = \left(\frac{s_e}{s} \right)^{0.55}$ for $s \geq s_e$ and $\chi = 1$ for $s \leq s_e$, s is the soil suction defined as $(p_a - p_w)$, and s_e suction value marking the transition between saturated and unsaturated states, for

wetting processes, s_e is equal to the air expulsion value, whereas for drying processes, s_e is equal to the air entry value. Khalili et al. (2004) provided experimental and literature evidences to the validity of the effective stress concept for unsaturated soils.

Sheng (1999) suggested that for certain soil, the effective stress concept is more efficient. The achievements presented in the literature are good evidences for the efficiency of the concept of effective stress.

For sandy soil, however, in partially saturated condition, when the volumetric water content exceeds certain value, 50% for example, the soil suction is negligible; the difference of pore-water pressure and pore-air pressure is close to zero. The contractile skin effects can be neglected.

1.10. Earthquake induced liquefaction

Soil liquefaction constitutes a major cause of damage induced by earthquakes. This phenomenon occurs in both saturated and unsaturated soils. Process of generation of excess pore-water pressure in sandy soil layers during the earthquakes causes the reduction in effective mean stresses, which leads to a loss in the rigidity and shear strength of the ground. Liquefaction was reported in moderate or large earthquake. For example: Loma USA 1989, Luzon Philippine 1990, Manjil Iran 1990, Kobe Japan 1995, Manzanillo Mexico 1995, Chi-Chi China 1999, Kocaeli Turkey 1999, Bhuj India 2001 (Singh et al., 2005), causing lots of damage (Bird et al., 2004). Liquefaction frequently occurs in reclaimed soils in coastal areas or poorly compacted man-made fills (e.g. Kobe Port; Marina District of San Francisco; Manzanillo, Mexico) and is also a common occurrence in alluvial or deltaic deposits including old or existing river beds (e.g. Dagupan, Luzon; Ceyhan, Turkey; the Rann of Kachchh in Gujarat, India).

Liquefaction-induced damage to buildings typically includes foundation settlement or tilting, or displacement due to lateral spreading. Foundation settlement occurs either where the soil beneath the building has settled due to volume change, or where the strength of soil has decreased causing the structure to sink into the ground in a bearing capacity failure. The secondary effect of building settlement is the dragging down of adjacent buildings, which, for various reasons do not settle by the same amount.

Liquefaction-induced disruption to transportation networks can be very significant, and its causes are damaged to road pavements or railway tracks due to settlement or lateral spreading, and damage to bridges. Ports and harbors tend to be particularly vulnerable to liquefaction due to the combination of fill and high water tables. Many of the dikes and embankments are

reported to failure due to the liquefaction induced by earthquakes and cause inundation in downstream area. The continued functioning of lifelines after an earthquake is of vital importance for both the emergency response and the recovery of a community. Buried utilities can be particularly vulnerable to permanent ground deformation resulting from liquefaction. They are similarly vulnerable to fault rupture deformation.

In fact, not only earthquakes cause liquefaction. The coastal or offshore structures such as pipelines installed in the seabed are subject to cyclic horizontal loads either by direct hydrodynamic wave action or through the cyclic movement of risers or flow lines transmitted by floating structures. In fine sandy or silty soils, such cyclic loads could lead to liquefaction of the surrounding bed, which can play an important damage to the pipe. On the express way or the railway, the vibration caused by the vehicle can also cause local liquefaction in the road foundation and cause the damage to the road.

It is widely recognized that the basic mechanism of liquefaction in a deposit of loose saturated sand during earthquakes is the progressive build-up of excess pore-water pressure due to the application of cyclic shear stresses induced by the upward propagation of shear waves from the underlying rock formation (Ishihara et al., 2004). Under ordinary condition prior to an earthquake, a soil element is subjected to a confining stress due to the weight of the overlying soils. When a series of cyclic stress is applied during an earthquake, the element of the loose sand tends to reduce its volume. However, since the duration of the cyclic stress application is so short as compared to the time required for drainage of water towards the surface from deposits of several meters depth, the volume contraction cannot occur immediately. In order to keep the potentially contracting loose sand at a constant volume, some change in the existing stress system must take place. The stress change is achieved in the form of a reduction in the existing confining stress due to the overlying soil, accompanied by concurrent increase of equal magnitude of pore-water pressure, therefore, the degree of pore-water pressure increase depends, on one hand, upon the looseness of the sand deposits indicatively of potential of the volume decrease tendency and, on the other hand, upon how largely the sand is sheared to extract the inherent volume decrease characteristics. When the state of sand packing is loose enough and the magnitude of cyclic shear stress is great enough, the pore-water pressure will build up to a full extent in which it becomes equal to the initially existing confining stress. At this state, no effective stress is acting on the sand and individual particles released from any confinement as if they are floating in water. Such a state is called liquefaction. Upon occurrence of liquefaction, individual particles of the sand start to sediment in water, thereby expelling pore-water towards the surface of the deposit and when the sedimentation has taken place throughout the depth, the sand is now deposited in a somewhat denser state.

1.11. Research on liquefaction

The liquefaction is caused by the contraction behaviour of granular material. To understand how soil liquefaction is initiated, some basic soil mechanics concepts are important, like the critical void ratio, the flow liquefaction and cyclic mobility. And then based on the experimental observation, the constitutive models are proposed for the granular material under cyclic loading conditions.

In 1936, Casagrande performed a series of drained strain-controlled triaxial tests and discovered that initially loose and dense specimens at the same confining pressure approached the same density when sheared to large strains. The void ratio corresponding to this density was called the critical void ratio. Performing tests at various effective confining pressures, Casagrande found that the critical void ratio varied with effective confining pressure. Plotting these on a graph produced a curve which is referred to as the critical void ratio (CVR) line. The CVR line constituted the boundary between dilative and contractive behavior in drained triaxial compression.

In the 1960s, Gonzalo Castro performed an important series of undrained, stress-controlled triaxial tests. Castro observed three different types of stress-strain behavior depending upon the soil state. Dense specimens initially contracted but then dilated with increasing effective confining pressure and shear stress. Very loose samples collapsed at a small shear strain level and failed rapidly with large strains. Castro called this behavior "liquefaction" - it is also commonly referred as flow liquefaction. Medium dense soils initially showed the same behavior as the loose samples but, after initially exhibiting contractive behavior, the soil "transformed" and exhibited dilative behavior. A key to understanding cyclic mobility came about with identification of the phase transformation line. Medium dense to dense sands subjected to monotonic loading will initially exhibit contractive behavior, but then exhibit dilative behavior as their strain toward the steady state.

Based on experimental observations, a large number of computational models have been, and continue to be developed for simulation of nonlinear granular soil response. Finn et al. (1977) and Martin et al. (1975) developed a model for the analysis of liquefaction of saturated cohesionless soil, this model, because of it simple form, has been introduced in the code FLAC (Itasca). Pastor and Zienkiewicz (1986, 1999) based on the general plasticity theory developed a numerical model. The bounding surface model developed by Dafalias (1997) has also been generally accepted. Elgamal et al. (2003) also based on the experimental observation developed a constitutive equation for the mobility behaviour of sand soil under undrained saturated conditions. In our laboratory, a robust constitutive equation, MODSOL, for granular material

was also developed (Chehade, 1991; Shahrour and Chehade, 1992; Khoshravan, 1995; Ousta and Shahrour, 1998, 2001). These are just several examples for the development of the constitutive models for granular material. However, until now reliable computational modelling of cyclic-mobility shear deformations remains a major challenge. Most of the developed constitutive model can be used within general fully coupled (solid–fluid) finite element formulations. In this dissertation, the MODSOL will be used.

It is interesting to indicate that, most of the constitutive models are based on the effective stress concept, and all these models can be applied successfully to the saturated condition. If the effective stress concept extended to partially saturated condition, these models could be used to predict the mechanical behaviour under unsaturated configurations.

1.12. Influence of the water saturation on liquefaction

Results of different investigators showed that a small reduction in the degree of water saturation from fully saturated sand can result in a significant increase in the shear strength against liquefaction. Martin et al. (1978) explained that a 1 % reduction in the degree of water saturation of a saturated sand specimen with porosity $n = 0.4$ can lead to 28 % reduction in the pore-water pressure increase per cycle. Figure 1.13 illustrates the influence of saturation on the cyclic liquefaction resistance. It is clear that, at the same stress ratio (loading level) with the decrease in water saturation, the number of cycles to liquefaction increases (liquefaction resistance increase).

According to Yang et al. (2003), a reduction of 1% in the water saturation led to a reduction in the excess pore-pressure ratio from 0.6 to 0.15 under pure horizontal excitation. Chaney (1978) and Yoshimi et al. (1989) have showed that the liquefaction resistance was about twice than that for fully saturated samples when the degree of water saturation reduced to 90%. Xia and Hu (1991) demonstrated that small quantities of entrapped air can significantly increase the liquefaction strength of a sand specimen. The laboratory tests showed that a reduction in the degree of water saturation from 100% to 97.8% led to more than 30% increase in the liquefaction resistance (Figure 1.14).

Tsukamoto et al. (2002) studied the liquefaction resistance of partially saturated sands. They concluded that the resistance to liquefaction increases with the decrease in the pore-pressure parameter B. When the B-value dropped to zero with a degree of water saturation $S_w = 90\%$, the cyclic strength became twice higher than that of the fully saturated condition. Ishihara and Tsukamoto et al. (2004) conducted a laboratory study on the undrained behaviour of near-saturated sand for both cyclic and monotonic loading. They showed that the decrease in

the water saturation (Skempton coefficient B) leads to an increase in the liquefaction resistance (Figure 1.15).

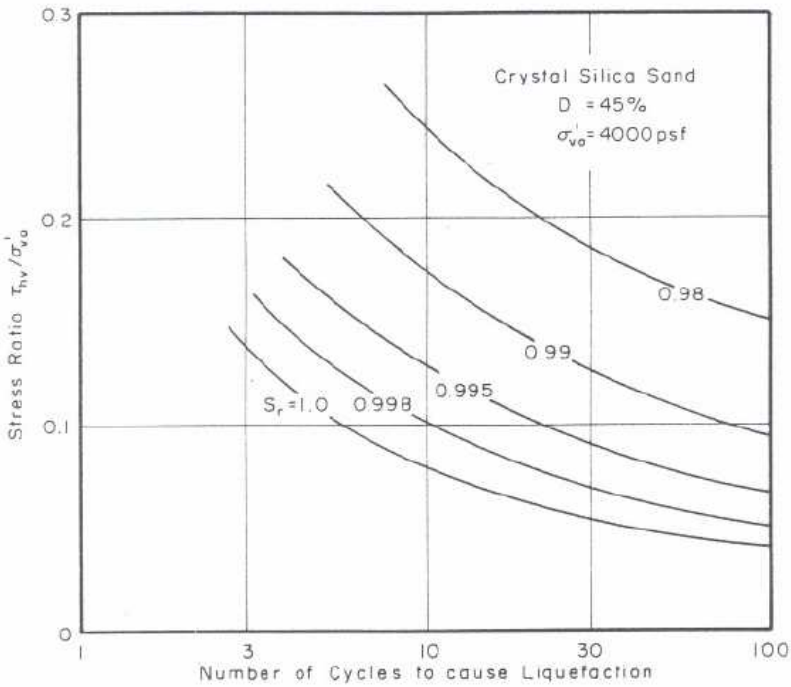

Figure 1.13: Influence of the water saturation on the liquefaction resistance (1psf=47.9 N/m^2) (Martin et al., 1978)

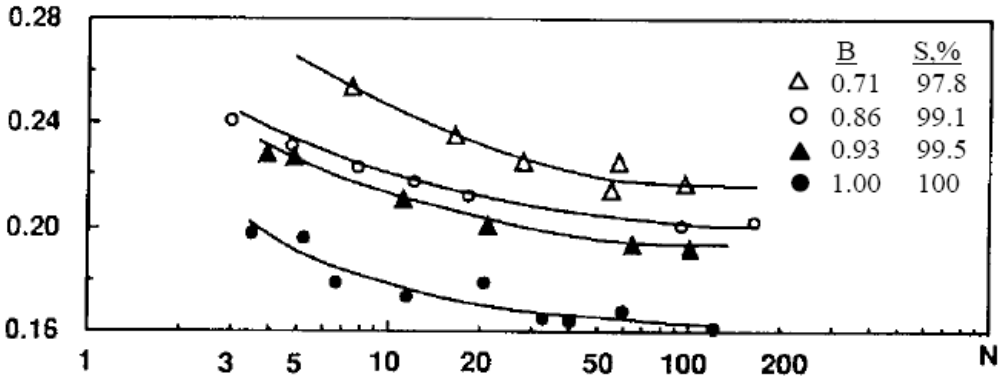

Figure 1.14: Influence of the water saturation on the liquefaction resistance (Xia et al., 1991)

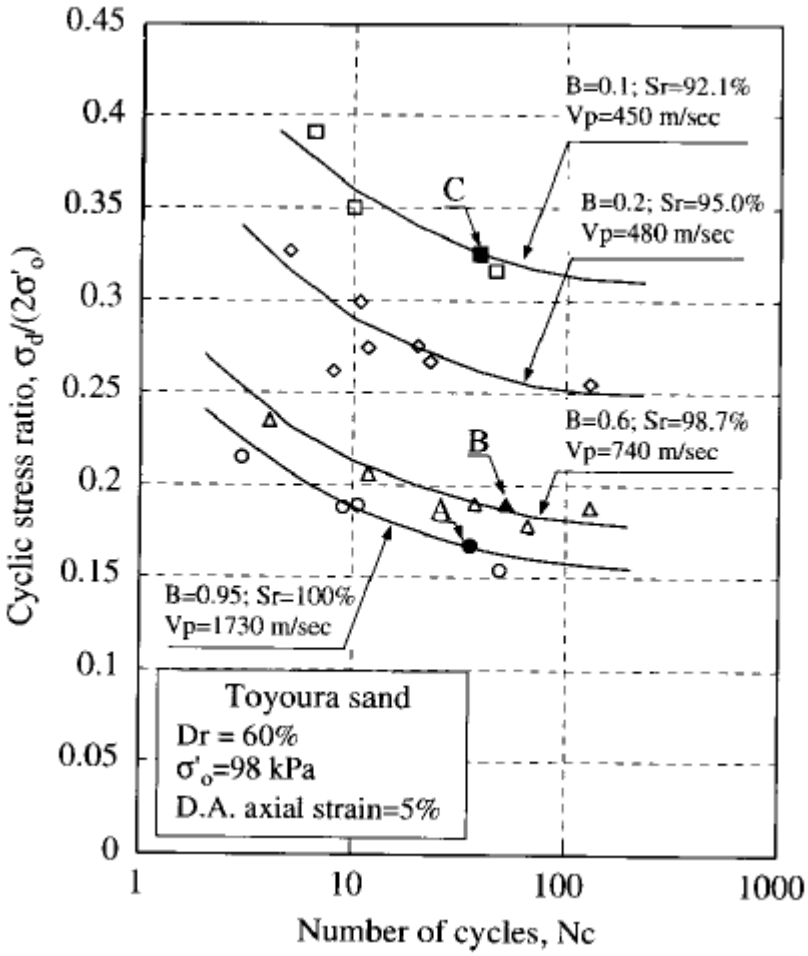

Figure 1.15: Influence of the water saturation on the liquefaction resistance (Ishihara et al., 2004)

Okamura et al. (2006) have conducted researches on the influence of the water saturation on the liquefaction resistance. The experimental results confirmed that the degree of water saturation had a significant effect on the liquefaction resistance.

Bouferra (2000) has conducted a series of undrained triaxial tests on Hostun sand with different water saturation. The water saturation is represented by the Skempton coefficient. The test results showed that the decrease in soil saturation leads to an increase in the liquefaction resistance. Arab (2007) confirmed these results as illustrated in Figure 1.16.

Singh et al. (2005) examined the damage of 6 earth dams in Bhuj earthquake. The 6 reservoirs were nearly empty prior to earthquake, and the liquefiable soil layers were in a state of partially saturated sate. The in-situ observations indicated that the downstream area of the dam has less damage than the upstream. The observation shows that the partially saturation reduces the liquefaction potential. It also shows that liquefaction could occur in partially saturated condition.

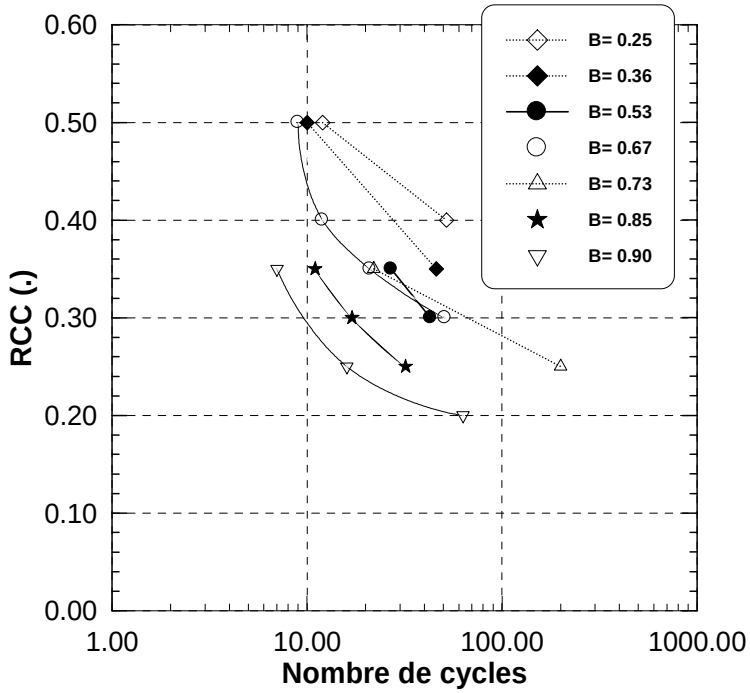

Figure 1.16: Influence of the water saturation on the liquefaction resistance Hostun sand (Arab, 2007)

Nagao et al. (2007) excited the report of Shiraishi, that 312 examples of structures having pneumatic caisson foundation were prevented from fatal damage by liquefaction in Kobe earthquake, because the ground surrounding the foundation were unsaturated by air entrapped during the construction. More detailed evidences are needed for further studies.

Zienkiewicz et al. (1999) conducted a pioneer work on the partially saturated liquefiable soils. Sheng (1999) gave some perspectives in the partial saturation condition for sandy soils. Jafari-Mehrabadi et al. (2007) conducted some work on the quasi saturated sands, the saturation greater than 90%.

1.13. Liquefaction mitigation

Remediation methods against liquefaction have been developed and applied since the 1964 Niigata earthquake. The efforts for liquefaction mitigations include 3 strategies:

a) Avoid locating buildings and infrastructure in areas with high liquefaction potential,
b) Foundations which can resist to liquefaction,
c) Improve the soil (including soil compactness and drainage)

The compactness of soil can be achieved by different techniques, like vibroflotation which is the process of inserting a vibrating probe into the ground to cause compaction of sediments, and dynamic compaction, where a heavy weight is dropped on to the soil surface to compact loose

sediments. Stone columns are used to decrease the liquefaction potential of soils. This method will increase the density of the soil and at the same time will increase the drainage capacity.

For the drainage, the main principle is to ensure the soil has sufficient drainage capacity. During the earthquake, the generated excess pore-pressure can be dissipated rapidly. Harada et al. (2006) reported the drainage techniques for pile foundation. The shaking table tests and in-situ experiments illustrate the efficiency of the drainage method. Brennan et al. (2006) used centrifuge model to investigate examines the drainage efficiency of the penetration depth of drain-well.

However, most of the countermeasures against liquefaction are designed for new constructions. Few remediation methods were developed for existing structures. Various soil remediation measures to reduce or eliminate liquefaction potential for existing structures have been summarised by Yasuda (2007).

As indicated in the precedent sections, when the water saturation in the soil decreases, the liquefaction resistances will greatly increase. This suggests that the induced partial saturation could be a potential liquefaction mitigation countermeasure which could be applied to both new and existed constructions.

The techniques of induced partial saturation in ground have been studied in USA by Yegian et al. (2007) and in Japan by Nagao et al. (2007). Yegian et al. suggested that the Electrolysis may be a good method to induce partial saturation in ground. He also suggested a drained-recharge method for inducing partial saturation during the laboratory research; this may be used to construction site too. Nagao, however advised a micro-bubble injection method to induce partial saturation in ground, he argued that as the micro-bubble is an independent small bubble of 10-100µm in diameter, it can easily permeate voids among sand particles.

1.14. Conclusion

The review of the researches on response of unsaturated soils to seismic loading shows that natural soils, even those under the water table, are in unsaturated condition. The contractile effects for sandy soil are negligible. At high degree of water saturation, the air flux could be neglected. The concept of effective stress could be used to study the partially saturated sandy soils. The laboratory experimental researches show that the degree of water saturation influences the response of soils to undrained paths and their resistance to liquefaction. Introducing air in the saturated soils could be used as liquefaction mitigation method.

In this work, the objective is to develop a numerical model within the framework of porous media and the concept of effective stress. The two chapters followed are:

In the second chapter, based on the laboratory and in-situ observation, three reasonable assumptions are taken for partially saturated sandy soils; the soil suction, the effect of air dissolved into water and the air flux are neglected. Based on Coussy's formulation, a numerical model is established for unsaturated sandy soils. This numerical model can deal with both saturated and unsaturated conditions. The implementation of this model in finite element code is presented. Finally some numerical applications and discussions are presented.

In the third chapter, a cyclic constitutive equation based on the concept of effective stress for granular material is presented. After implementation of this model in the numerical model, some applications are illustrated. Firstly, the simulations of triaxial experiment in both monotonic and cyclic loading are presented; the influence of the water saturation on liquefaction resistance is analyzed by the numerical simulation. The numerical model is used to study the influence of the water saturation on the free-field response. Some key factors, namely the permeability and relative density are studied. At last the tests conducted by Yegian et al. are reviewed and discussed.

Chapter 2: Numerical model for unsaturated sandy soils

2.1. Introduction

Since the 1964 Niigata earthquake, extensive researches have been carried out on liquefaction. However, most of these researches were conducted on saturated soils. Recent observations indicate that soils encountered in geotechnical engineering are generally unsaturated (Fredlund et al., 1993; Sheng, 1999; Fredlund, 2006; etc.). The soils under water table are not, as usually assumed, fully saturated (Ishihara et al., 2004; Tsukamoto et al., 2007; etc.). They are in the state of near-saturated state with individual air bubbles. The liquefiable soils are generally located in partially saturated soil layers. On the other hand, experimental results show that the liquefaction resistance depends strongly on the water content of sandy soils. for example: a little decrease in water saturation, especially with high water saturation, results in an significant increase in the liquefaction resistance (Martin et al., 1978; Yoshimi et al., 1989; Ishihara et al., 2004; Arab, 2007; ect.). So it is of a major interest to investigate the liquefaction in partially saturated condition.

The partially saturated media can be described as the supposition of $n+1$ mechanically interacting media: n represents the saturating fluids while the remainder corresponds to the skeleton. It is considered partially saturated for a referenced fluid, generally chosen in liquid form. For the saturated case, the hydro-mechanic coupled theory founded by Biot (1941, 1956 and 1962) together with the concept of effective stresses proposed by Terzaghi (1936) are used to study the liquefaction phenomena in saturated soils (Zienkiwicz et al., 1980, 1984, 1999). New developments in the area of unsaturated soils (Fredlund, 1993, 2006; Coussy, 1991, 2004) together with the generalization of the concept of effective stress to unsaturated soils (Bishop, 1959) allow to deal the unsaturated problem as a coupled problem.

In this chapter, firstly, the theory for saturated pore material will be reviewed. Then, based on the formulation of Coussy (2004), this theory will be extended to partially saturated condition. Based on experimental observations, some assumptions will be discussed and used to elaborate a numerical model for unsaturated sandy soils. Later, we will present successively the formulation of the numerical model, the variation of the water saturation. This numerical model will be implemented into a finite element code. Finally some validation tests will be presented.

Because we emphasize on the coupled hydromechnical behavior of partially saturated sandy soils, so our research is limited to isothermal condition. In this chapter, the mechanical convention will be used as: compression stress is negative, while for the pore-pressure, compression pressure is positive.

2.2. Theory of saturated Poro-Mechanics

The hydro-mechanic coupled theory founded by Biot (1941, 1956, 1962) together with the concept of effective stresses proposed by Terzaghi (1936) are used to study the liquefaction phenomena of saturated soils (Zienkiwicz et al., 1980, 1984, 1999). Soils are considered as the superposition of two continua: the skeleton continuum and the fluid continuum. With the hypothesis of small deformations ε and small variation of fluid masse m, it is justified to adopt a quadratic form of the free energy with regard to the constituents m, ε:

$$\psi = \sigma^0 : \varepsilon + g_m^0 m + \frac{1}{2}\varepsilon : C : \varepsilon - (\frac{m}{\rho_w^0})MB\varepsilon_{kk} + \frac{1}{2}M(\frac{m}{\rho_w^0})^2 \tag{2.1}$$

In this potential function, M is the Biot's modulus. The second order tensor B is Biot's coefficient tensor. C is the stiffness tensor of isothermal undrained elastic moduli. ε is the strain tensor of soil skeleton. m is mass flux of pore-water and ρ_w^0 is the initial pore-water density. σ^0 and g_m^0 are the initial stresses and initial free enthalpy of the pore-water, respectively. The state equations can be derived by the derivation of the free energy:

$$\sigma = \frac{\partial \psi}{\partial \varepsilon} = \sigma_0 + C : \varepsilon - \left(\frac{m}{\rho_w^0}\right)MBI \tag{2.2}$$

$$g_m - g_m^0 = \frac{\partial \psi}{\partial m} = -\left(\frac{1}{\rho_w^0}\right)MB\varepsilon_{kk} + \left(\frac{1}{\rho_w^0}\right)M\left(\frac{m}{\rho_w^0}\right) \tag{2.3}$$

The free enthalpy is defined as (Coussy, 1991):

$$g_m = g_m^0 + \frac{p_w - p_w^0}{\rho_w} - \frac{\left(p_w - p_w^0\right)^2}{2\rho_w K_w} \tag{2.4}$$

The linear form is used here as:

$$g_m = g_m^0 + \frac{p_w - p_w^0}{\rho_w} \tag{2.5}$$

Combination of Equations (2.3) and (2.5) leads to the expression of the pore-pressure:

$$p_w = p_w^0 - M\left(B\varepsilon_{kk} - \frac{m}{\rho_w}\right) \tag{2.6}$$

Introducing Equation (2.6) into (2.2), by eliminating the mass flux of pore-water, after rearranging the equation, it becomes:

$$\begin{aligned} &\sigma = \sigma_0 + C_0 : \varepsilon - B(p - p_0)I \\ &C_0 = C - MB \otimes B \end{aligned} \tag{2.7}$$

Where C_0 is the tensor of isothermal drained elastic moduli. For an isotropic thermoporoelastic porous material, the Biot's coefficient tensor can be expressed as scalar-valued function of b as, $B = bI$. In the case of natural stresses sate, the constitutive equations can be presented as follow:

$$\sigma = C : \varepsilon - \left(\frac{m}{\rho_w^0} \right) MbI \tag{2.8}$$

$$p_w = M \left(b\varepsilon_{kk} - \frac{m}{\rho_w} \right) \tag{2.9}$$

The Biot's coefficient b and Biot's modulus M can be identified by laboratory tests. Coussy (2004) proposed:

$$b = 1 - \frac{K_0}{K_m}; \frac{1}{M} = \frac{b-n}{K_m} + \frac{n}{K_w} \tag{2.10}$$

K_0 is the drained bulk modulus of soil skeleton, K_m and K_w are the bulk moduli of soil grains and the pore-water, respectively. n is the porosity. If the soil grain is supposed as incompressible, that means $K_m \to \infty$, we have $b = 1$. Equation (2.10) can be rewritten in the form:

$$b = 1; \quad \frac{1}{M} = \frac{n}{K_w} \tag{2.11}$$

In consequence, Equation (2.8) will be rewritten as:

$$\sigma' = \sigma + bp_w I \quad \text{with} \quad \sigma' = C_0 : \varepsilon \tag{2.12}$$

The tensor σ' is called the elastic effective stresses tensor and can be interpreted as the stress tensor that produces the (elastic) strain of the skeleton. In the case of incompressible soil grains ($b = 1$), the effective stresses concept of Terzaghi (1936) is proved. This function has been used by Zienkiwicz et al. (1980, 1984 and 1999) to study the liquefaction of saturated sandy soils.

2.3. Theory of unsaturated Poro-Mechanics

In many engineering practices, such as drying, drainage or the imbibitions of soils, the soil is said to be unsaturated. The partially saturated media can be viewed as the supposition of $n+1$ mechanically interacting media: n saturating fluids plus one deformable skeleton. It is considered partially saturated for a referenced fluid, generally chosen in the liquid form. The sate equations of saturated media presented in the last section can be extended to unsaturated media.

Based on the thermodynamic theory of Coussy (1991, 2004), the fluid components of unsaturated soils include a liquid (index w), its vapour (index v) and the dry air (index a). In isothermal condition, the interaction of water/vapour and dry air /water-vapour is so weak that it could be neglected in the liquefaction problem. For the sake of simplicity, the water-vapour and the dry air will not be distinguished. The unsaturated soil can be considered as the superposition of the soil skeleton, the pore-water (index w) and the pore-air (index a).

Since the pore-air and pore-water occupy the total porous space, the following equation is obtained:

$$n = n_w + n_a \tag{2.13}$$

The saturation of each fluid can then be defined as:

$$S_w = \frac{n_w}{n}; S_a = 1 - S_w = \frac{n_a}{n} = \frac{n - n_w}{n} \tag{2.14}$$

The linear model in saturated soil is based on the linearization of the free mass enthalpy g_m^j of the fluid j and the free energy ψ, with respect to variables ε and m_j, by retaining only the second order expansions. However, if the saturating fluid is highly compressible gas, the linearization of g_m^j is irrelevant. Furthermore, since the saturation with respect to any of the fluid phases can vary form 0% to 100%, the linearization with respect to the variations in fluid mass content m_j is generally also irrelevant. Moreover, as the water saturation decreases, suction effects arise, and these are nonlinear. Hence, a non linear formulation of thermoporoelastcity is necessary for unsaturated soils. With the extension of equations (2.2) and (2.3), the state equations can be derived as follows:

$$\delta\sigma = C : \delta\varepsilon - \left(\frac{\delta m}{\rho_0}\right)_j M_{jk} B_k I \tag{2.15}$$

$$\delta g_{mi} = -(\frac{\delta_{ij}}{\rho_{0j}})M_{jk}B_k\delta\varepsilon_{mm} + \frac{1}{2}\left[(\frac{\delta_{ij}}{\rho_{0j}})M_{jk}(\frac{\delta m_k}{\rho_{0k}}) + (\frac{\delta m_j}{\rho_{0j}})M_{jk}(\frac{\delta_{ki}}{\rho_{0k}})\right] \tag{2.16}$$

Where I is a unit second order tensor and δ_{ij} is the Kronecker's delta. The tensors B_k are symmetric second order tensors, and moduli M_{jk} are the components of a symmetric matrix $\left(M_{jk} = M_{kj}\right)$.

By using the linear form of the free enthalpy defined in Equation (2.4), the state equation of pore-pressure can be written as:

$$\delta p_i = -M_{ij}\left\{B_j\delta\varepsilon_{mm} - \left(\frac{\delta m}{\rho_0}\right)_j\right\} \tag{2.17}$$

Combining equation (2.15) and (2.17), allows to eliminate the mass flux, and to get the state equation in pore-pressure:

$$\begin{aligned}\delta\sigma &= C_0 : \delta\varepsilon - B_i\delta p_i I \\ C_0 &= C - B_i M_{ij} B_j\end{aligned} \tag{2.18}$$

State equations for saturated case have been extended to the case of n saturating fluids. Therefore, the tensors C_0 and C have the same signification as in the saturated condition. The specific properties to partially saturated media are moduli M_{ij}, with $i \neq j$, which are associated with coupling phenomena. Equation (2.17) shows that M_{ij} is the modulus linearly linking the pressure variation $p_i - p_{0i}$ of fluid i to m_j, the increase in the fluid masse content of phase j.

With the expression of Biot's coefficients for unsaturated soils (Coussy, 2004):

$$B_i = b_i I; b_i = bS_i; b = \sum b_i = b\left(S_a + S_w\right) \tag{2.19}$$

The variable b is the Biot's coefficient for saturated case. So the equation (2.18) with zero initial stress can be arranged as:

$$\delta\sigma_{ij}^{'} = C_0 : \varepsilon = \left(\delta\sigma_{ij} + b\delta p_a\delta_{ij}\right) + bS_w\left(\delta p_w - \delta p_a\right)\delta_{ij} \tag{2.20}$$

Under the assumptions of incompressible soil grain $\left(b = 1\right)$, the Bishop's (1959) effective stresses for partially saturated porous media are proved:

$$\sigma' = (\sigma + p_a) + \chi(p_w - p_a) \tag{2.21}$$

For the isotropic material, the sate equations are rewritten as follow:

$$\delta\sigma_{ij} = \lambda\delta\varepsilon_{kk}\delta_{ij} + 2\mu\delta\varepsilon_{ij} - \begin{Bmatrix} \dfrac{\delta m_w}{\rho_w^0} & \dfrac{\delta m_a}{\rho_a^0} \end{Bmatrix} \begin{bmatrix} M_{ww} & M_{wa} \\ M_{aw} & M_{aa} \end{bmatrix} \begin{Bmatrix} S_w \\ S_a \end{Bmatrix} b\delta_{ij} \tag{2.22}$$

$$\begin{Bmatrix} \delta p_w \\ \delta p_a \end{Bmatrix} = \begin{bmatrix} M_{ww} & M_{wa} \\ M_{aw} & M_{aa} \end{bmatrix} \left(-b \begin{Bmatrix} S_w \\ S_a \end{Bmatrix} \delta\varepsilon_{kk} + \begin{Bmatrix} \delta m_w / \rho_w^0 \\ \delta m_a / \rho_a^0 \end{Bmatrix} \right) \tag{2.23}$$

$M_{ww}, M_{wa}, M_{aw}, M_{aa}$ depend fundamentally on the porosity; the compressibility of the soil grains, the pore-water and the pore-air; the fluid saturations; and also the soil water characteristic curve. Their expressions will be detailed in the following section.

2.4. Assumptions for unsaturated sandy soils

The numerical model is based upon the following assumptions:

1) The hypothesis of infinitesimal transformations with respect to the skeleton between the initial state and the current state:

$$\|grad\,\xi\| << 1 \tag{2.24}$$

Where ξ is the displacement vector. Furthermore, the Jacobin J of transformation reads:

$$J = 1 + tr\varepsilon \tag{2.25}$$

2) The solid matrix is supposed as incompressible;
3) Under unsaturated condition, the pore-water is supposed as pure saturated water;
4) The pore-air is supposed as ideal gas;
5) The soil suction is neglected;
6) The interaction between pore-water and pore-air is neglected;
7) Null air flux $dm_a = 0$ is assumed.

The last three hypotheses will be discussed in the following paragraphs.

2.4.1. The soil suction

The main differences between saturated and unsaturated soil lies in the existence of soil suction, which is defined as the difference between the pore-air pressure and the pore-water pressure. It is an important parameter for unsaturated soils. However, for sandy soils, because of the big diameter of soil grains; the soil suction in certain water saturation range is so small that it can be neglected. Figure 1.10 in section 1.6 shows the soil water characteristic curve for the Hostun sand and other sands. It can be observed that the soil suction is very small over a very wide range of water saturation: suction remains lower than 5kPa when the degree of water saturation is higher than 40%. This value is so small that it can be neglected. Consequently, the soil suction is neglected, which means: the pore-water pressure is equal to the pore-air pressure ($p_a = p_w$).

This assumption is reasonable, especially for the high water saturation. With the increase in water saturation, the capillary effect decreases. In addition, in the equilibrium condition, the pore-air pressure is equal to pore-water pressure in the water/air mixture. It means that the effect of surface tension (soil suction) is neglected. Martin et al. (1978) indicated that for air bubbles having a radius lower than 0.03mm, the error in using this assumption is less than 5%.

2.4.2. The diffusion of air into water

As discussed in the first chapter, the water volumetric coefficient of solubility is about 2% in natural condition. And the diffusion of air into water will greatly influence the compressibility of air and water mixture. On the other hand, the diffusion of air into water is very slow.

The process of air diffusion into water is described by Fick's law, which states that the rate of air mass dissolved into water is proportional to the contacted surface and to the gradient of air concentration which is related to the air pressure.

$$\frac{dm_a}{dt} = -DA\frac{\partial C}{\partial x} \tag{2.26}$$

As discussed in the first chapter, the coefficient of diffusion D for natural air through free water is about $2.2\times10^{-9}\,\mathrm{m^2/s}$. In the case of high water saturation, the free air in the air-water mixture is in the form of individual air bubbles. The pore-water is saturated with its vapour. As a result it needs a long time for the air to pass through the interface and into the water. Martin et al. (1978) indicated that the influence of air going into solution due to the increase in the pressure may be neglected. This is appropriate for the dynamic loading portion of the test in

view of the large time required to dissolve air. Nagao et al. (2007) confirmed this conclusion, when the confining pressure is less than 400kPa.

2.4.3. Air flux in partially saturated sandy soils

In partially saturated soils, the fluid fluxes are described by Darcy's law, which defines that the mass flux of each fluid is proportional to the pressure gradient, as:

$$\frac{\vec{w}_i}{\rho_i} = -k_i \, grad(p_i); \quad i = a, w \tag{2.27}$$

The most important parameter is the permeability as discussed in section 1.7. In fact, for a single fluid (i.e. saturated case), the permeability has a clear significant; however if there are two or more fluids, it should take the interaction between fluids into consideration. The presence of one fluid will eventually have some impacts on the other. The concept of relative permeability (Luckner et al., 1989), which assumes that the permeability is an intrinsic property and the permeability of each fluid is just a fractional part of this property permeability, is used. As illustrated in Figure 1.11 in section 1.7, when the saturation exceeds 80%, the relative permeability of pore-air is close to zero; that means that the pore-air is entrapped in the soil and there is no air flux.

The in-situ observation of the air entrapped below the phreatic surface for 26 years was observed by the Okamura et al. (2006). The Laboratory study for "long term air diffusion test" by Yegian et al. (2007) confirmed that the air entrapped in the soil with high water saturation will survive for long time. All these facts suggest that for high water saturation, the air flux could be neglected.

2.4.4. Conclusion

In order to take the influence of water saturation on the liquefaction phenomena into consideration, the several reasonable assumptions are taken. In addition, the isothermal condition is supposed. In fact, the temperature has so many influences on both pore fluids and soil grains. However, only in special case such as the reservoir of radwaste, the temperature will be taken into consideration. Generally, the thermal effects are neglected in geotechnical engineering.

2.5. General equations for unsaturated sandy soils

With the assumptions presented in the precedent section, based on the general theory of unsaturated soils, the numerical model for unsaturated sand soils will be established. By using the stresses partition concept, under the assumption of infinitesimal transformations, the incremental mean stress is expressed as follows (Coussy, 2004):

$$\delta\sigma_m = (1-n)\delta\sigma_m^s - n_j\delta p_j \tag{2.28}$$

Where $\delta\sigma_m$ is the mean stress increment defined as $\delta\sigma_m = tr(\delta\sigma_{ij})/3$, n_j is the porosity of the fluid j. n is the current porosity. $\delta\sigma_m^s$ is the matrix mean stress increment (i.e. the partition stresses act on the soil grains), which can be expressed as:

$$\delta\sigma_m^s = K_s\delta\varepsilon_{kk}^s \tag{2.29}$$

K_s is the matrix bulk modulus, $\delta\varepsilon_{kk}^s$ is the matrix volumetric deformation increment. Moreover, the matrix volumetric deformation increment $\delta\varepsilon_{kk}$ is linked the skeleton volumetric deformation increment $\delta\varepsilon_{kk}^s$ and the variation of porosity δn (Coussy, 1991):

$$(1-n)\delta\varepsilon_{kk}^s = (1-n)\delta\varepsilon_{kk} - \delta n \tag{2.30}$$

Where $\delta n = n_0 - n$ is the variation of porosity, n_0 is the initial porosity.

The incremental constitutive equations of the saturating fluids may be expressed as:

$$\delta p_j = K_j\frac{\delta\rho_j}{\rho_j} \tag{2.31}$$

Generally, the pore-air is considered as an ideal gas, so the bulk modulus of the pore-air is associated with the absolute pore-air pressure:

$$K_a = \overline{p}_a = p_a + p_{a0} \tag{2.32}$$

Where $\overline{p}_a$ is the absolute pore-air pressure, and p_a is the measured pore-air pressure, p_{a0} is the atmospheric pressure (101.3kPa). While for the pore-water, the bulk modulus of full saturated pure water is about 2.23GPa. Comparing that of pore-air, the linear property is assumed for the pore-water (constant bulk modulus).

From equations (2.28) to (2.31), the incremental macroscopic mean stress can be expressed by:

$$\delta\sigma_m = (1-n)K_s\delta\varepsilon_{kk} - n_j K_j \frac{\delta\rho_j}{\rho_j} - K_s\delta n \tag{2.33}$$

The combination of the conservation of mass ($\delta m_j = J\rho_j n_j - \rho_{0j} n_{0j}$) and the infinitesimal transformation ($J \approx 1+\delta\varepsilon_v$) allow us to obtain the derivation of the following expression for the variation of the porosity.

$$\frac{\delta m_j}{\rho_j} = \frac{\delta\rho_j}{\rho_j} n_j + n_j\delta\varepsilon_{kk} + \delta n_j \tag{2.34}$$

As a result, the variation of porosity can be written in the form:

$$\delta n = \sum_{j=1}^{n} \delta n_j = \sum_{j=1}^{n} \left(\frac{\delta m_j}{\rho_j} - \frac{\delta\rho_j}{\rho_j} n_j - n_j\delta\varepsilon_{kk}\right) \tag{2.35}$$

The combination of equations (2.30), (2.31) and (2.35) leads to:

$$\delta\varepsilon_{kk} = \frac{\delta m_a}{\rho_a} + \frac{\delta m_w}{\rho_w} - \frac{n_a}{K_a}\delta p_a - \frac{n_w}{K_w}\delta p_w \tag{2.36}$$

Under the assumption of the equality of pore-air pressure and pore-water pressure (presented in section 2.4.1) in unsaturated sandy soils, the pore-air pressure or the pore-water pressure could be determined:

$$\delta p_a = \delta p_w = M'\frac{\delta m_a}{\rho_a} + M'\frac{\delta m_w}{\rho_w} - M'\delta\varepsilon_{kk} \tag{2.37}$$

With the Biot modulus for unsaturated soil M':

$$\frac{1}{M'} = \frac{n_a}{K_a} + \frac{n_w}{K_w} = \frac{n(1-S_w)}{p_w + p_{a0}} + \frac{nS_w}{K_w} \tag{2.38}$$

The constitutive equations for unsaturated sandy soils become:

$$\begin{aligned}\delta p_a &= -M_{aa}S_a b\delta\varepsilon_{kk} - M_{aw}S_w b\delta\varepsilon_{kk} + M_{aa}\frac{\delta m_a}{\rho_a} + M_{aw}\frac{\delta m_w}{\rho_w}\\ \delta p_w &= -M_{wa}S_a b\delta\varepsilon_{kk} - M_{ww}S_w b\delta\varepsilon_{kk} + M_{wa}\frac{\delta m_a}{\rho_a} + M_{ww}\frac{\delta m_w}{\rho_w}\end{aligned} \tag{2.39}$$

With the no-air flux assumption $\delta m_a = 0$ (presented in section 2.4.2), the equation (2.39) could be rewritten as the following:

$$\begin{aligned}\delta p_a &= -M_{aa}S_a b\delta\varepsilon_{kk} - M_{aw}S_w b\delta\varepsilon_{kk} + M_{aw}\frac{\delta m_w}{\rho_w}\\ \delta p_w &= -M_{wa}S_a b\delta\varepsilon_{kk} - M_{ww}S_w b\delta\varepsilon_{kk} + M_{ww}\frac{\delta m_w}{\rho_w}\end{aligned} \tag{2.40}$$

In fact, with any deformation and any water flux, the pore-air pressure is assumed to be equal to the pore-water pressure, together with equation (2.37) and equation (2.40), we get:

$$M_{aa} = M_{aw} = M_{wa} = M_{ww} = M' \tag{2.41}$$

The constitutive equations are governed by the following expressions:

$$\delta\sigma = C:\delta\varepsilon - M'\frac{\delta m_w}{\rho_w}bI \tag{2.42}$$

$$\delta p_w = \delta p_a = -M'b\delta\varepsilon_{kk} + M'\frac{\delta m_w}{\rho_w} \tag{2.43}$$

Which are similar to that used for saturated soils (equation (2.2) and (2.6)), but with a Biot modulus depending on the porosity, pore-pressure and water saturation, while for saturated soils, the modulus is constant. It is of interest to indicate that, in Equation (2.38), if the water saturation is unit, which means the soil is saturated, the formulation for saturated soils is recovered. It means that this formulation could be used for both saturated and unsaturated soils.

2.6. Variation of water saturation

The water saturation is a key variable for unsaturated soils. In the constitutive equation, it should be determined. Generally, for unsaturated soils, the water saturation could be determined by using the soil water characteristic curve. However, for sandy soils, the ideal gas law will be used to determine the water saturation. In addition, the assumption of null air flux which is used for deriving the constitutive equations will also be used to determine the water saturation. With the null air flux, all the pore-air will rest in its original place or dissolved in the pore-water. We consider an unsaturated soil specimen, with a volume V and initial measured pore-pressure p_{0w}. The initial porosity is n_0 and the initial water saturation is S_w^0. So the initial pore-air and pore-water volume are:

$$\begin{aligned} V_a^0 &= n_0(1-S_w^0)V \\ V_w^0 &= n_0 S_w^0 V \end{aligned} \tag{2.44}$$

After a small perturbation, under drained or undrained conditions (for pore-water only; while for pore-air the condition is always supposed as undrained), the measured pore-pressure becomes p_w, the volumetric deformation is ε_v. Because the soil grain is incompressible, the variation of the soil volume is equal to the variation of the pore volume:

$$\delta V = \varepsilon_v V = (n-n_0)V \tag{2.45}$$

Because the soil grain is incompressible, the variation of the soil volume is composed of the variation of the pore-air volume and pore-water volume as:

$$\delta V = \delta V_a + \delta V_w \tag{2.46}$$

Since the pore-air is assumed as an ideal gas, it obeys the ideal gas law.

$$(p_a + p_{a0})V_a = N_m RT \tag{2.47}$$

With V_a the current volume of air, T is the absolute air temperature, R is the universal gas constant, and N_m is the number of air moles. For an isothermal process the ideal gas law reduces to the Boyle's law. According to (2.47), we can calculate the variation of the pore-air volume as:

$$\delta V_a = \left(\frac{p_{0w} + p_{a0}}{p_w + p_{a0}} - 1 \right) V_a^0 \tag{2.48}$$

Current pore-water volume will change because of the drainage or/and the compressibility of water. Combination of equations (2.44) and (2.46) gives the current pore-water and pore-air volume:

$$V_w = V_w^0 + \delta V - \delta V_a; \quad V_a = V_a^0 + \delta V_a \tag{2.49}$$

So the current water saturation can be expressed as its definition:

$$S_w = \frac{V_w}{V_w + V_a} \tag{2.50}$$

Combination of equations (2.44) to (2.50) allows the determination of the current water saturation as follow:

$$S_w = \frac{n_0 S_w^0 + \varepsilon_v - \left(\frac{p_{0w} + p_{a0}}{p_w + p_{a0}} - 1 \right) n_0 (1 - S_w^0)}{n_0 + \varepsilon_v} \tag{2.51}$$

It should be indicated that, in Equation (2.48), it is supposed that no interaction between pore-air and pore-water. However, as discussed in the first chapter, the air dissolved in water will greatly influence the mechanical behaviour of the water-air mixture. The volumetric coefficient of solubility of the air in water at certain temperature is relatively stable. So it can be used to calculate the water saturation and taking the effect of dissolution into consideration:

$$\left(p_{0w} + p_{a0} \right)(V_a^0 + hV_w) = \left(p_w + p_{a0} \right)(V_{fa} + hV_w) \tag{2.52}$$

With h volumetric coefficient of solubility of air in water and V_{fa} the current free air volume after the perturbation, by using the same method, we can get the expression of water saturation, as:

$$S_w = \frac{n_0 S_w^0 + \varepsilon_v - \left(\frac{p_{0w} + p_{a0}}{p_w + p_{a0}} - 1 \right) (n_0 (1 - S_w^0) + hV_w)}{n_0 + \varepsilon_v} \tag{2.53}$$

This is similar to equation (2.51) with a additional part related with the current water volume V_w which can be determined using the state equation (2.42):

$$V_w = V_w^0 + \frac{p_w - p_{0w}}{M} + \varepsilon_v \tag{2.54}$$

2.7. Finite element modelling

This part is devoted to solve the poroelastic problem by the finite element method. The attention will mainly focus on the non-linear poroelastic problem. By choosing the displacement and the water pressure as principal variables, the general set of field equations of unsaturated soil can be firstly derived. The fluid diffusion process is then analyzed. Finally, some problems of poroelasticity are solved. The finite element method is used to solve the dynamic problem which is governed by the following expressions:

1) The balance equation:
When adopting the small perturbation hypothesis and neglecting the body force, the balance equation is:

$$div(\sigma) - \rho\ddot{u} = 0 \tag{2.55}$$

u, $\dot{u}$ and $\ddot{u}$ are the displacement, velocity and acceleration vectors of soil skeleton, respectively. ρ is the soil density, which depends on soil porosity, the densities of the solid grains and pore-water, respectively:

$$\rho = (1-n)\rho_s + nS_w\rho_w \tag{2.56}$$

The density of the pore-air is neglected.

2) The diffusion law:
For instance, the generalized Darcy's law is used:

$$\frac{\vec{w}}{\rho_w} = -k_{ins}\frac{k_{rl}^w}{\mu}\left[grad(p_w) + \rho_w\ddot{u}\right] \tag{2.57}$$

Where $\vec{w}$ is the pore-water mass flux, k_{ins} and k_{rl}^w are the soil intrinsic permeability and the permeability relative to water, respectively. μ is the water viscosity.

3) The conservation of the mass:

The expression of the overall mass conservation must take into account the relative masse flow of each fluid phase: pore-water and pore-air. In the absence of overall creation and null gas flux, the overall mass conservation can be written as follows:

$$\dot{m}_w = div(\vec{w}) \tag{2.58}$$

The constitutive equations (2.42) are used to solve the coupled dynamic problem, by eliminating the water mass content in first equation; we get the total stresses in function of pore-water pressure and the deformation as:

$$\delta\sigma = C_0 : \delta\varepsilon - \delta p_w I \tag{2.59}$$

Where C_0 is the drained elastic matrix.

Combination of equations (2.57), (2.58) and the second equation in (2.42) leads to the diffusion equation of the pore-water as:

$$div\left\{\frac{k}{\mu}\left[grad(p_w) + \rho_w \ddot{u}\right]\right\} + \frac{1}{M}\frac{\partial p_w}{\partial t} + \frac{\partial \varepsilon_v}{\partial t} = 0 \tag{2.60}$$

Using the finite element discretization, the displacement in an element can be expressed in a function of nodal displacements:

$$u = NU^e \tag{2.61}$$

N and U^e are the interpolation function for displacement and the elemental nodal displacement vector, respectively. Similarly, the pore-pressure in the element can be written as:

$$p = N'P^e \tag{2.62}$$

N' and P^e are the interpolation function for pore pressure and the elemental nodal pore-water pressure vector, respectively.

The strain in an element is expressed as:

$$\varepsilon = BU^e \tag{2.63}$$

B is the gradient of the interpolation function N.

The application of the finite element approach to Equation (2.60) and the combination of (2.59) and (2.55) lead to the following expressions:

$$\begin{aligned} M_{ss}\ddot{U} + RU + C_{up}P &= F_u \\ M_{pu}\ddot{U} + C_{pu}\dot{U} + C_{pp}\dot{P} + K_{pp}P &= F_p \end{aligned} \tag{2.64}$$

U and P denote the nodal displacement and the pore-water pressure vectors, respectively. The matrixes of finite element method in (2.64) are given by:

$$\begin{aligned} M_{ss} &= \int_\Omega N^t \rho N d\Omega & R &= \int_\Omega B^t C_0 B d\Omega & C_{up} &= -\int_\Omega B^t m b N' d\Omega \\ F_u &= \int_\Gamma N^t f_s d\Gamma & C_{pp} &= \int_\Omega N'^t \frac{1}{M} N' d\Omega & C_{pu} &= \int_\Omega N'^t m b B d\Omega \\ K_{pp} &= \int_\Omega B'^t \frac{k}{\mu} B' d\Omega & M_{pu} &= \int_\Omega B'^t \rho_w \frac{k}{\mu} m N d\Omega & F_p &= -\int_\Gamma N' f_{flux} d\Gamma \end{aligned} \tag{2.65}$$

It is of interest to indicate that the formulations above are used for poroelastic problems. However, for sandy soils the problems are generally elasto-plastic. The strain increment and the variation of the pore space are divided into two parts: the elastic part and the plastic part. As:

$$\begin{aligned} \delta\varepsilon &= \delta\varepsilon^e + \delta\varepsilon^p \\ \delta n &= \delta n^e + \delta n^p \end{aligned} \tag{2.66}$$

Equation (2.59) then is rewritten as:

$$\sigma = C_0 : (\delta\varepsilon - \delta\varepsilon^p) - \delta p_w I \tag{2.67}$$

And the plastic pore space variation is related to the plastic strain increment, as (Coussy, 2004):

$$\delta n^p = \beta \delta\varepsilon^p \tag{2.68}$$

β is the plastic parameter.

2.8. The Newmark method

The generalized Newmark method is used to integrate the equations in the time domain. The idea is that: the displacement and the velocity at time $t+\Delta t$ can be expressed in mathematic as:

$$\begin{aligned} U_{t+\Delta t} &= U_t + \Delta t \dot{U}_t + \frac{\Delta t^2}{2}\ddot{U}_t + \frac{\Delta t^3}{6}\dddot{U}_t + \ldots \\ \dot{U}_{t+\Delta t} &= \dot{U}_t + \Delta t \ddot{U}_t + \frac{\Delta t^2}{2}\dddot{U}_t + \ldots \end{aligned} \tag{2.69}$$

And the linear variation of the acceleration is approximate as:

$$\dddot{U} = \frac{\ddot{U}_{t+\Delta t} - \ddot{U}_t}{\Delta t} \tag{2.70}$$

We limit the expression of (2.69) as function of displacement, velocity and acceleration by introducing two parameters a and b, which are referred as the Newmark coefficients. The limited expression can be written as:

$$\begin{aligned} U_{t+\Delta t} &= U_t + \Delta t \dot{U}_t + \frac{\Delta t^2}{2}\ddot{U}_t + \frac{b}{2}\Delta t^3 \dddot{U} \\ \dot{U}_{t+\Delta t} &= \dot{U}_t + \Delta t \ddot{U}_t + a\Delta t^2 \dddot{U} \end{aligned} \tag{2.71}$$

While for the pore-pressure, the linear variation is assumed, and the formulation is written as:

$$\dot{P}_{t+\Delta t} = \frac{P_{t+\Delta t} - P_t}{\Delta t} = \frac{\Delta P}{\Delta t} \tag{2.72}$$

By introducing Equations (2.71) and (2.72) into Equation (2.64), we can get the two equations which represent the nodal pore-pressure and nodal displacement at time $t+\Delta t$. After arranging the two equations, the incremental nodal displacement and pore-water pressure can be expressed as:

$$\begin{bmatrix} \overline{R} & \overline{C}_{up} \\ \overline{M} & \overline{C}_{pp} \end{bmatrix} \begin{Bmatrix} \Delta U \\ \Delta P \end{Bmatrix} = \begin{Bmatrix} \overline{F}_u \\ \overline{F}_p \end{Bmatrix} \tag{2.73}$$

Where ΔU and ΔP are the incremental displacement and pore-pressure vectors at element nodes. The mathematical expressions of the matrix in Equation (2.73) are given by:

$$\begin{aligned} \overline{R} &= M_{ss}\frac{2}{\Delta t^2} + bR; & \overline{C}_{up} &= bC_{up} \\ \overline{M} &= M_{pu}\frac{2}{b\Delta t} + C_{pu}\frac{2a}{b}; & \overline{C}_{pp} &= C_{pp} + \Delta t K_{pp} \end{aligned} \tag{2.74}$$

$$\begin{aligned} \overline{F}_u &= bF^u_{t+\Delta t} - bC_{up}P_t + M_{ss}\left(\frac{2}{\Delta t}\dot{U}_t + (1-b)\ddot{U}_t\right) - bRU_t \\ \overline{F}_p &= \Delta t F^p_{t+\Delta t} - \Delta t K_{pp}P_t + \left[M_{pu}\frac{2}{b} + \Delta t C_{pu}(\frac{2a}{b}-1)\right]\dot{U}_t + \left\{\Delta t M_{pu}\frac{(1-b)}{b} + \Delta t^2 C_{pu}\frac{(a-b)}{b}\right\}\ddot{U}_t \end{aligned} \tag{2.75}$$

These formulations were introduced into the finite element program, PECPLAS.

2.9. Validation of the program

In this section, the finite element code will firstly be validated on the Terzaghis's 1-D consolidation problem. The constitutive equations of the proposed model will be verified. After that a numerical example will be used to illustrate the proposed model.

2.9.1. 1-D consolidation problem

Because the presented numerical model can deal with both saturated and unsaturated problems, the Terzaghis's 1-D consolidation problem is used to validate the program (Coussy, 1991, 2004; Wang, 2000). This problem has an analytical solution, as illustrated by Coussy and Wang. Figure 2.1 and Table 2.1 show the geometric and mechanical characteristics used in this example. The base and the lateral boundaries are assumed impervious, while free flow condition is assumed at the top of soil column. A constant pressure (P_s =100kPa) is applied at the top of the soil column. The water is assumed compressible ($K_w = 100MPa$) and the initial water saturation is unit.

Figure 2.2 presents the numerical and the analytical variation of the pore-water pressure at different depths for initial water saturation $S_w = 1.0$. The pore-pressure and the position (in Y direction) are normalized by the constant pressure P_s and the high of the soil column H, respectively. It can be observed that the numerical results agree well with the analytical results. The oscillation of numerical results at the beginning is due to the compressibility of the pore-water and the inertial effects. It is also of interest to indicate that although the problem is saturated, the water with a constant bulk modulus about 100MPa. That means the pore-water is not pure saturated water, but a water-air mixture.

Table 2.1: Material properties of the 1-D consolidation example

Young's Modulus	E	30MPa
Poisson Ratio	v	0.2
Mass density of solid	ρ_s	2000kg/m^3
Mass density of fluid	ρ_w	1000kg/m^3
Permeability	K	0.01m/s
Porosity	n	0.3
Newmark parameter	a	0.5
Newmark parameter	b	0.5

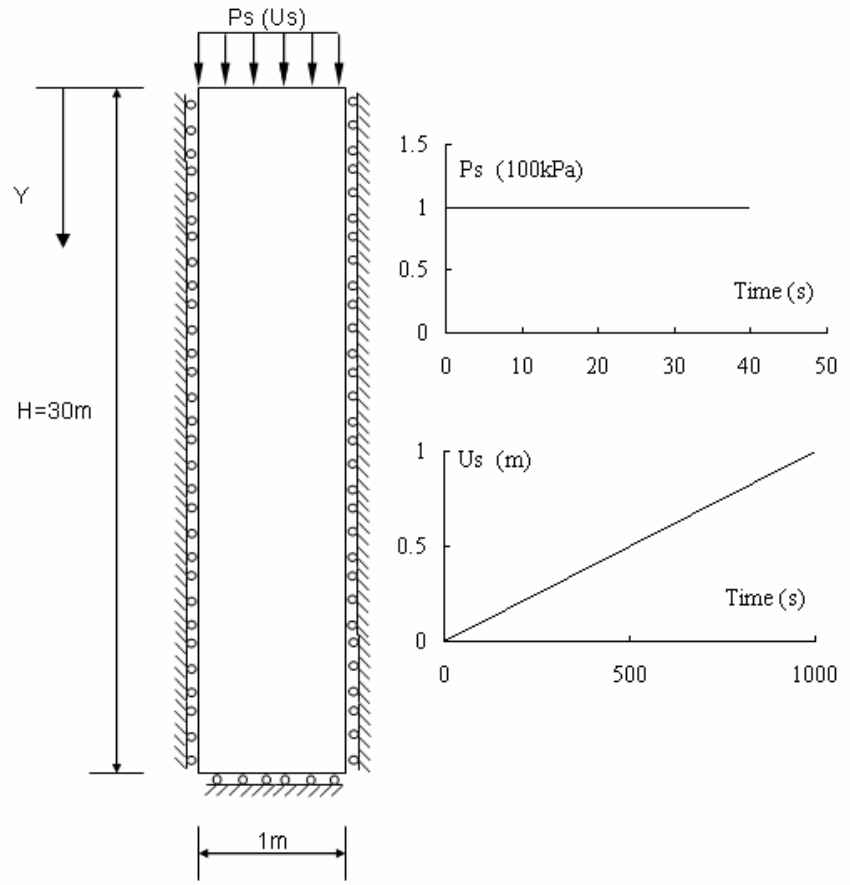

Figure 2.1: Geometric of 1-D validation test

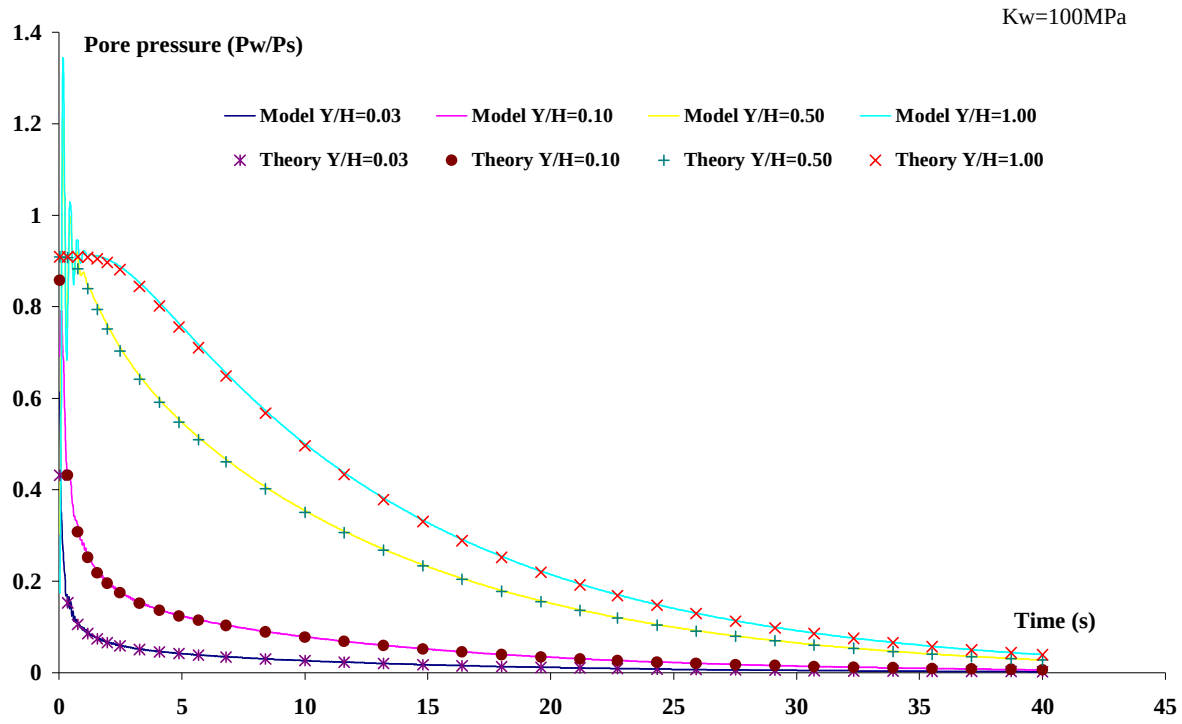

Figure 2.2: Pore-water pressure Vs time of saturated sandy soil

2.9.2. Constitutive equation

For verifying the constitutive equations, an unsaturated soil under undrained condition is considered. Under undrained condition, the water saturation and the pore-pressure depend on the volumetric deformation, which could be determined by mathematical analysis. Comparing the pore-pressure and the water compressibility, the deformation of pore-water can be neglected (the pore-pressure ranges from zero to 140kPa), so Equation (2.46) becomes:

$$\delta V = \delta V_a \tag{2.76}$$

According to Equation (2.48), (2.45) and (2.44), the pore-water pressure could be determined in function of the volumetric deformation:

$$p = (p_0 + p_{a0})\frac{n_0(1-S_w^0)}{n_0(1-S_w^0)+\varepsilon_v} - p_{a0} \tag{2.77}$$

We can also write the water saturation in function as the volumetric deformation as:

$$S_w = \frac{n_0 S_w^0}{n_0 + \varepsilon_v} \tag{2.78}$$

The analytical results are presented in Figures 2.3 and 2.4.

For the numerical analysis, the problem in Figure 2.1 is reconsidered. The soil is considered as unsaturated with the initial porosity $n=0.3$ and the initial water saturation $S_w=80\%$. The lateral displacements are blocked. Instead of the surface pressure, the vertical displacement at the top of soil column in function of time $U_s(t)$ is imposed as illustrated in Figure 2.1. The influence of initial stress is neglected, i.e. the gravity stress is not taken into consideration. The soil column is considered as homogenous.

Figure 2.3 and Figure 2.4 show the numerical and analytical results, the pore-pressure and the water saturation are given in terms of volumetric deformation. It shows that the unsaturated constitutive equations are exactly reproduced by the program. It can be observed that the mechanical behaviour of the pore-fluid is nonlinear.

If the dissolution of air into water is taken into consideration, in undrained condition, the variation of the water saturation could also have an analytical expression. Because of the high value of water bulk modulus and the undrained condition, the volume of pore-water is supposed constant. Using the same method, the pore-pressure is given by:

$$p_w=\left(p_{0w}+p_{a0}\right)\frac{(n_0(1-S_w^0)+hn_0S_w^0)}{(n_0(1-S_w^0)+\varepsilon_v+hn_0S_w^0)} \tag{2.79}$$

The variation of the water saturation has the same formulation as (2.78). The analytical and numerical results are given in Figure 2.5. Except for the solubility, the other configurations for the two cases are the same as the example above. It can be observed that at the high pore-pressure, the errors are significant. However, for liquefaction, the confining is generally less than 400kPa. So the consideration of the dissolution process is not important, even with enough time for the diffusion.

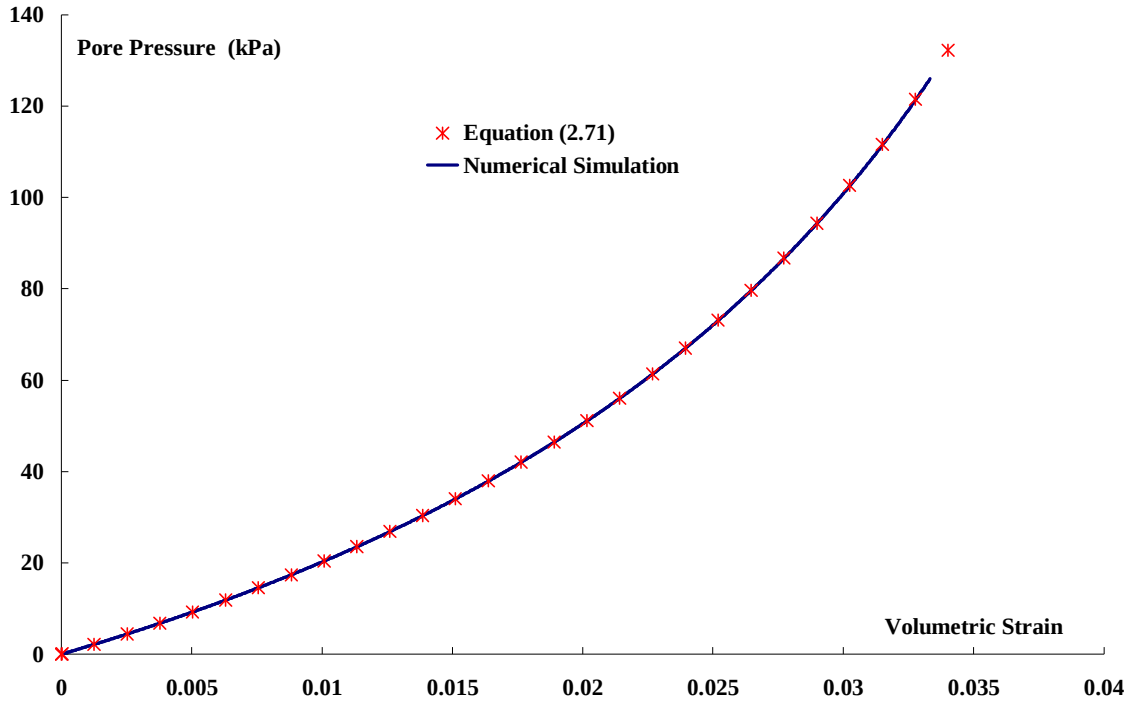

Figure 2.3: Pore-water pressure Vs. Volumetric strain of unsaturated sandy soil

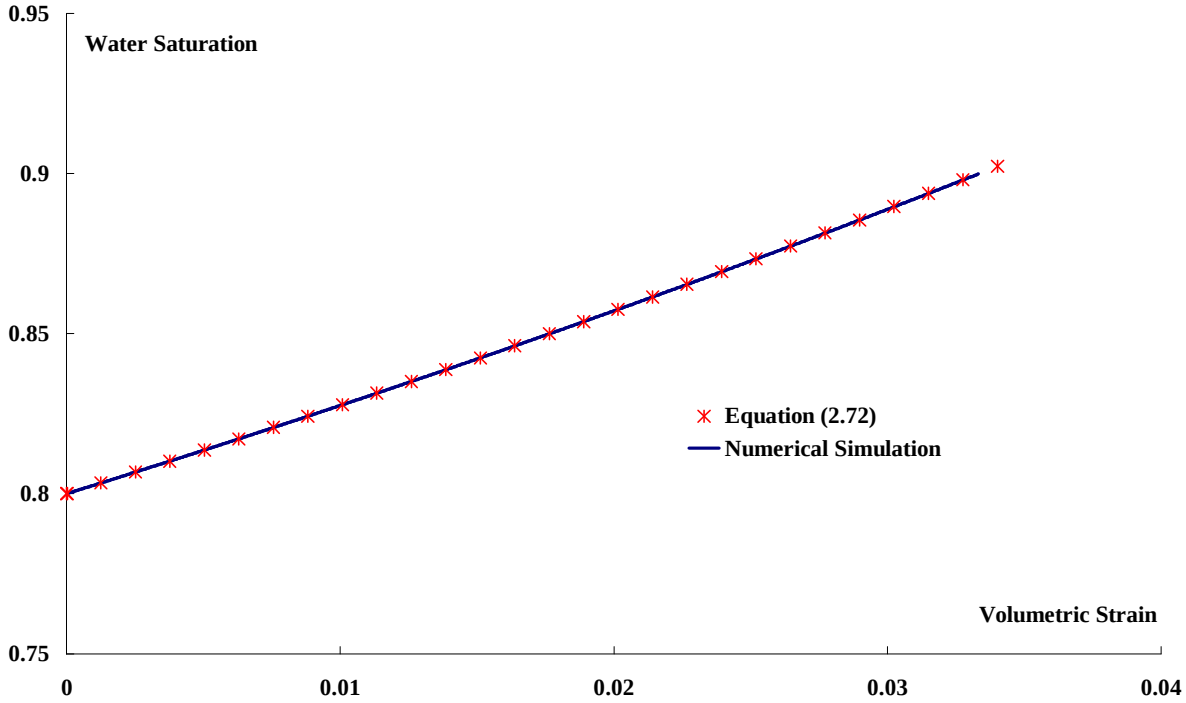

Figure 2.4: Water saturation Vs. Volumetric strain of unsaturated sandy soil

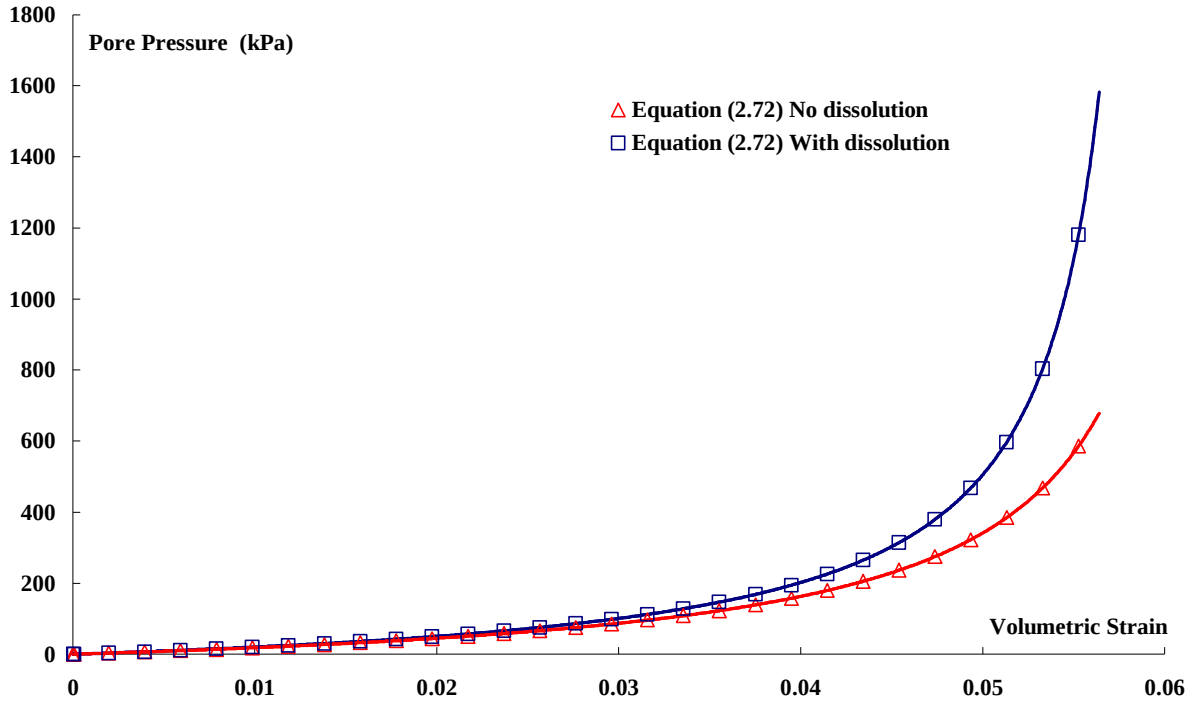

Figure 2.5: Pore-water pressure Vs. Volumetric strain of unsaturated sandy soil

2.9.3. Application

In the unsaturated case, it is difficult to drive analytical solution. Here we just present a numerical application of this model to a partially saturated soil in order to illustrate the performance of the proposed numerical model and the calculation code. The geometric and mechanical characteristics of the two precedent examples are used. The initial water saturation is changed from saturated to $S_w = 99\%$. And the water compressibility of the pure water is used ($K_w = 2GPa$). The other conditions are the same as that of 1-D consolidation example in Figure 2.1. Figure 2.6 presents the variation of the pore-water pressure at different depths vs. time for an initial water saturation $S_w = 99\%$. Comparison with Figure 2.2, it can be observed that the water saturation has an important influence on both the generation of pore-pressure and its dissipation. A decrease of 1% in the water saturation reduces the pore-pressure generation up to 50%. The oscillation of numerical results at the beginning is due to the compressibility of the pore-water and inertial effects. Because of the presence of air in the pores, the oscillation of unsaturated case is more pronounced than that of saturated soils. The dissipation of excess pore-pressure is slower than that of saturated case. Figure 2.7 illustrates the distribution of the water saturation at different instance during the dynamic consolidation. It can be seen that, at first, the water saturation is the highest at the base of the soil column, just like the distribution of excess the pore-water pressure; and then the water saturation approaches the initial water saturation. This is due to the assumption of no air fluxes.

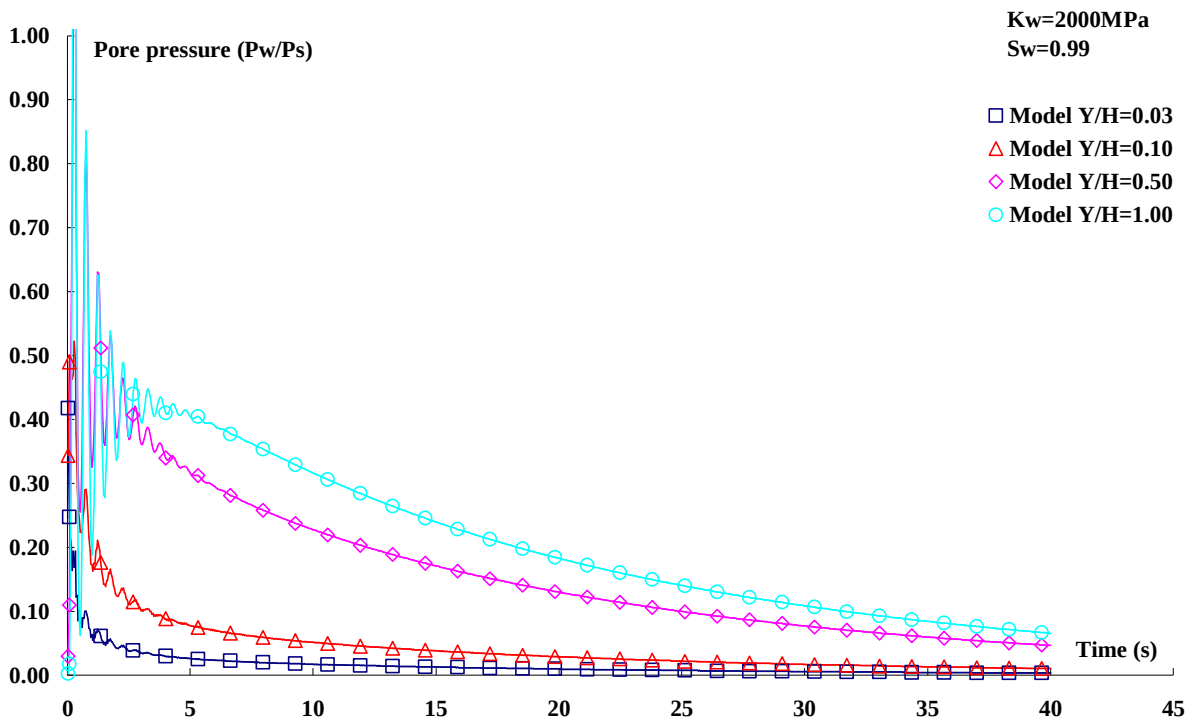

Figure 2.6: Pore-water pressure Vs time for unsaturated sandy soil
Example of application of the numerical model and calculation code

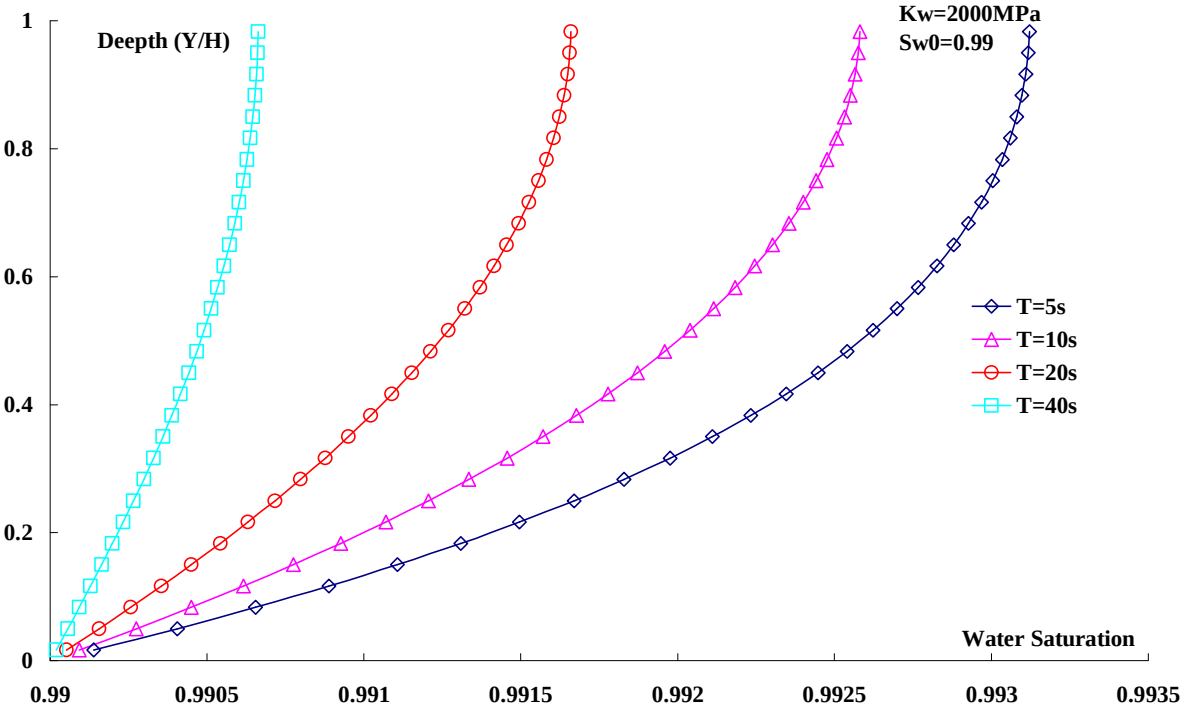

Figure 2.7: Distribution of water saturation at different times
Example of application of the numerical model and calculation code

However, by comparing the two numerical examples, the saturated consolidation and that of unsaturated, it can be seen that the water saturation has a great influence on the generation of the excess pore-pressure, even with a little perturbation in the water saturation (for example 1% variation). It is necessary to consider the unsaturated condition which exists in natural conditions.

2.10. The compressibility of the water-air mixture

One of the most important characteristic of the present model is the nonlinear compressibility of the water-air mixture. As indicated in 1-D consolidation example, the saturated numerical model has a constant bulk modulus for the mixture. However, researches indicate that the bulk modulus of the water-air mixture depends on the pore-pressure, water saturation and initial pore-pressure (Tsukamoto et al., 2002; Ishihara et al., 2004; Okamura et al., 2006). For example, Okamura (2006) showed that the degree of water saturation has a significant effect on the liquefaction resistance. He also found that the liquefaction resistance depends on the initial confining pressure and the initial pore-pressure: the higher the confining pressure and the lower the initial pore-pressure, the higher the liquefaction resistance of partially saturated sand. This conclusion suggests the use of varied water-air mixture compressibility.

If the water-air mixture is regarded as a single fluid, the saturated theory can be used. From the presented model, the bulk modulus of the mixture can be derived from Equations (2.38) and (2.42):

$$\frac{1}{K_{wa}} = \frac{S_w}{K_w} + \frac{1-S_w}{p_w + p_{a0}} \tag{2.80}$$

In conclusion, the water-air mixture bulk modulus K_{wa}, depends on the water saturation, pore-pressure and initial pore-pressure. Based on the theory of Koning, Martin et al. (1978) indicated that the water bulk modulus containing air bubbles can be expressed as a function of water saturation and absolute pore-pressure, which in turn is the same expression as (2.80). The ratio of water-air bulk modulus to pure water bulk modulus in function of water saturation and initial pore-water pressure is shown in the Figure 2.8. It can be observed that, the bulk modulus of the mixture increases with the water saturation. When the initial water saturation increases, the bulk modulus increases. This result agrees well with the experimental observations of Okamura et al. (2006).

As indicated in the validation examples (section 2.9.1), the soil is not really full-saturated. The word "saturated" could be regarded as that the water-air mixture saturated all the pores. With the value of mixture bulk modulus 100MPa and zero initial pore-pressure, the relative ratio of bulk modulus is about 0.045 at the initial state. It is noticed (Figure 2.8) that this assumption will eventually reduce some errors. Consequently, the varied water-air mixture bulk modulus should be used. Fortunately, this concept has been applied in the proposed model.

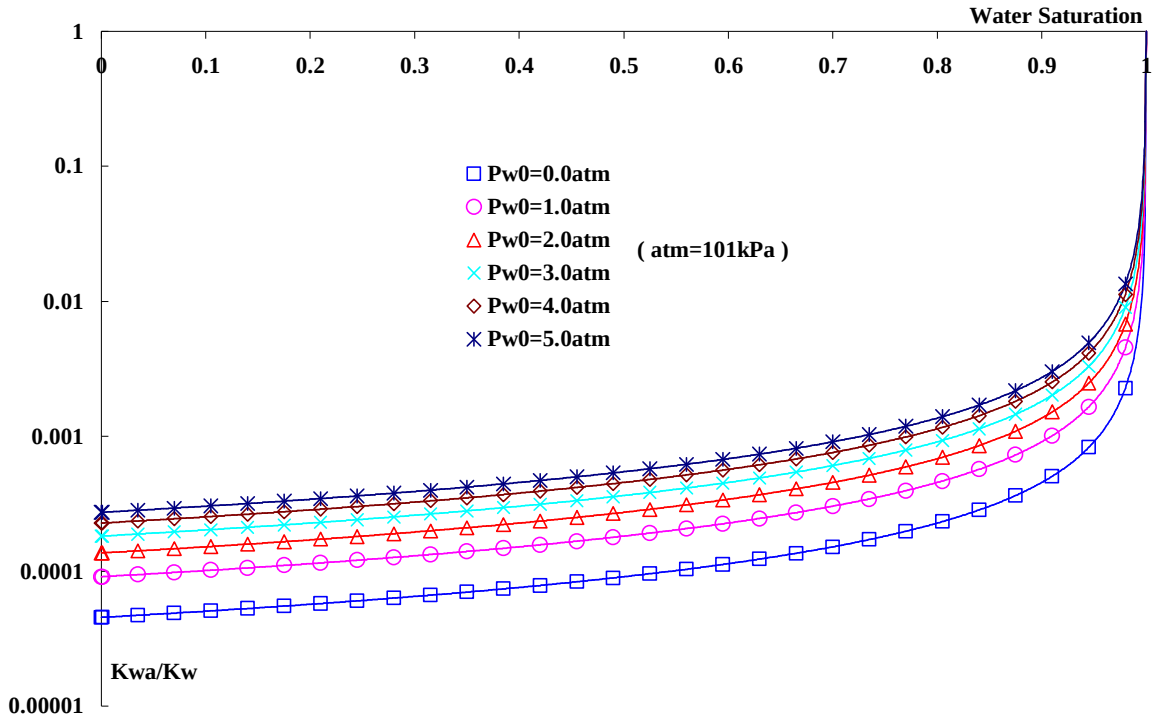

Figure 2.8: The bulk Modulus of Water-Air mixture in function of water saturation at different values of the initial pore-pressure

2.11. The Skempton coefficient

It is generally difficult to determine precisely the water saturation degree particularly when the soil is partially saturated near the state of full saturated. The Skempton coefficient B (or pore-pressure parameter, or B-value) is used as indicator of the water saturation (Martin et al., 1978; Yoshimi et al., 1989; Bouferra, 2000; Arab, 2007). It is defined as the ratio between the pore-pressure increment and the stress increment under undrained conditions. Martin indicated that the Skempton coefficient could be defined as:

$$B = \frac{1}{1 + n\dfrac{K_0}{K_{wa}}} \tag{2.81}$$

Where K_0 is the bulk modulus of the soil skeleton, or the drained bulk modulus of the soil. By introducing (2.80) into Equation (2.81), the Skempton coefficient for partially saturated soils could be expressed as follows:

$$B = \frac{1}{1 + nK_0\left[\frac{S_w}{K_w} + \frac{1 - S_w}{p_w}\right]} \tag{2.82}$$

This formulation is used by Yoshimi et al. (1989) on the bases of experiments on the Toyoura sands, as indicated in Figure 2.9. The circles in Figure 2.9 show the experimental relationship between the B-value measured before liquefaction test and the degree of saturation. The curve in Figure 2.9 shows the theoretical relationship proposed by Lade and Hernandez, that is the same of (2.82), in which the membrane penetration effects and the compliance of the pore-pressure measuring system are ignored.

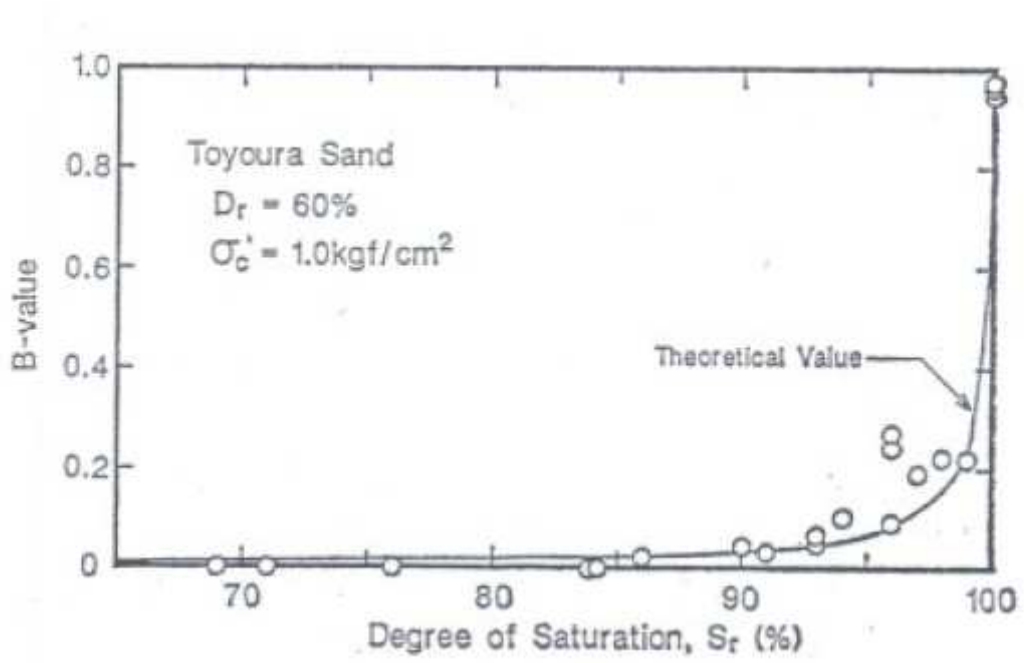

Figure 2.9: The B value vs. water saturation (Yoshimi et al., 1989)

Yoshimi et al. (1989) also gave the value of each parameter in the formulation: n is the porosity (0.48), K_0 bulk modulus of soil skeleton (6.7×10^4kPa), K_w bulk modulus of water (2.23×10^6kPa), and absolute pressure in pore fluid (343kPa for saturated specimens and 98kPa for partially saturated specimens). These values were used for obtaining the theoretical curve. The elastic shear modulus of the specimens measured before liquefaction test was 7.65×10^4kPa .

Once again, we translate the partially saturated soil as saturated problem, by regarding the water-air mixture as a compressible single fluid. Thus, by using the results of saturated theory, the Skempton parameter is expressed as (Coussy, 1991):

$$B = \frac{\left(\frac{1}{K_0} - \frac{1}{K_s}\right)}{\left(\frac{1}{K_0} - \frac{1}{K_s}\right) + n\left(\frac{1}{K_w} - \frac{1}{K_s}\right)} \tag{2.83}$$

However, here the bulk modulus of the pore-water should be replaced by bulk modulus of water-air mixture as:

$$B = \frac{\left(\frac{1}{K_0} - \frac{1}{K_s}\right)}{\left(\frac{1}{K_0} - \frac{1}{K_s}\right) + n\left(\frac{1}{K_{wa}} - \frac{1}{K_s}\right)} \tag{2.84}$$

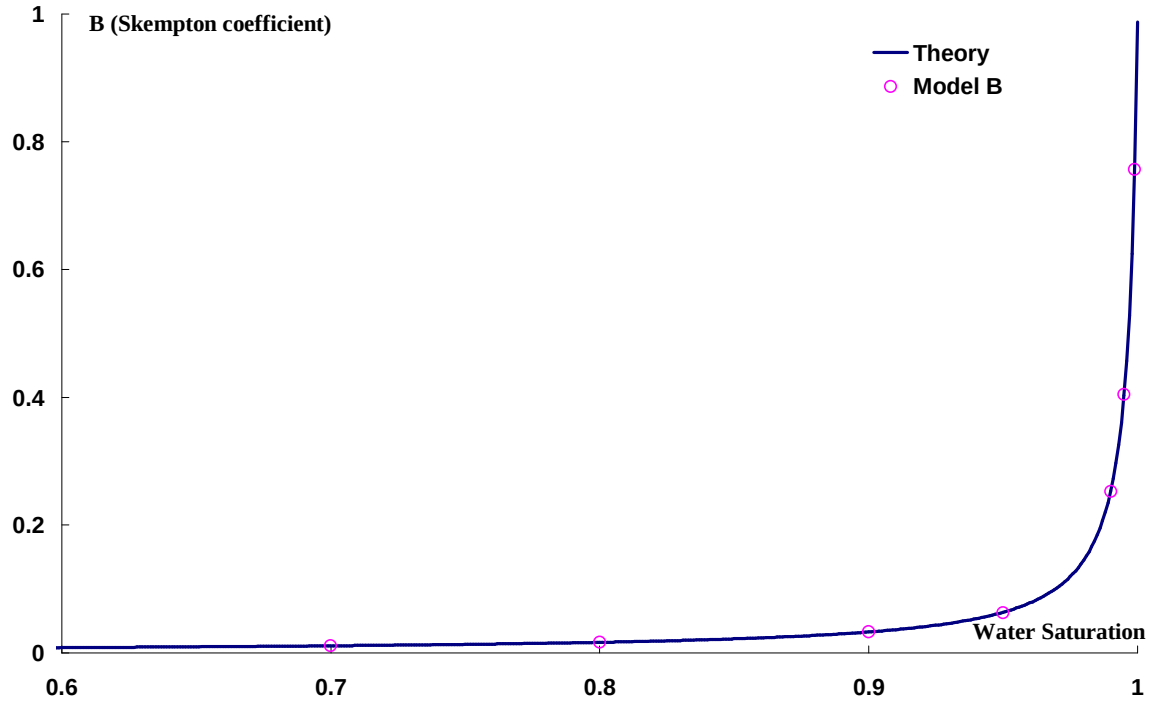

Figure 2.10: The Skempton coefficient vs. water saturation (Model and Theory)

K_s is the bulk modulus of the soil grains. Compared to that of water, the soil grain is assumed incompressible. So Equation (2.84) reduces to:

$$B = \frac{1}{1 + K_0 n \frac{1}{K_{wa}}} \tag{2.85}$$

By using Equation (2.80), Equation (2.82) can be reproduced.

From the measured parameters of Yoshimi, the Young's modulus and the Poisson ratio can be determined as: E=1.662×10^{8}Pa, v=0.086 . These values will then be used for the calculation of the theoretical analysis and numerical simulation. A one-element model is used to simulate the undrained problem, and then the Skempton parameters are calculated for different water saturation when the absolute pore-pressures arrive at 98kPa. The calculated B-values are presented in Figure 2.10 in circles. It can be observed that, the numerical simulation agrees well with the theoretical results. This result constitutes a good example of validation of the program.

However, a crucial disadvantage of using either the Skempton coefficient or the saturation degree is that it is practically impossible to monitor these quantities in soil deposits in the field. Tsukamoto et al. (2002) and Yang (2002) suggested the use of the propagation velocity of shear wave and longitudinal wave as an indicator of the degree of saturation. Tsukamoto et al. (2002) indicate that the velocity of P-wave tends to increase from about 500m/s to about 1800m/s when the B-value increase form near zero to 0.95 corresponding respectively to the water saturation about 90% and 100%.

2.12. Conclusion

This chapter presented the formulation and validation of a numerical model for unsaturated sandy soils. The model is based upon the following assumptions: the equality of the pore-air pressure and the pore-water pressure; no dissolution of pore-air into pore-water; null air flux , etc..

The numerical model was implemented in a finite element program which can deal with coupled problems under seismic loadings. The model was validated on some examples. The first example concerned the 1-D consolidation problem. The second example concerned the constitutive equations. The two validation examples showed that the program correctly reproduced the analytical results. The application example illustrated the good implementation of the model in the code.

Analysis of the bulk modulus of the water-air mixture and the Skempton coefficient showed the importance of the variation of the compressibility of the pore fluids under partially saturated conditions. They also serve as the validation examples of the model.

In all examples, elastic model is used for soils. In the next chapter, elasto-plastic constitutive model will be presented. The numerical model will be used to study the influence of water saturation on the dynamic response of sandy soils, particular to the liquefaction potential.

Chapter 3: Influence of water saturation on liquefaction

3.1. Introduction

This chapter includes an application of the proposed model on the analysis of the influence of water saturation on the soil liquefaction. Firstly, an elasto-plastic constitutive model for the sandy soils under both monotonic and cyclic loadings will be presented and then implanted in the numerical model proposed in Chapter 2. Then, some numerical simulations of triaxial tests with different water contents will be simulated in order to illustrate the influence of water saturation on the mechanical behaviour of partially saturated loose sand. Moreover, the influence of water saturation on the free filed response is also investigated using the proposed model. In addition, some key factors on the layer liquefaction will be analysed, namely: the water saturation, the permeability and the relative density. Finally, the experiments conducted by Yegian (2007) will be discussed.

3.2. Constitutive equation for Sandy soils

MODSOL is a constitutive equation which captures the main features of sandy soils under both monotonic and cyclic loadings. It is developed in LML (Laboratory of Mechanics of Lille). At the beginning, Chehade and Shahrour, based on observation of experimental results and plasticity framework, proposed a simple constitutive equation for sandy soils under monotonic loading (Chehade, 1991; Shahrour and Chehade, 1992). This constitutive equation was extended to cyclic loading conditions by Khoshravan (1995), and introduced into the finite element calculation code PECPLAS. This model was calibrated using the experiments realized in centrifuge within the projects VELCAS (Verification of liquefaction analysis by centrifuge studies). Later this model was used by Ousta and Shahrour (1998, 2001) to study the mechanical behaviour of micro-piles under seismic loading; and by Khoshnoudian (1999) to study the behaviour of tunnels under seismic loading. The application showed that, this model is capable in capturing well the behaviour of granular soils. This model is based on the concept of effective stresses, so it could be easily integrated into the numerical model presented in Chapter 2.

3.2.1. Elastic part

The elastic part of the model is nonlinear. The shear modulus and the bulk modulus are function of stresses, as follows:

$$K = K_0 (\frac{p}{p_a})^N A(p,q); \quad G = G_0 (\frac{p}{p_a})^N \tag{3.1}$$

Where p_a is the reference pressure. N is the parameter which controls the variation of the bulk and shear moduli. While p and q are the mean stress and the deviatoric stress respectively. K_0 and G_0 are the bulk and shear moduli at the reference pressure p_a . They can be derived from the drained Young's modulus and drained Poisson ratio as:

$$K_0 = \frac{E_0}{3(1-2v_0)}; \qquad G_0 = \frac{E_0}{2(1+v_0)} \tag{3.2}$$

The function $A(p,q)$ is defined as:

$$A(p,q) = \left[1 - \frac{1}{9}.(\frac{1-v_0}{1-2v_0}).N.(\frac{q}{p})^N\right]^{-1} \tag{3.3}$$

If the function $A(p,q)$ is unit, constant Poisson ratio will be assumed. In the calculation code, the drained Young's modulus and drained Poisson ratio are used. They are derived from the bulk and shear moduli as:

$$E_0 = \frac{9K_0G_0}{3K_0+G_0}; \quad v_0 = \frac{3K_0-2G_0}{6K_0+2G_0} \tag{3.4}$$

3.2.2. The Monotonic part

The constitutive model includes two loading surfaces as illustrated in Figure 3.1 and Figure 3.2. The first one is called the limit surface (represents the monotonic loading surface); while the second is the cyclic loading surface (describes the cyclic behaviour). The monotonic loading surface is defined by:

$$f_m = q - M_f\, pR_m \tag{3.5}$$

The hardening function R_m expressed as:

$$R_m = \frac{\varepsilon_d^p}{b+\varepsilon_d^p} \tag{3.6}$$

In which b is a constitutive parameter. ε_d^p is the plastic deviatoric deformation. M_f takes into consideration the second principal stress, as proposed by Zienkiewicz and Pande (1977):

$$M_f = \frac{6\sin\varphi}{3-\sin\varphi\sin 3\theta} \tag{3.7}$$

φ is the internal friction angle. θ is the Lode's angle:

$$\theta = \frac{1}{3}\arcsin\left(-\frac{3\sqrt{3}J_3}{2(J_2)^{1.5}}\right) \tag{3.8}$$

J_2 and J_3 are the second and third invariants of the deviator stresses tensor, respectively. The monotonic loading surface described by Equation (3.5) is an open cone in stress space. This does not exactly represent the laboratory observations; however, our interests focus on the shear deformation caused by the seismic or cyclic loadings.

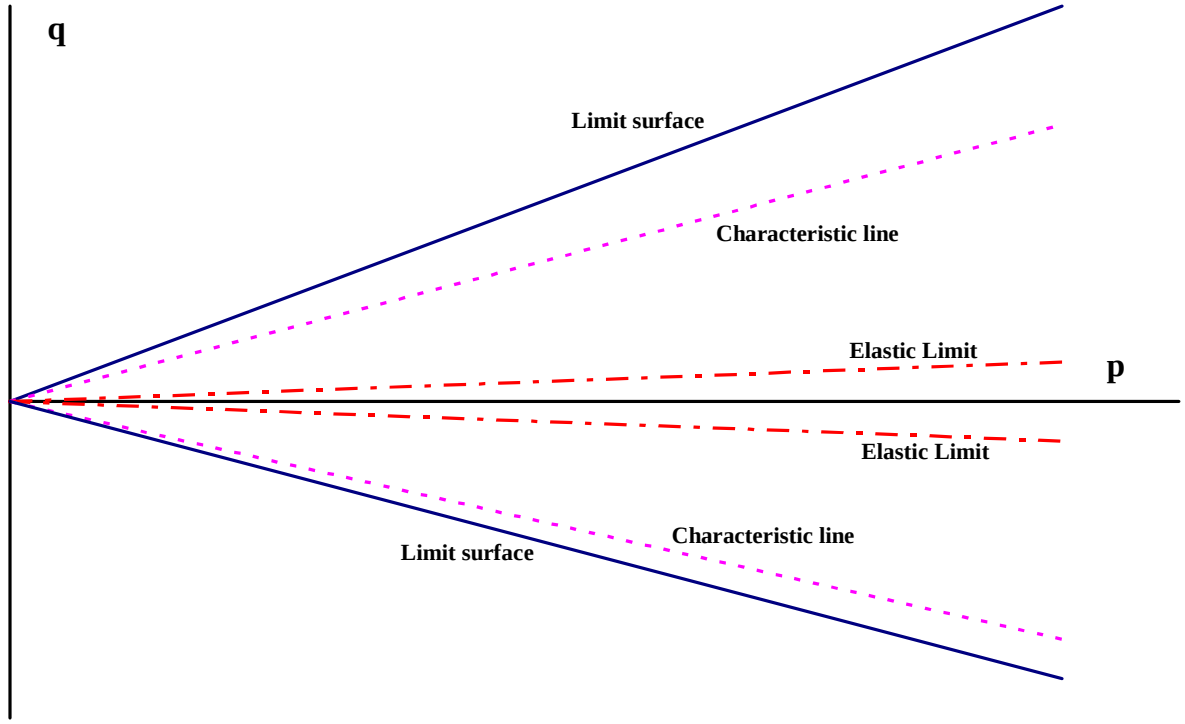

Figure 3.1: The limit surface, characteristic line and elastic domain of proposed model

The non-associate plastic flow is used; the plastic potential is given directly as:

$$\begin{cases} \dfrac{\partial g_m}{\partial p} = \dfrac{\exp(-\alpha_0 \varepsilon_d^p)}{M_c p}\left(M_c - \dfrac{q}{p}\right) \\ \dfrac{\partial g_m}{\partial q} = \dfrac{1}{M_c p} \end{cases} \tag{3.9}$$

α_0 is the model parameter, which controls the rate of dilatation. It is worth to indicate that when α_0 equal to zero, the plastic potential of Cam-Clay is reproduced. The use of parameter α_0, is to eliminate the volumetric deformation when the critical state is arrived. Another variable M_c is expressed similar to that of M_f in Equation (3.7), as:

$$M_c = \frac{6\sin\varphi_{cv}}{3 - \sin\varphi_{cv}\sin 3\theta} \tag{3.10}$$

φ_{cv} is the characteristic angle, which is related to the "characteristic state line" or the "line of phase transformation", which corresponds to the transition between the contracting and dilating phases.

3.2.3. The Cyclic part

A first step towards modelling cyclic behaviour of sands is to understand what happens during unloading and reloading. Concerning the former, the response is characterized elastic in most classical plasticity models. The cyclic loading surface is applied to simulate the unloading and reloading behaviour until the monotonic loading surface is reactive.

The cyclic loading surface is a cone in the stress space, as illustrated in Figure 3.2 and Figure 3.3. Its axis, which has been defined by the normalized tensor α_{ij}, turns with the process of loading. In the same time, its radius could change. The cyclic loading surface is defined by the following function:

$$f_c = q^l - p^l R_c \tag{3.11}$$

With:

$$q^l = \sqrt{s_{ij}^l s_{ij}^l} \qquad s_{ij}^l = \sigma_{ij} - p^l \alpha_{ij}$$

$$p^l = \alpha_{ij}\sigma_{ij} \qquad R_c = \frac{\varepsilon_{dc}^p}{b + \varepsilon_{dc}^p}$$

R_c is used to describe the isotropic hardening of the cyclic loading surface, which defining the radius of the cyclic loading surface, and ε_{dc}^p is the plastic deviatoric deformation associated with the cyclic loading, which should be initialized at each inversion of loading direction. s_{ij}^l is the equivalent deviator stresses tensor. p^l and q^l are the equivalent mean stress and deviator stress, respectively, similar to p, q in the limit surface.

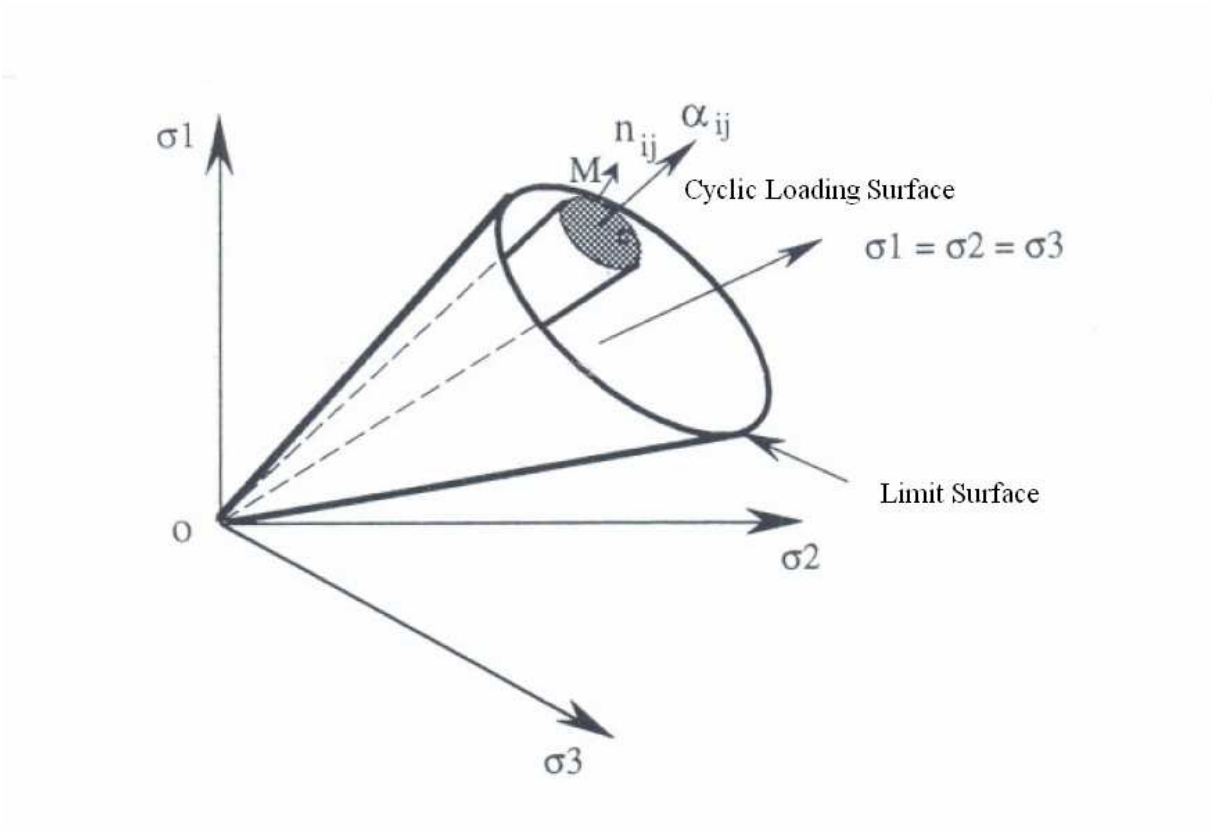

Figure 3.2: Limit surface and Cyclic loading surface

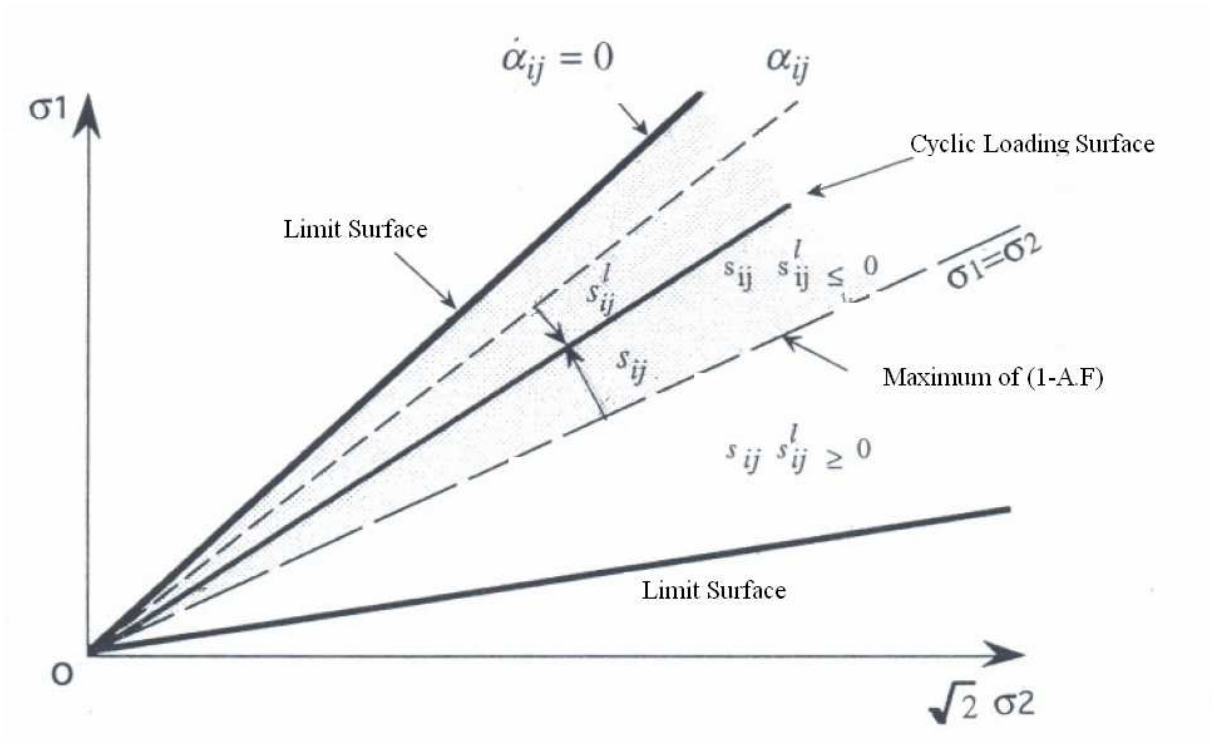

Figure 3.3: Evolution of the cyclic loading surface

The unit tensor α_{ij} represents the axis of the cyclic loading surface as illustrated in Figure 3.2 and Figure 3.3. Its evolution is defined as:

$$\begin{aligned} \delta\alpha_{ij} &= \delta\lambda H_{ij} \\ H_{ij} &= c_c(1-AF)R_c s_{ij}^l \end{aligned} \tag{3.12}$$

Where $\delta\lambda$ is the plastic multiplier. The model parameter c_c controls the kinetic of the cyclic loading surface axis. The two variables A and F are calculated as:

$$\begin{aligned} &A=1 \quad \text{if} \quad s_{ij}s_{ij}^l \geq 0 \\ &A=-1 \quad \text{if} \quad s_{ij}s_{ij}^l < 0 \\ &F=\frac{q}{M_f\, pR_m} \qquad (F \leq 1) \end{aligned} \tag{3.13}$$

The evolution of the cyclic loading surface is illustrated in Figure 3.3.

A non associated plastic potential is used for the cyclic surface. The plastic potential is given as follows:

$$\begin{aligned} &\text{if} \quad \frac{\partial g_m}{\partial \sigma_{ij}} d\sigma_{ij} \geq 0 \qquad \frac{\partial g_c}{\partial \sigma_{ij}} = \frac{B\exp(-\alpha_0 \varepsilon_d^p)}{3M_c p}(M_c - \frac{q}{p})\delta_{ij} + \frac{3}{2M_c p}\frac{s_{ij}}{q} \\ &\text{if} \quad \frac{\partial g_m}{\partial \sigma_{ij}} d\sigma_{ij} < 0 \qquad \frac{\partial g_c}{\partial \sigma_{ij}} = \frac{B\exp(-\alpha_0 \varepsilon_d^p)}{3M_c p^l}(M_c - \frac{3\sqrt{j_2^l}}{p^l})\alpha_{ij} + \frac{3}{2M_c p^l}\frac{1}{\sqrt{j_2^l}} s_{ij}^l \end{aligned} \tag{3.14}$$

With $B=\exp(-b_c\left|\varepsilon_v^p\right|)$, ε_v^p is the plastic volumetric deformation, b_c is used to control the plastic deformation due to cyclic loading.

One of the key points in this model is to determine which loading surface should be used during the loading process. The criterion is defined as follows: firstly, the loading process is checked with the monotonic loading surface, in the event of unloading, the current active loading surface (monotonic loading surface) is memorized and a new loading surface (cyclic loading surface) is initialized and activated. During the loading process, at each loading increment, we check the monotonic loading surface. If this surface is checked as active, the cyclic loading surface is deactivated; the behaviour is controlled by the monotonic loading surface.

At each inverse in loading direction, the cyclic loading surface should be initialized. In the stress space, the point O is considered as a reference point (origin). At the moment of discharge, the stress is at point M located at the monotonic loading surface; the stress tensor then can be represented by the vector $\overrightarrow{OM}$. It is supposed that, each cyclic loading surface with the same

initial radius R_{co}. So the vector, which represents the axis of the new cyclic loading surface, can be represented by:

$$\overrightarrow{OC} = \overrightarrow{OM} - n_{ij} R_{co} \tag{3.15}$$

Where n_{ij} is the unit normal tensor of the monotonic loading surface at the point of unloading; it can be calculated as:

$$n_{ij} = \frac{\partial f_m}{\partial \sigma_{ij}} / \left(\frac{\partial f_m}{\partial \sigma_{kl}} \frac{\partial f_m}{\partial \sigma_{kl}}\right)^{0.5} \tag{3.16}$$

After normalization of the axis tensor, the unit tensor α_{ij} is given:

$$\alpha_{ij} = \frac{\overrightarrow{OC}}{\left|\overrightarrow{OC}\right|} \tag{3.17}$$

There are nine parameters for the constitutive equations: the drained Young's modulus E_0, the drained Poisson ratio v_0, the nonlinear elastic parameter N, the internal friction angle φ, the characteristic angle φ_{cv}, the hardening parameter b, the model parameter α_0, and two cyclic parameters c_c, b_c. The first seven parameters are used to describe the monotonic behaviour, they can be determined from standard triaxial tests; while the two latter should be determined from the cyclic triaxial tests. The method and procedure for determining the model parameters can be founded in the dissertations of Chehade (1991) and Khoshravan (1995). The model was implemented in the proposed numerical model for partially saturated sandy soils.

3.3. Influence of water saturation on monotonic behaviour

We consider a loose sand specimen, with different values of initial water saturation ($S_w = 100\%$, 99%, 95% and 90%). The monotonic loading is controlled by the axial deformation. The amplitude of the deformation is controlled as +10%. The initial pore pressure is supposed as zero (measured pressure). The confining pressure is 80kPa. The tests are conducted under undrained conditions.

It should be mentioned here, for the fully saturated case, the formulation of the proposed model reduces to that of Zienkiwicz; the bulk modulus of water is 100MPa, while for partially saturated cases, the proposed model is used, and the bulk modulus for water is 2.23GPa, which means the use of pure saturated water.

The nine model parameters of MODSOL are listed in Table 3.1, which are adopted from Ousta (1998) for loose sand.

Table 3.1: Model parameters for sandy soils (Ousta, 1998)

1	2	3	4	5	6	7	8	9
E_0	v_0	N	ϕ	φ_{cv}	b	α_0	c_c	b_c
100kPa			°	°			1/100kPa	°
200	0.3	0.5	33	30	0.001	12	0.005	500

The numerical simulations are presented in Figure 3.4. It can be seen that, the initial water saturation has a significant influence on the response of sandy soils. For the fully saturated case, the deviator stress has a plate, that corresponding to the transition from contraction to dilation phase. With the decrease in initial water saturation, this plate firstly reduces and then disappears. This corresponds to the effective stresses path in Figure 3.4 (b). All these changes are due to the generation of the pore pressure as illustrated in Figure 3.4 (c). Because the specimens have different initial water saturations, the fluid mixture has different compressibilities. Under the same excitation the rate of the pore-water pressure generation is different. With more air (lower water saturation), the fluid has greater compressibility, and consequently lower rate of excess pore pressure generation.

For saturated case under undrained conditions, the volumetric strain is assumed as zero. This, however, is not exact. The excess pore-water pressure is generated from the contraction of the pore space. As the bulk modulus of the pore-water is relatively high, so the volumetric deformation is relatively small; sometimes, it is so small that it is difficult to measure. However, for partially saturated cases, the bulk modulus of the water-air mixture is relatively small comparing with that of saturated case. As a consequence, greater deformation is needed for the excess pore pressure generation. The volumetric deformation vs. the axial deformation for different water saturation under undrained condition is presented in Figure 3.4(d). Comparing Figure 3.4(d) and Figure 3.4(c), it can be observed that the trends are different. For example: the smaller the volumetric deformation, the greater the excess pore pressure, this is the case of fully saturated.

It also can be observed that the contraction-dilation behaviour of the sand is not changed. All the specimens, either fully saturated or partially saturated, exhibit a contracting-dilating behaviour. However, for partially saturated case, it needs more excitation to reach the phase transition. It can be seen from Figure 3.4(d) that the axial strain at peak value of the volumetric strain increases with the decrease in water saturation.

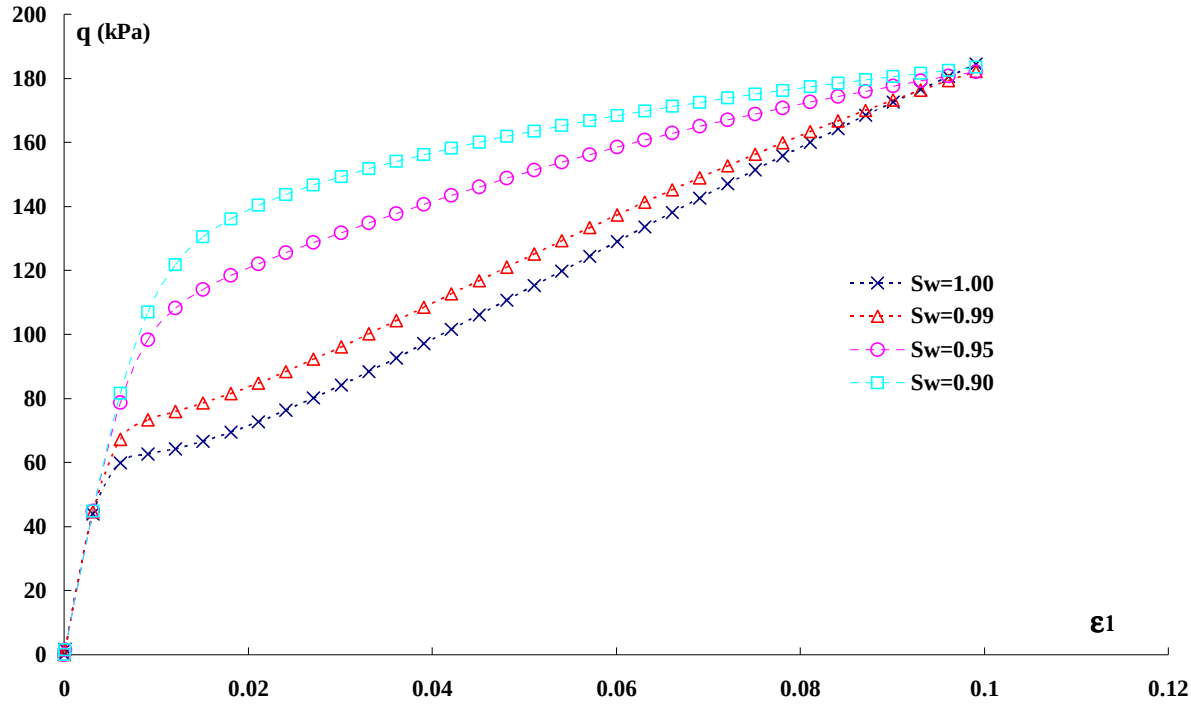

Figure 3.4 (a): Influence of initial water saturation on the undrained response of loose sand In the ($\varepsilon_1 - q$) plane

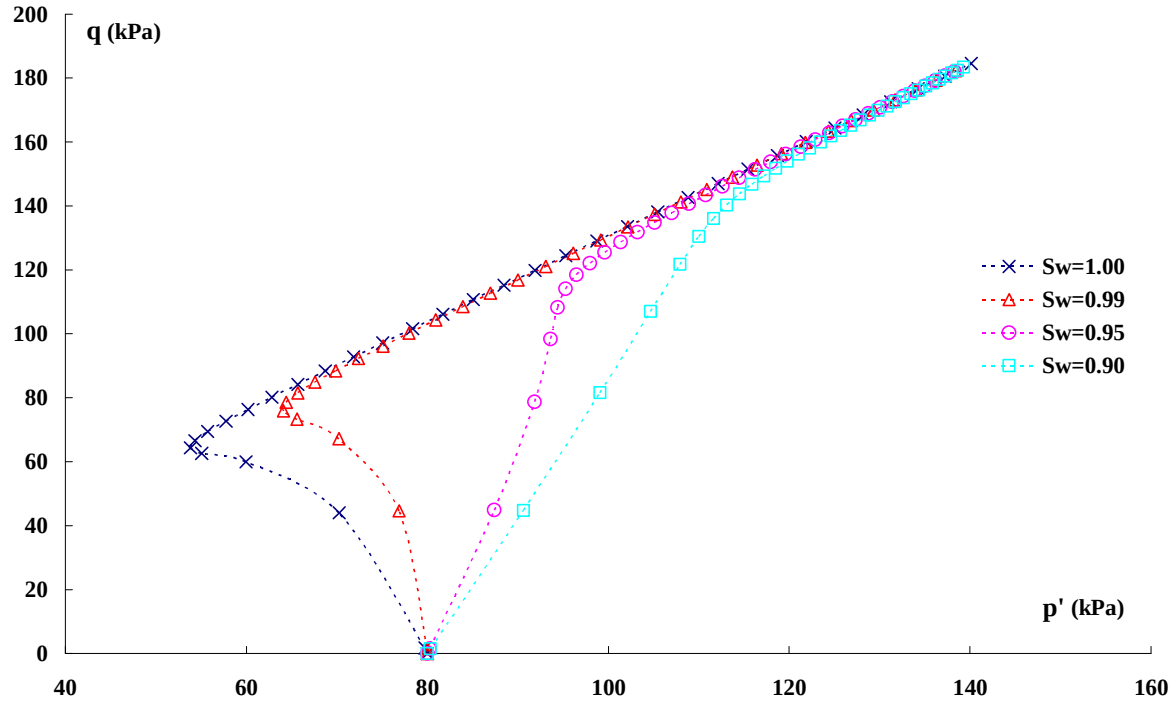

Figure 3.4 (b): Influence of initial water saturation on the undrained response of loose sand In the ($p' - q$) plane

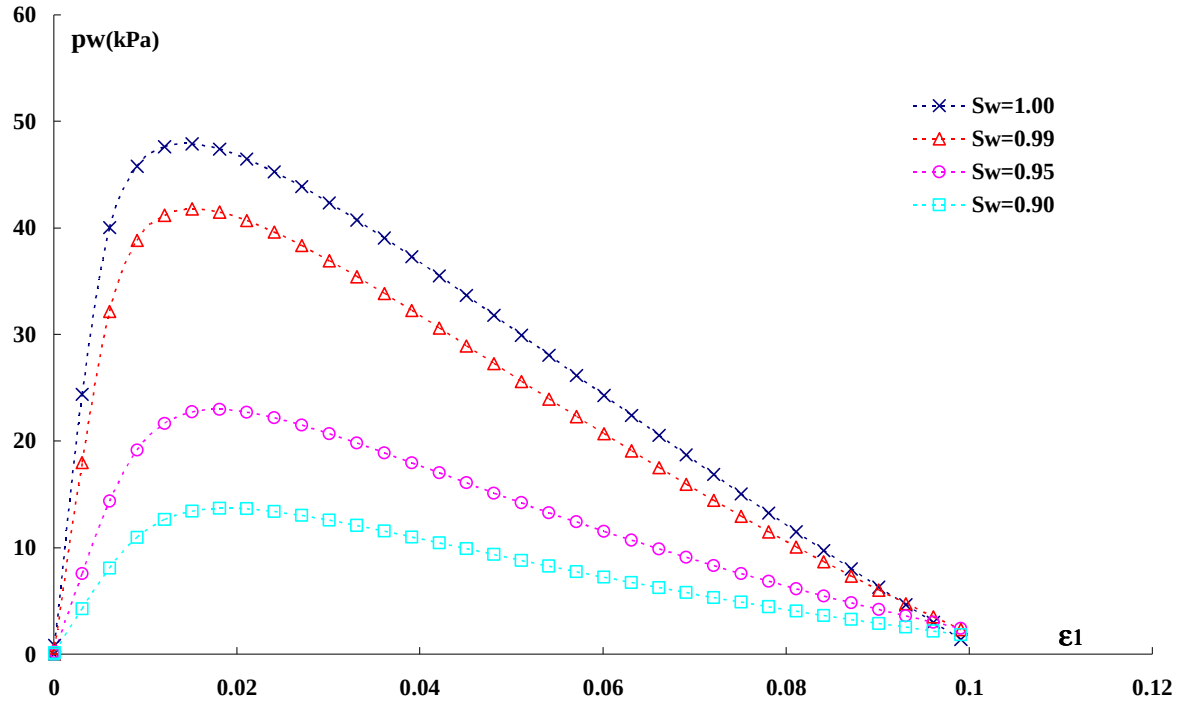

Figure 3.4 (c): Influence of initial water saturation on the undrained response of loose sand In the ($\varepsilon_1 - p_w$) plane

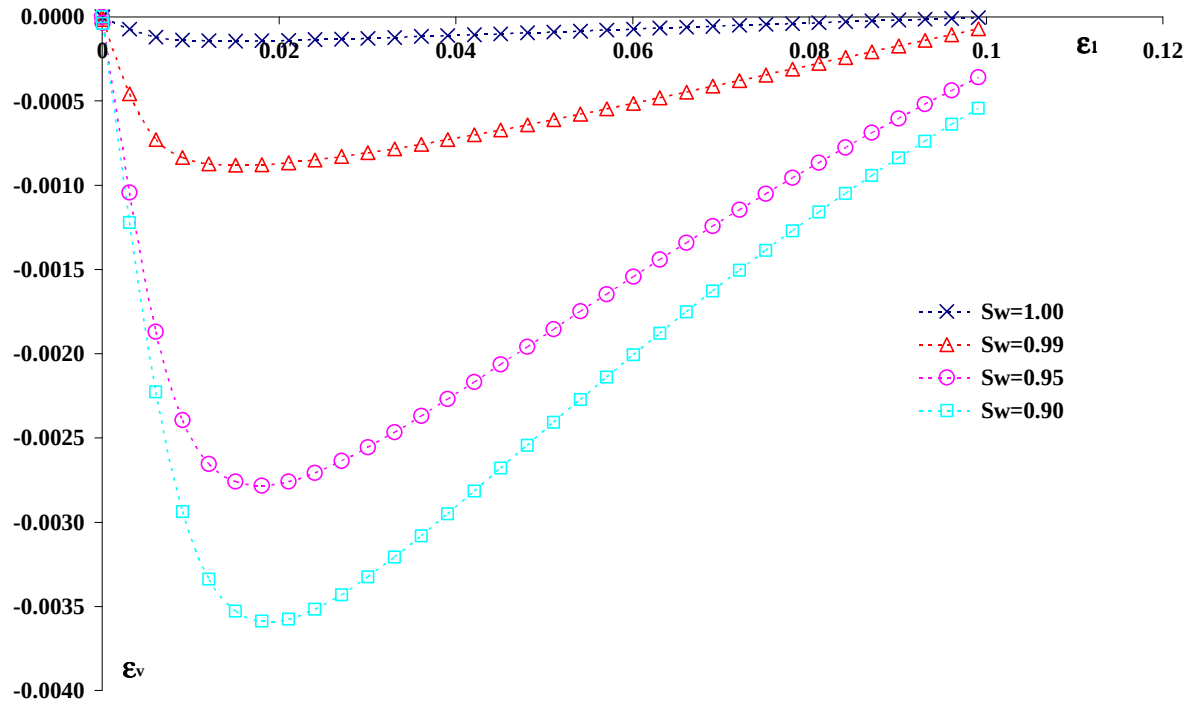

Figure 3.4 (d): Influence of initial water saturation on the undrained response of loose sand In the ($\varepsilon_1 - \varepsilon_V$) plane

3.4. Influence of water saturation on cyclic behaviour

The undrained cyclic triaxial tests have been simulated using the parameters of Table 3.1 under the following conditions: confining pressure 80kPa, initial pore pressure $p_{w0} = 0$. The Loading is controlled by the axial deformation, the amplitude of the deformation varies between -1% and +1%. Simulations are carried out for 4 different initial water saturations ($S_w = 100\%$, 99%, 95% and 90%).

Figure 3.5 presents the deviator stress vs. the axial deformation, for the different water saturations. It shows that the decrease in initial water saturation, leads to an increase in the liquefaction resistance. For fully saturated specimen, the initial liquefaction occurs after 3 cycles, while for Sw=99%, the liquefaction occurs after 4 cycles. And for the sandy soils with low water saturations $S_w = 95\%$ and $S_w = 90\%$, the liquefaction occurs after 7 and 12 cycles, respectively.

Figure 3.6 presents the evolution of the pore-water pressure vs. the axial deformation for different initial water saturations. It can be observed that the decrease in the initial water saturation leads to a decrease in excess pore-pressure generation rate. For example, after one cycle, the increments in pore pressure are 70kPa, 65kPa, 38kPa and 21kPa for $S_w = 100\%$, 99%, 95% and 90%, respectively.

These examples show that the initial water saturation has a significant influence on the soil liquefaction: the increase in water content will accelerate the liquefaction processes. This result agrees well with the laboratory observations (Bouferra, 2000; Arab, 2007). So the response of partially saturated sandy soils is well predicated by the proposed model.

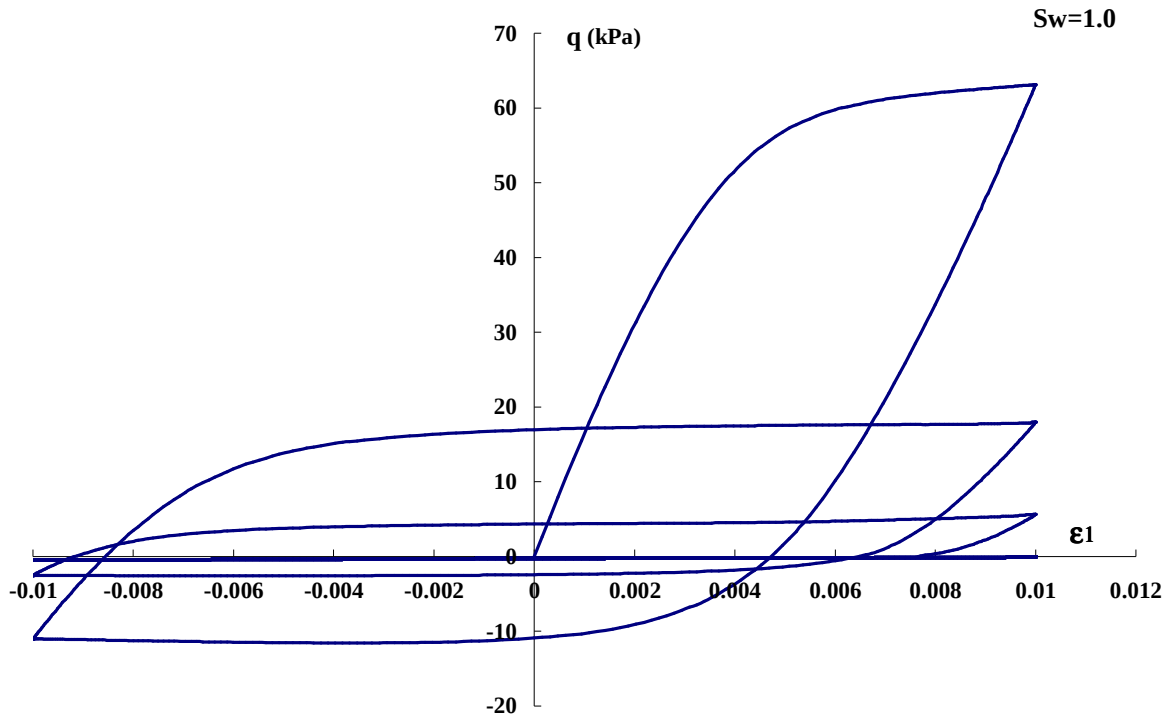

Figure 3.5 (a): Influence of initial water saturation on the cyclic response of undrained loose sand in ($\varepsilon_1 - q$) plan (Sw=100%)

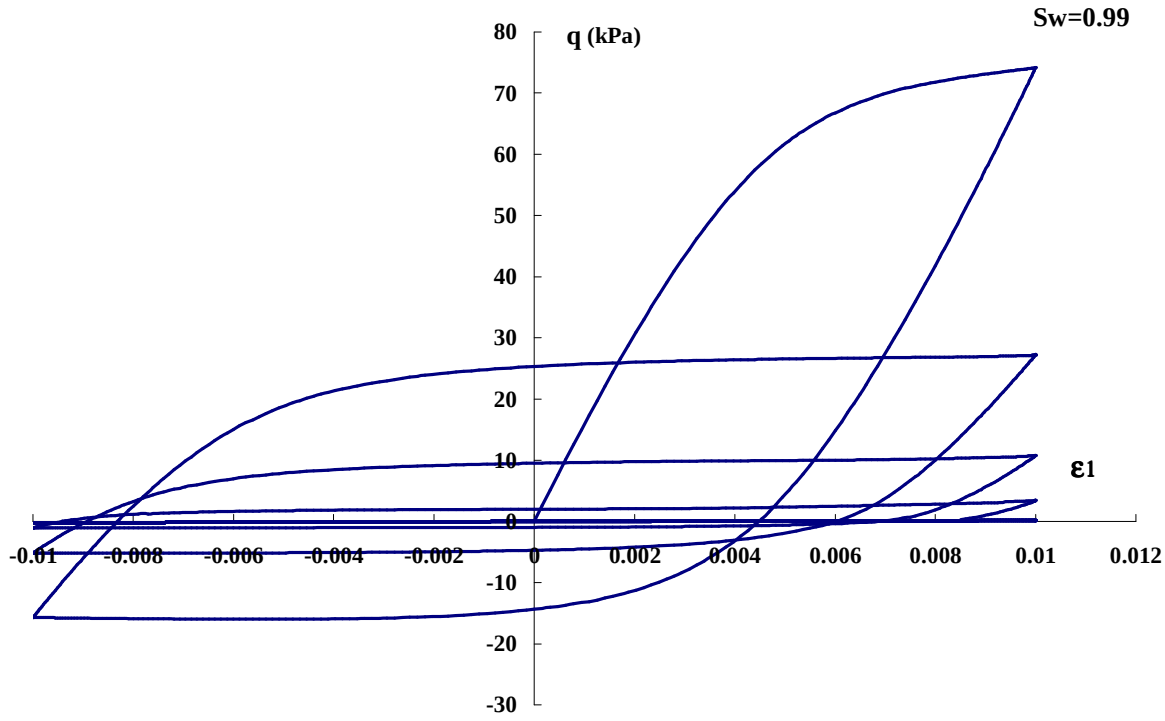

Figure 3.5 (b): Influence of initial water saturation on the cyclic response of undrained loose sand in ($\varepsilon_1 - q$) plan (Sw=99%)

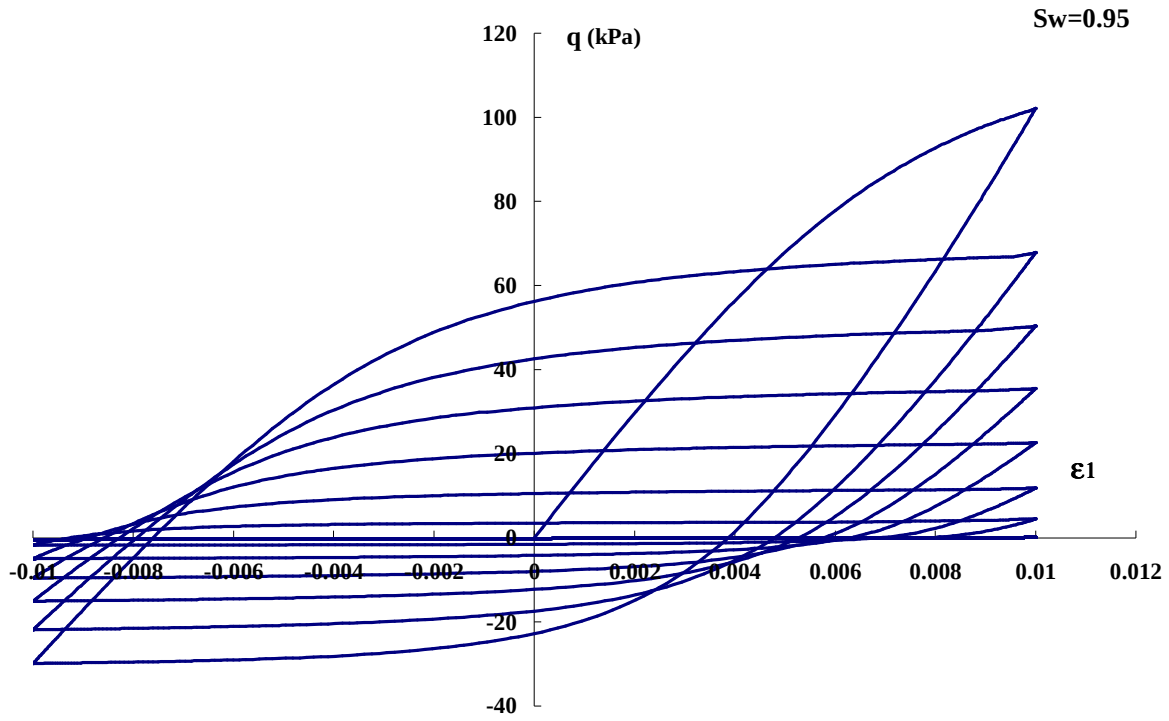

Figure 3.5 (c): Influence of initial water saturation on the cyclic response of undrained loose sand in ($\varepsilon_1 - q$) plan (Sw=95%)

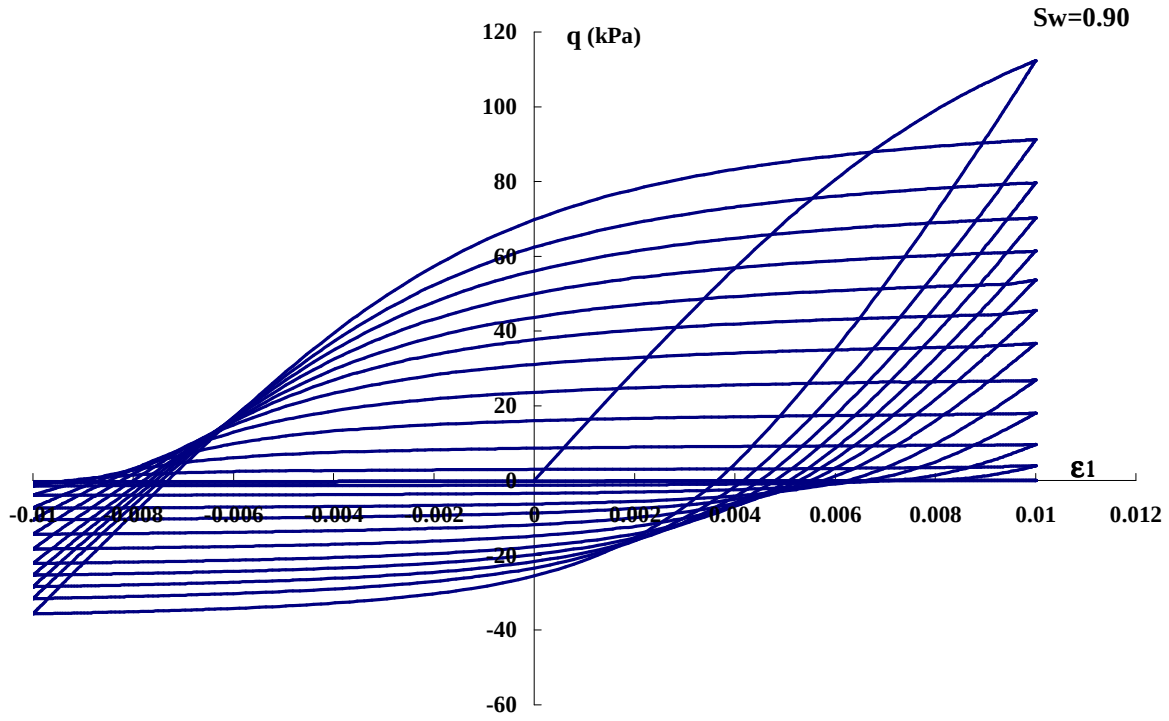

Figure 3.5 (d): Influence of initial water saturation on the cyclic response of undrained loose sand in ($\varepsilon_1 - q$) plan (Sw=90%)

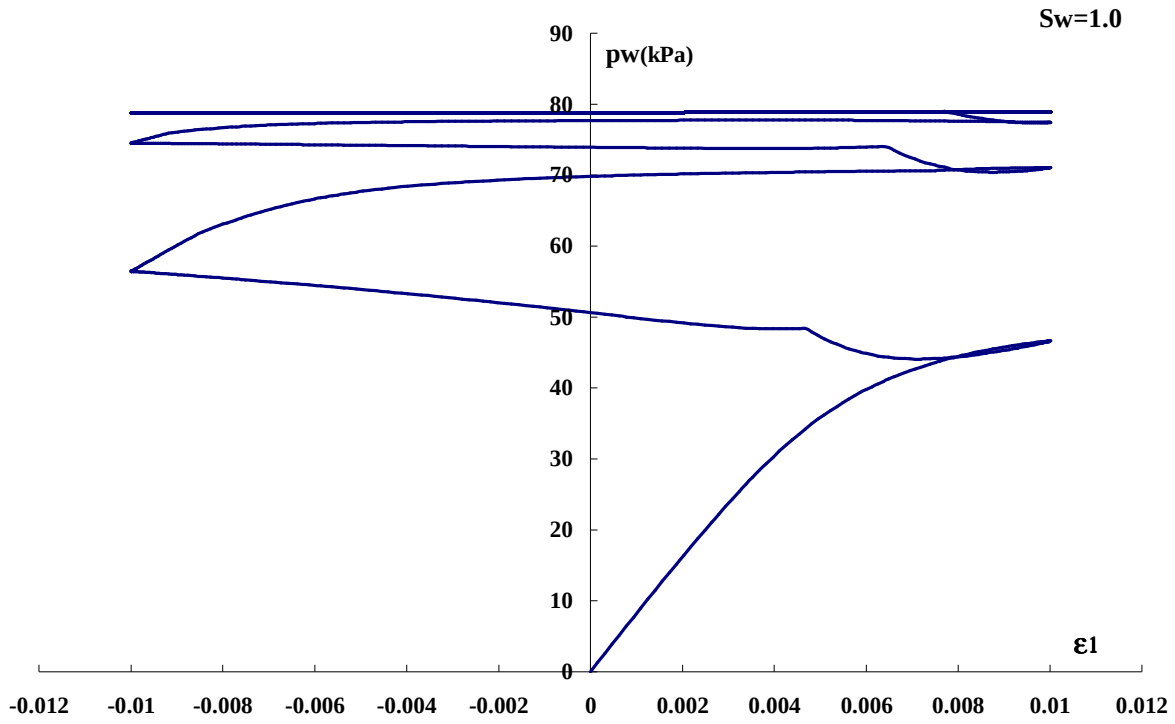

Figure 3.6 (a): Influence of initial water saturation on the cyclic response of undrained loose sand in ($\varepsilon_1 - p_w$) plan (Sw=100%)

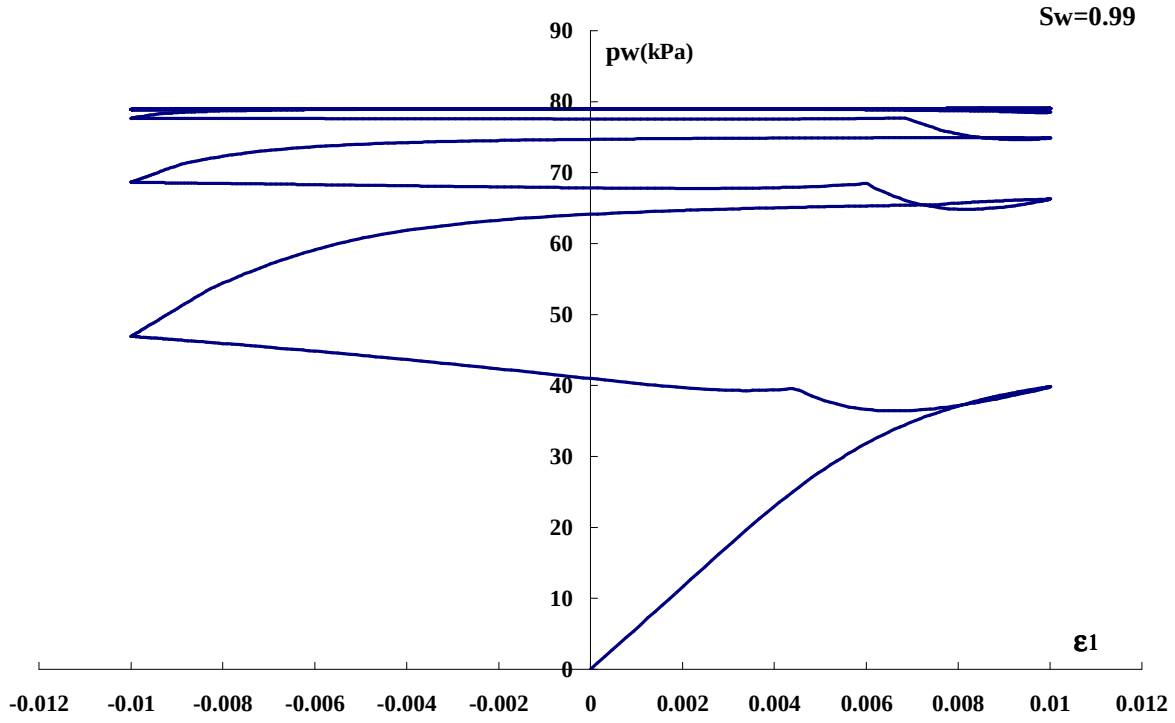

Figure 3.6 (b): Influence of $\varepsilon_1 - q$ initial water saturation on the cyclic response of undrained loose sand in ($\varepsilon_1 - p_w$) plan (Sw=99%)

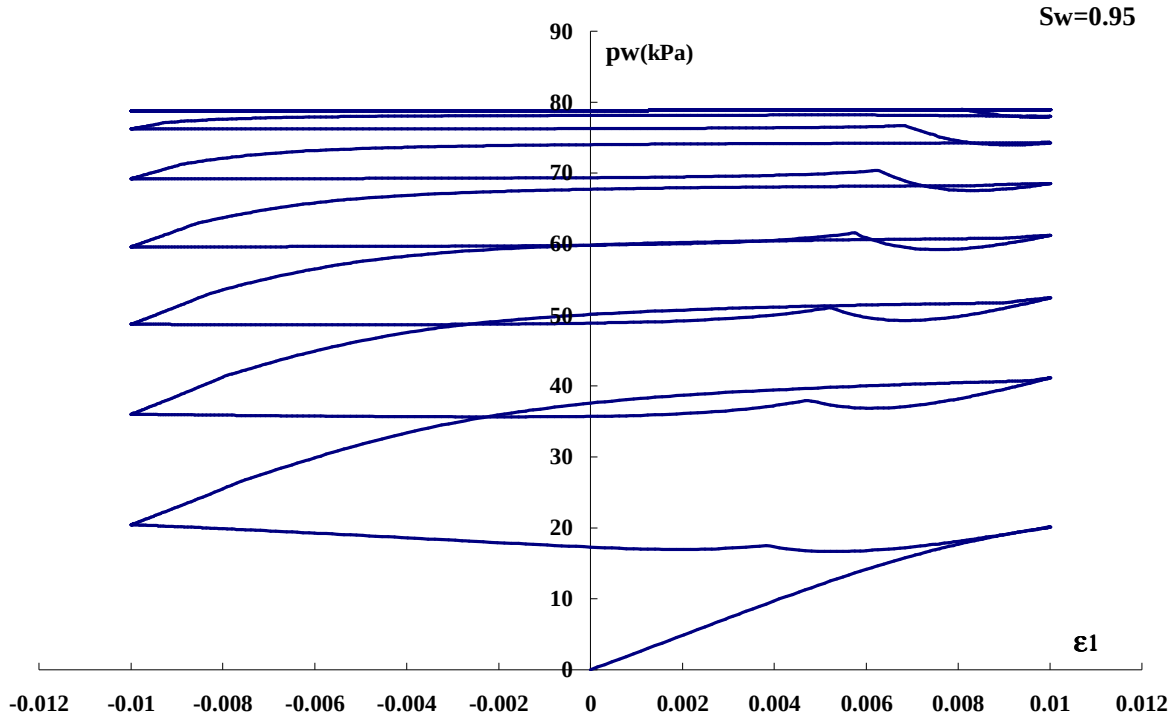

Figure 3.6 (c): Influence of initial water saturation on the cyclic response of undrained loose sand in ($\varepsilon_1 - p_w$) plan (Sw=95%)

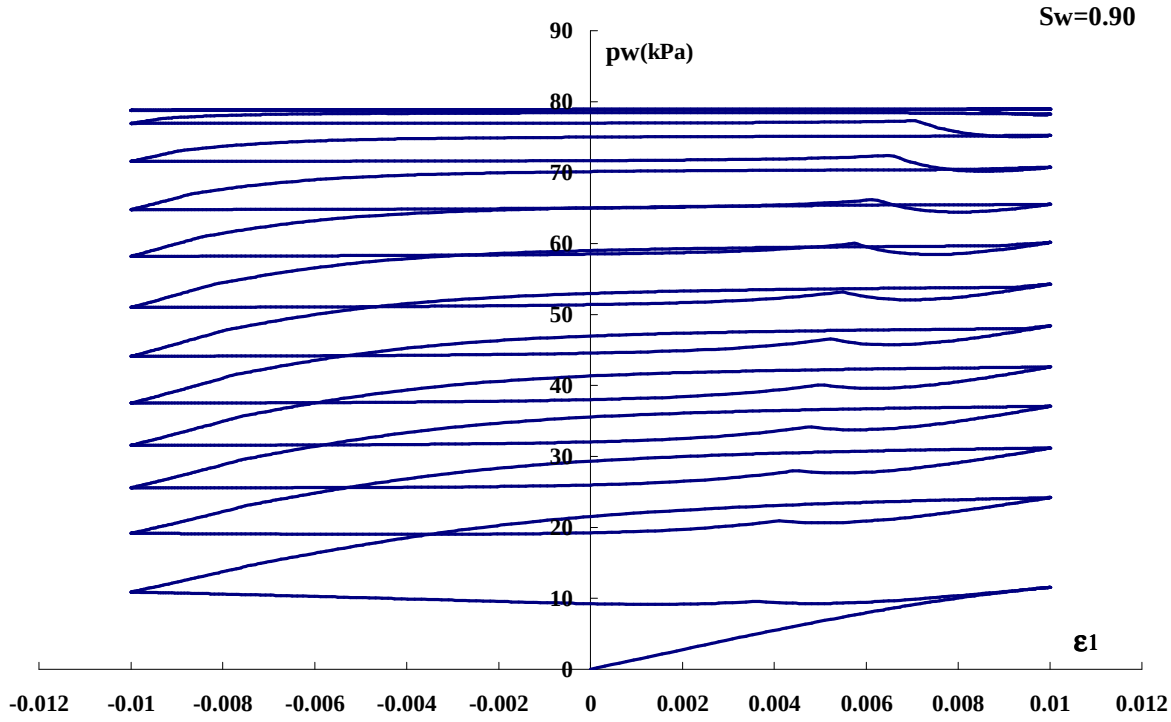

Figure 3.6 (d): Influence of initial water saturation on the cyclic response of undrained loose sand in ($\varepsilon_1 - p_w$) plan (Sw=90%)

3.5. Free filed response of liquefiable layer

The precedent sections showed that the decrease in water content in sandy soils leads to a reduction in the generation of excess pore-water pressure and in the liquefaction risk. In this section, the influence of water saturation on the free filed response is investigated. The geometry of the layer is shown in Figure 3.7. The water table is at the top of the soil column. The initial water saturation is supposed uniform. The boundary conditions are defined as following:

- At the base of soil column, the vertical displacement is blocked, and it is impermeable;
- At the lateral boundaries, the equivalent displacement and pore pressure are imposed;
- At the top of the soil layer, null water pressure is applied, and it is permeable.

The soil used is Nevada sand. The physical properties of this sand are extracted from the VELCAS experiment report (Arulmoli et al., 1992). They are listed in Table 3.2. Different densities are also taken into consideration (the relative density I_d =0.4 and I_d =0.6). The void ratio, porosity, density and permeability are listed in Table 3.2(b).

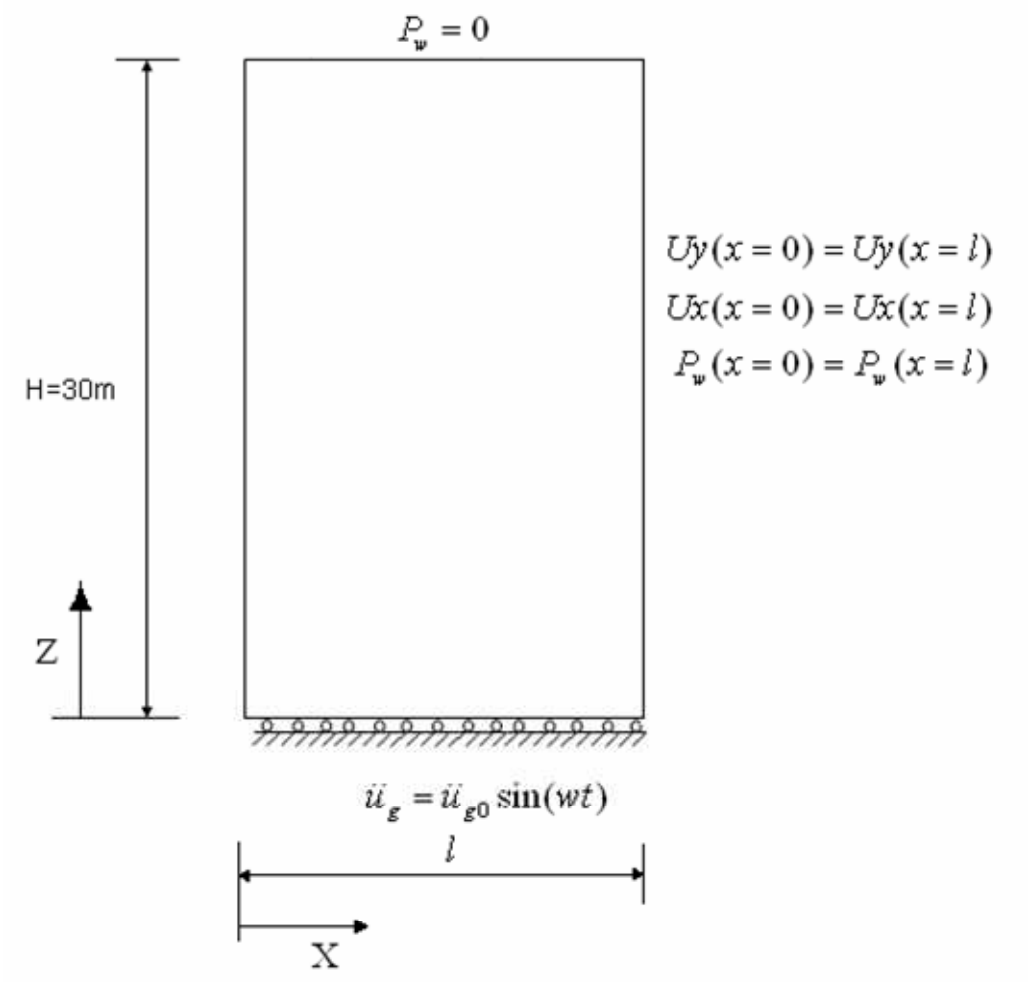

Figure 3.7: Geometry of the liquefiable free filed (Nevada sand)

Table 3.2 (a): Material Properties of Nevada sand (Arulmoli et al., 1992)

G_s	$e_{\min}$	$e_{\max}$	$r_{d\min}$	$r_{d\min}$
			kN/m^3	kN/m^3
2.67	0.511	0.887	13.87	17.33

Table 3.2 (b): Material Properties of Nevada sand (Arulmoli et al., 1992)

I_d	e	n	r_d	r_{satu}	k	ρ_d
			kN/m^3	kN/m^3	m/s	kg/m^3
0.4	0.736	0.42	15.08	19.20	6.6×10^{-5}	1540
0.6	0.661	0.40	15.76	19.68	5.6×10^{-5}	1610

The model parameters of the Nevada sand for MODSOL were determined by Khoshravan (1995) to simulate the centrifuge tests of VELCAS. They are listed in Table 3.3.

Table 3.3: Model Parameters of Nevada sand (I_d =0.4) for MODSOL (Khoshravan, 1995)

1	2	3	4	5	6	7	8	9
E_0	ν_0	N	ϕ	φ_{cv}	b	α_0	c_c	b_c
100kPa			°	°			1/100kPa	°
450	0.23	0.5	34.8	30.5	0.00094	8	0.024	100

Table 3.4: Model Parameters Nevada sand (I_d =0.6) for MODSOL (Khoshravan, 1995)

1	2	3	4	5	6	7	8	9
E_0	ν_0	N	ϕ	φ_{cv}	b	α_0	c_c	b_c
100kPa			°	°			1/100kPa	°
650	0.24	0.5	36	33.2	0.00017	5	0.05	100

The height of the soil column is equal to 30meters. The mesh should be chosen according to the material and loading properties as:

$$l_{\max} \le \frac{\lambda}{6 \sim 8} \tag{3.18}$$

In which, $l_{\max}$ is the maximum length of the element in the wave transmission direction, while λ is the wave length, it is calculated as:

$$\lambda = \frac{V_s}{f_{\max}} \tag{3.19}$$

V_s is the wave transmission velocity. In our case, it is the shear wave velocity, which is calculated as $V_s = \sqrt{G/\rho}$, and $f_{\max}$ is the maximum frequency concerned.

The water saturation varies as $S_w = 100\%$, 99%, 95% and 90%. For unsaturated case, the density of soil, because of the presence of air, will decrease with the decrease in water

saturation, it should be calculated as $\rho_{unsaturated} = \rho_{grain}(1-n) + \rho_{water} n S_w$. A uniform water saturation distribution is assumed. Theoretically, this could exist in the reality, as reported by Okamura et al. (2006).

The loads frequency is equal to 2Hz and its amplitude is $\ddot{u}_g = 0.25g$. It is applied at the base of the soil column during 5s. The time step is also chosen according to the wave transmission velocity and the mesh, $\Delta t = 0.001s$ was used here.

The problem considered is nonlinear; the initial stresses may have a great influence on the numerical results. The initial stress used is due to the gravity action.

3.5.1 Response of free filed (I_d =0.4)

Firstly, the results of relative density I_d =0.4 are presented. Figure 3.8 presents the distribution of the excess pore pressure at different time for different initial water saturations. The pore-pressure is normalised by the initial effective stresses; while the depth is normalised by the total height of the soil column. Figure 3.8 (e) presents the distribution of the maximum excess pore pressure for the different values of the initial water saturation.

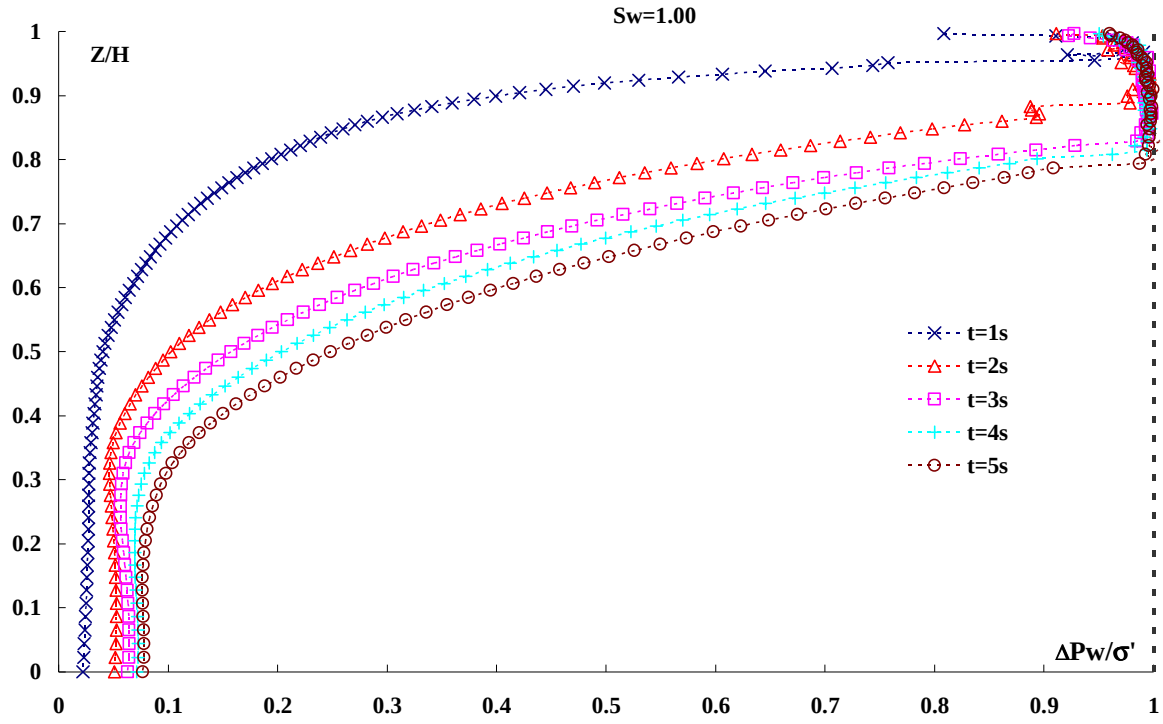

Figure 3.8 (a): Influence of water saturation on the distribution of excess pore-pressure (Nevada sand I_d =0.4) (Sw=100%)

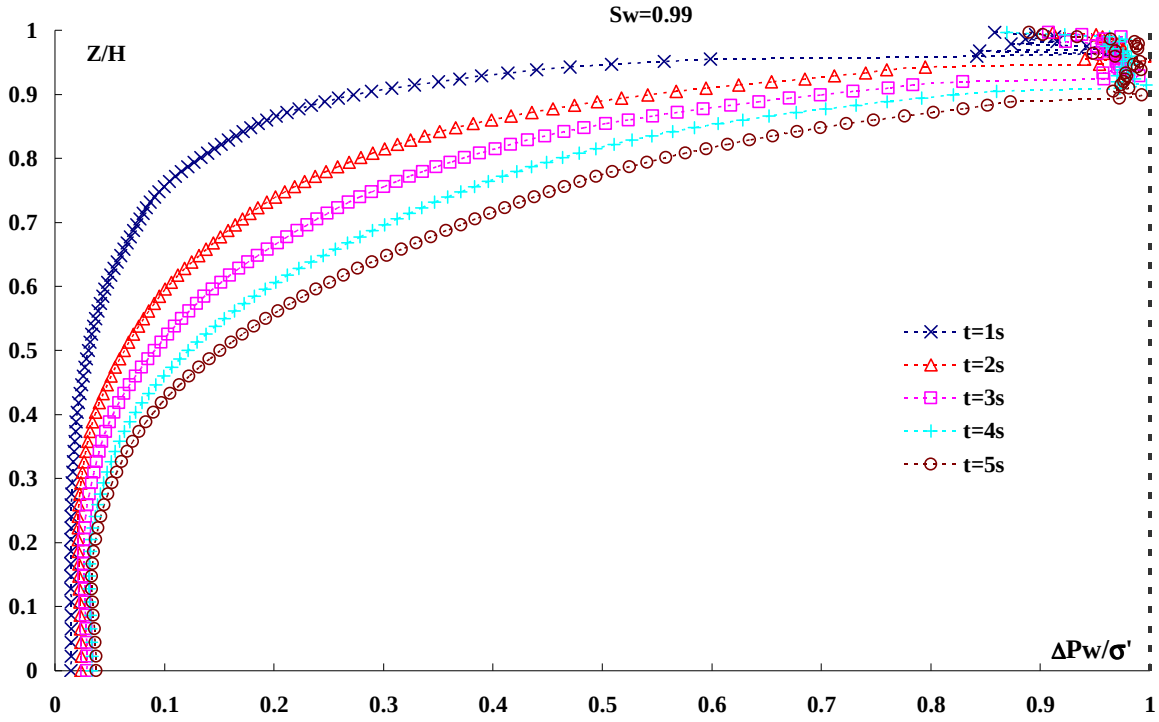

Figure 3.8 (b): Influence of water saturation on the distribution of excess pore-pressure (Nevada sand I_d =0.4) (Sw=99%)

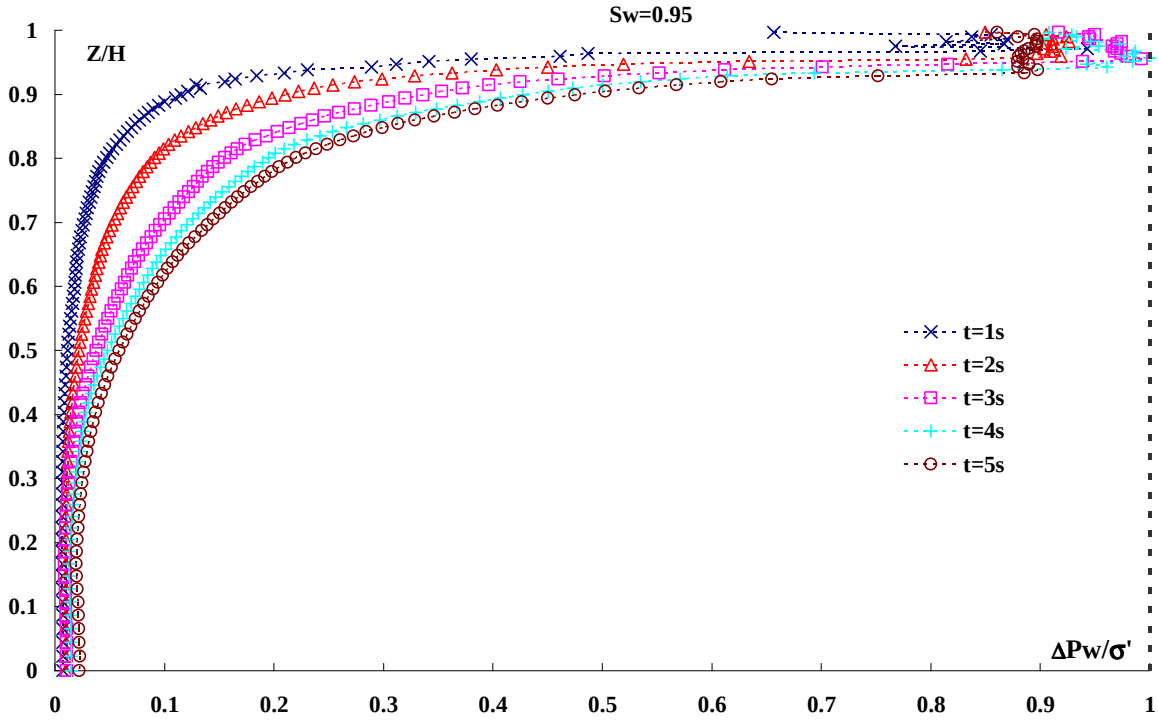

Figure 3.8 (c): Influence of water saturation on the distribution of excess pore-pressure (Nevada sand I_d =0.4) (Sw=95%)

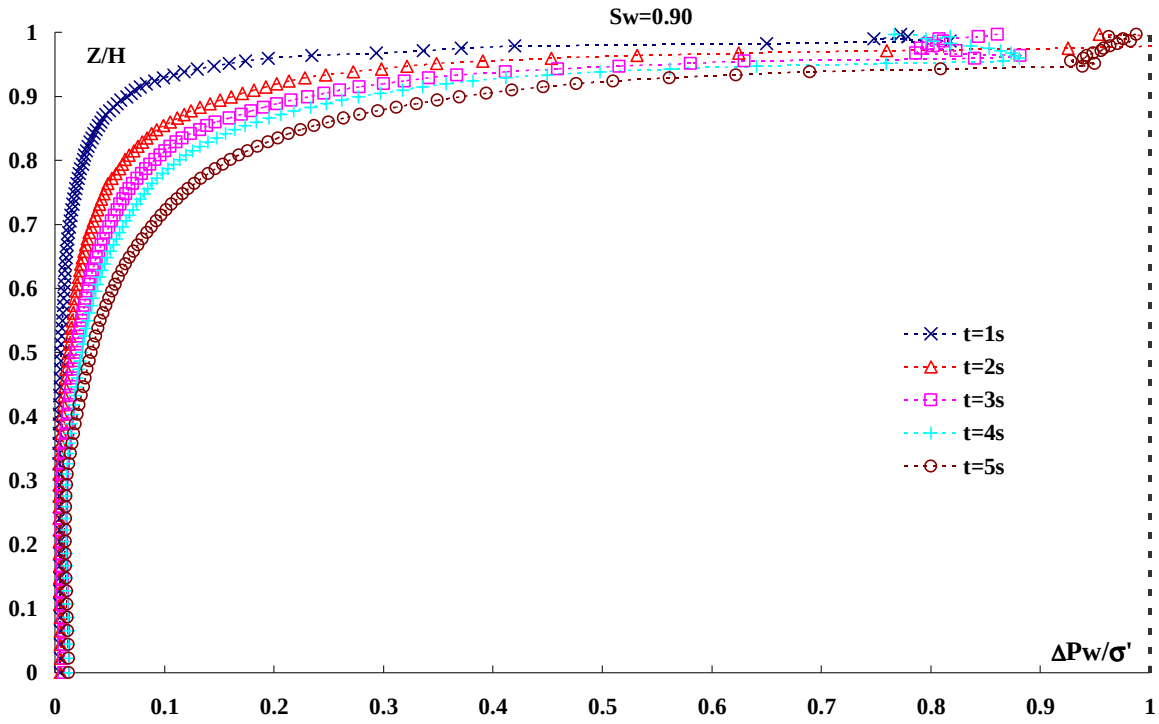

Figure 3.8 (d): Influence of water saturation on the distribution of excess pore-pressure (Nevada sand I_d =0.4) (Sw=90%)

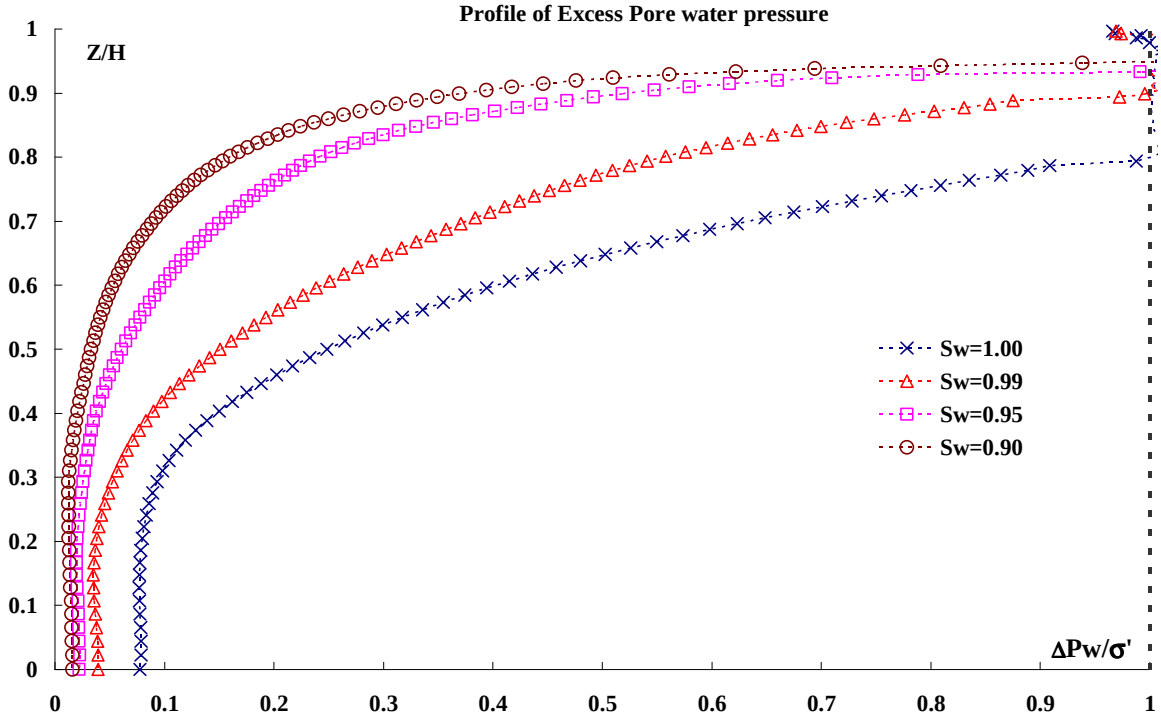

Figure 3.8 (e): Influence of water saturation on the distribution of excess pore-pressure (Nevada sand I_d =0.4)

From Figure 3.8, we can see that the variation of the water saturation has a significant influence on the excess pore-water pressure generation. With the decrease in the initial water saturation, the generation of excess pore pressure decreases, and the risk of liquefaction will be reduced. When the water saturation is less then 0.90, the liquefaction could not occur.

Figure 3.8 (e) illustrates the distribution of the maximum generated excess pore-water pressure for the different initial water saturations. It can be seen that with the decrease in the water saturation, the liquefaction zone will decrease. For example, for fully saturated case, the liquefaction zone concerns about 20% of the layer. In the case of water saturation $S_w = 99\%$, the liquefaction zone is reduced to 10%. The liquefaction resistance of partially saturated soil is greater than that of saturated soil. For instance, at the depth $Z = 0.6\text{H}$, the ratio excess pore-water pressure to effective stresses is about 0.42, while this ratio decreases to 0.25, 0.1 and 0.05 for the initial water saturation $S_w = 99\%$, 95% and 90% respectively.

In order to well explain the effects of water saturation, we give the excess pore pressure generation history of Node37 (Z=25m) in Figure 3.9. For the fully saturated case, at time about 2.66s, the excess pore-pressure is equal to the initial effective stresses (liquefaction occurs), while for the partially saturated cases, there is no liquefaction. The effect of the water saturation is demonstrated by the slope in Figure 3.9, the slope decreases with the decrease in the initial water saturation. This conclusion is confirmed by the results at deeper point in the soil layer, the history of Node73 (Z=15m), (Figure 3.10). It can be seen that the presence of gas in the pore-water reduces the excess pore-water generation. The increase in the amount of gas in soil voids leads to a reduction in the excess pore pressure generation.

It is of interest to remark that, in Figure 3.8, at the top the soil column the excess pore pressure, some times is greater than the initial confining pressure. This could be due to the very low value of the effective stresses.

Figure 3.11 gives the distribution of the vertical displacement for the different values of the initial water saturation. Figure 3.12 gives the history of the settlements at the top of soil layer for different values of the initial water saturation. For the fully saturated case (Figure 3.11 a) in the zone of liquefaction, the settlement seems greater than that of other regions. However, for partially saturated case, the distribution of settlement seems more uniform. In Figure 3.12, it could be observed that the influence of the initial water saturation is very significant. It seems that, for partially saturated cases, the settlements are greater than that of fully saturated case. And the settlement increases with the decrease in the initial water saturation. This is because the pore fluid for partially saturated cases has greater compressibility than that of fully saturated case. The settlement is mainly caused by two factors: the compressibility of both the soil skeleton and pore fluid and the permeability. The four cases have the same permeability, so the settlement is caused by the compressibility of the fluid, because the soil grain is supposed incompressible. This has been confirmed by the experimental results of Sawada et al. (2006).

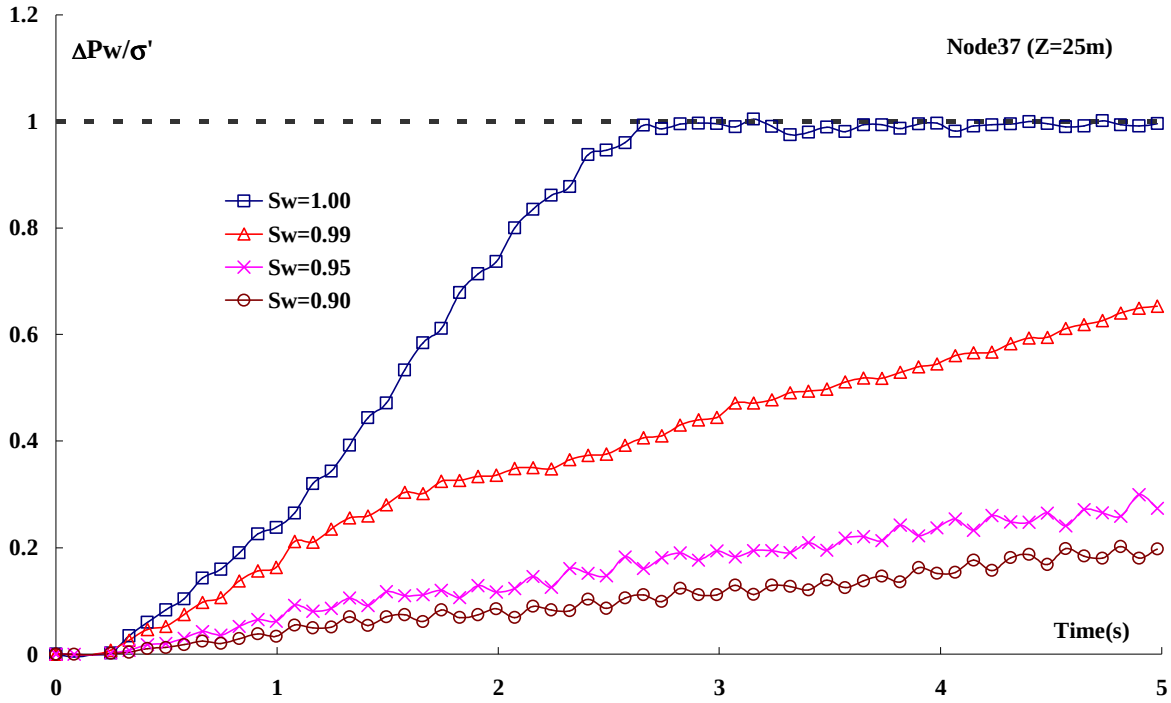

Figure 3.9: History of the excess pore-water pressure at Node37 (Z=25m) for different initial water saturations (S_w = 100%, 99%, 95% and 90%) (Nevada sand I_d =0.4)

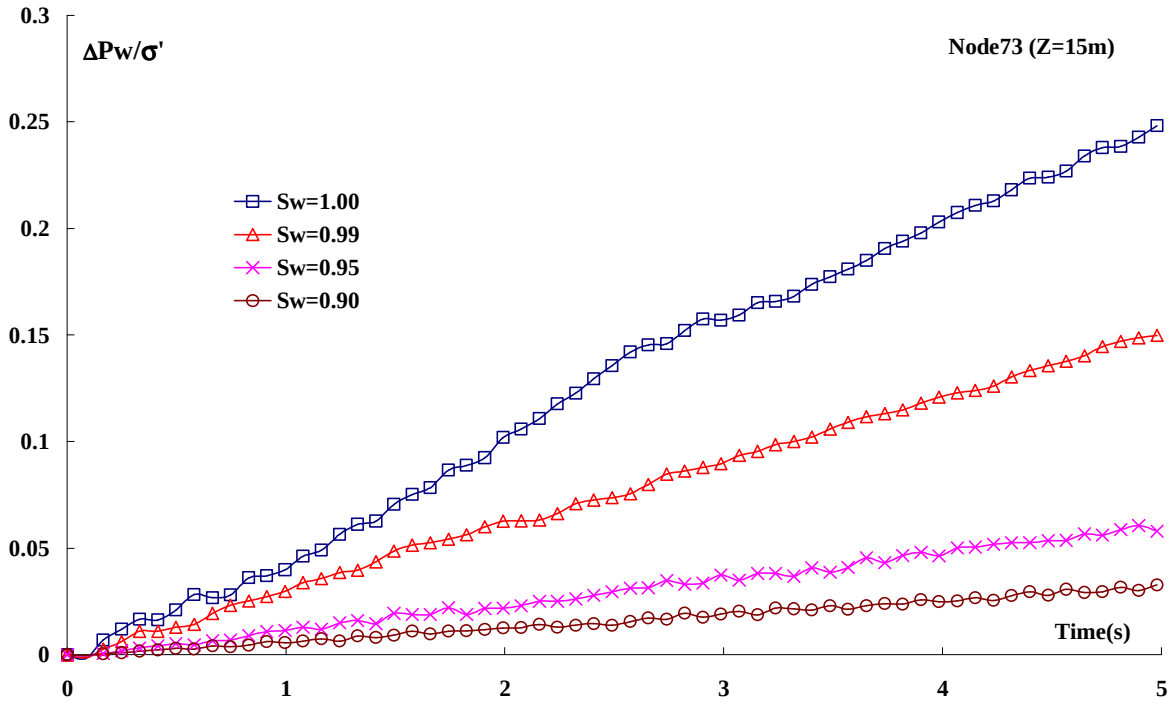

Figure 3.10: History of the excess pore-water pressure at Node73 (Z=15m) for different initial water saturations (S_w = 100%, 99%, 95% and 90%) (Nevada sand I_d =0.4)

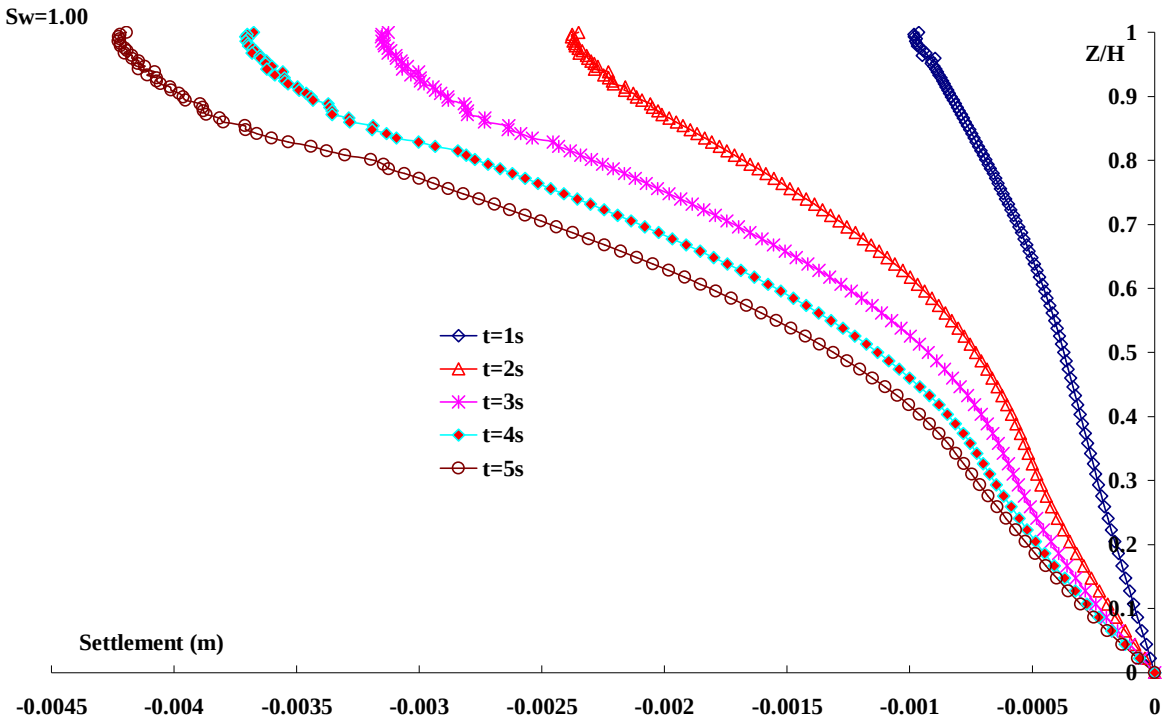

Figure 3.11 (a): Variation of the vertical displacement (S_w = 100%, Nevada sand I_d =0.4)

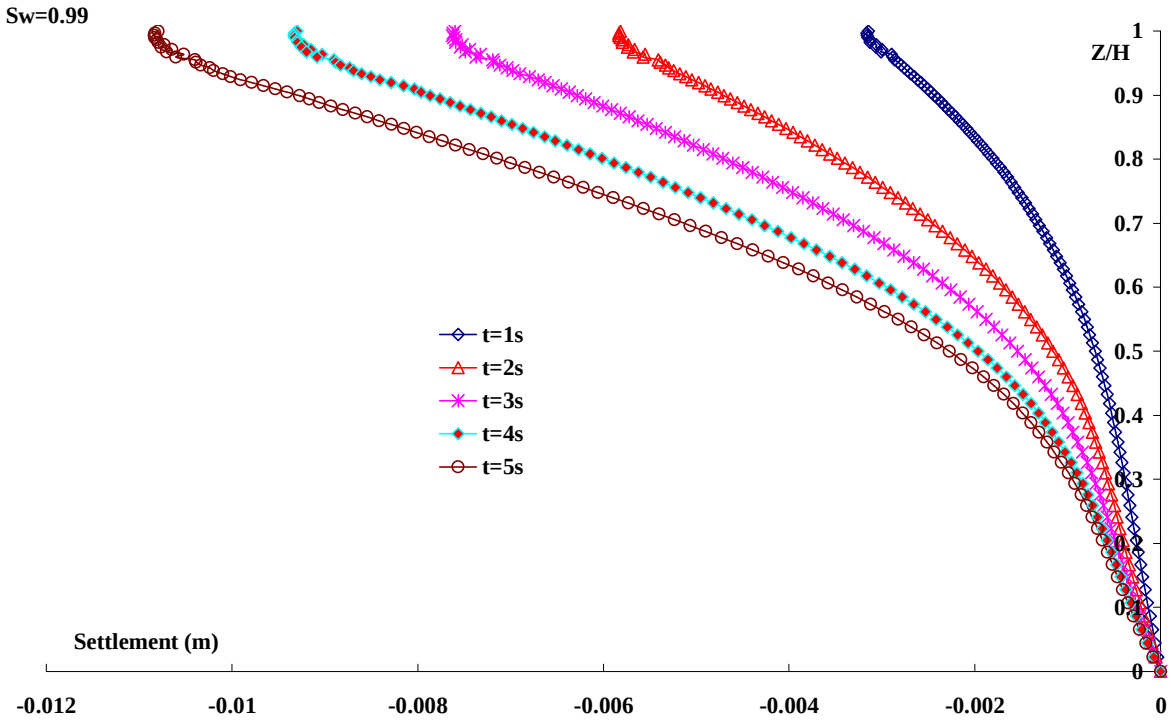

Figure 3.11 (b): Variation of the vertical displacement (S_w = 99%, Nevada sand I_d =0.4)

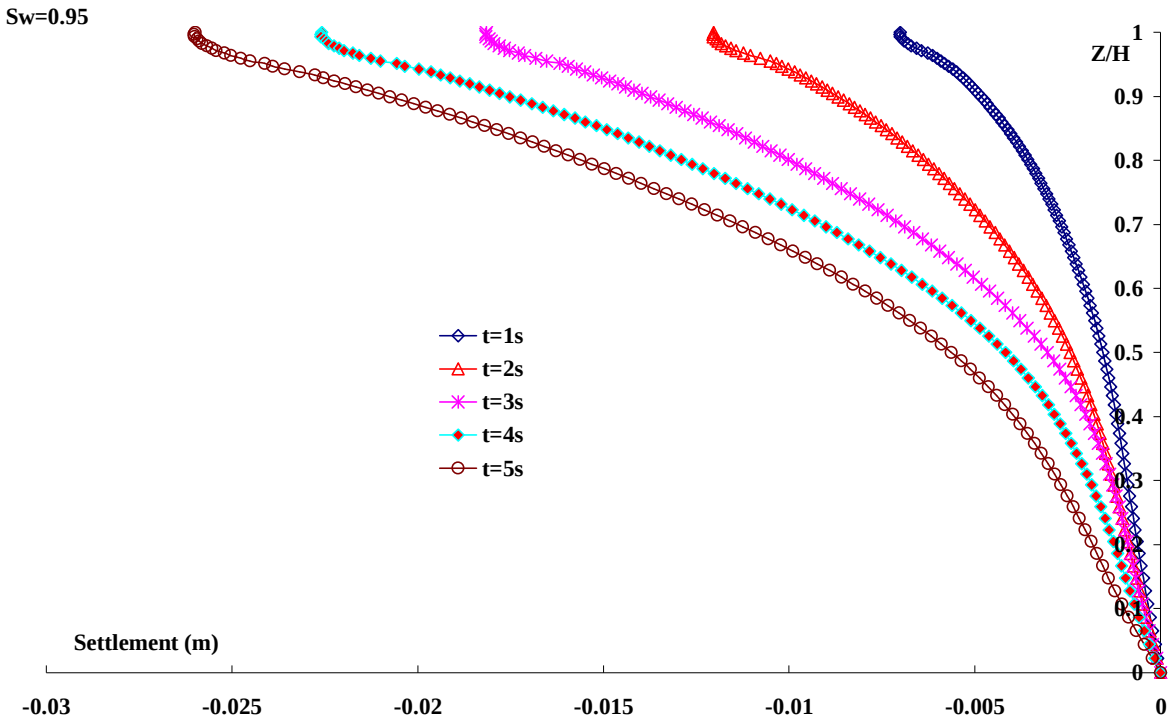

Figure 3.11 (c): Variation of the vertical displacement ($S_w = 95\%$, Nevada sand I_d =0.4)

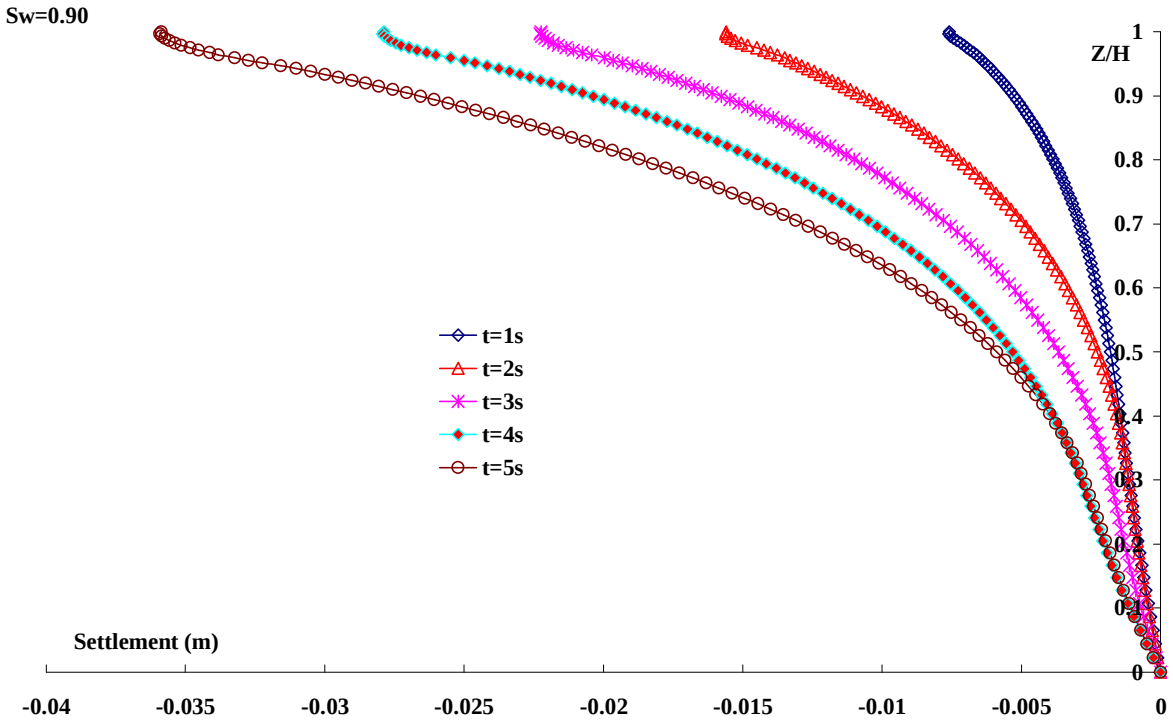

Figure 3.11 (d): Variation of the vertical displacement ($S_w = 90\%$, Nevada sand I_d =0.4)

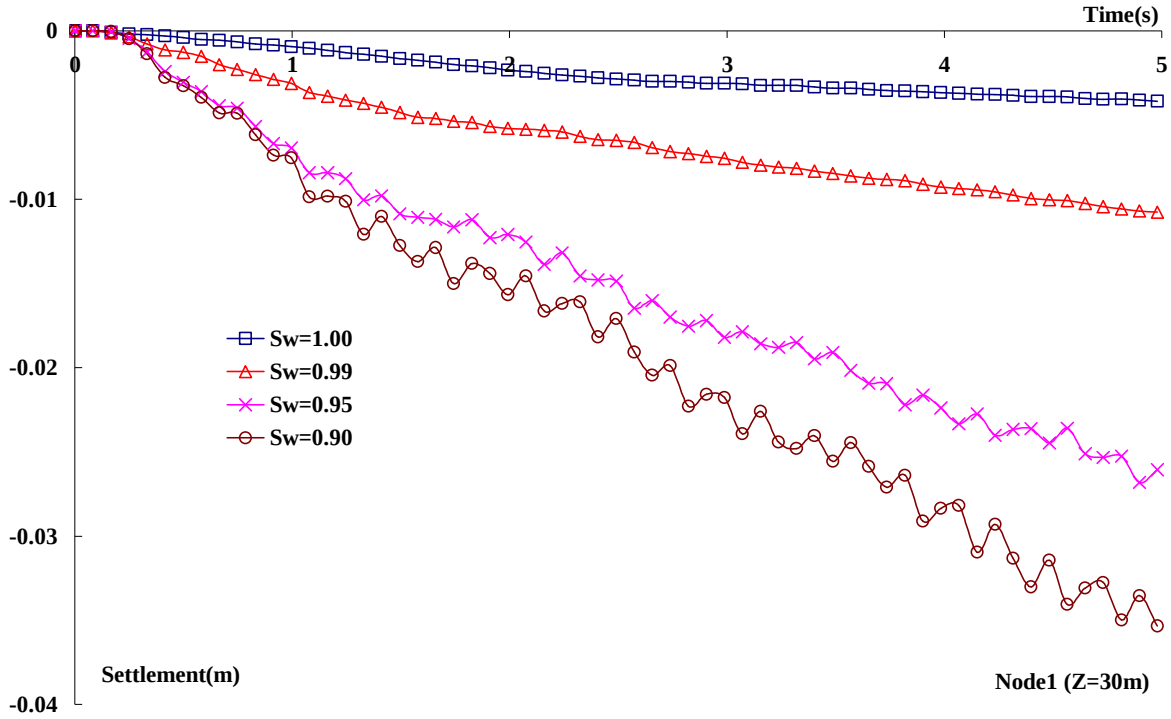

Figure 3.12: Influence of the initial water saturation on the column settlement (S_w = 100%, 99%, 95% and 90%) (Nevada sand I_d =0.4)

3.5.2 Influence of the permeability

Note that the settlement is controlled by the compressibility of both the soil skeleton and the pore fluid, as well as the permeability. In this part, the influence of the permeability will be analysed. For the fully saturated case, four different permeabilities (k=1K0, 10K0, 100K0 and 1000K0, where K0 is the permeability of Nevada sand with the relative density I_d =0.4, see Table 3.4) are used to study the influence of permeability on the free filed response.

(A) Saturated soil

The results are presented in Figures 3.13 and 3.14. The distributions of the excess pore pressure for different permeabilities are presented in Figure 3.13. With the increase in the permeability, the liquefaction zone decreases. For the case k=10K0, the liquefaction zone is reduced by comparing with the case k=K0 (Figure 3.8a). For the case k=100K0, the liquefaction zone is greatly reduced; the liquefaction zone is very small. The location of liquefaction zone varies with time. When the permeability attains 1000K0, no liquefaction occurs. This is because: the increase in permeability increases the dissipation of the excess pore pressure and the outflow of pore-water.

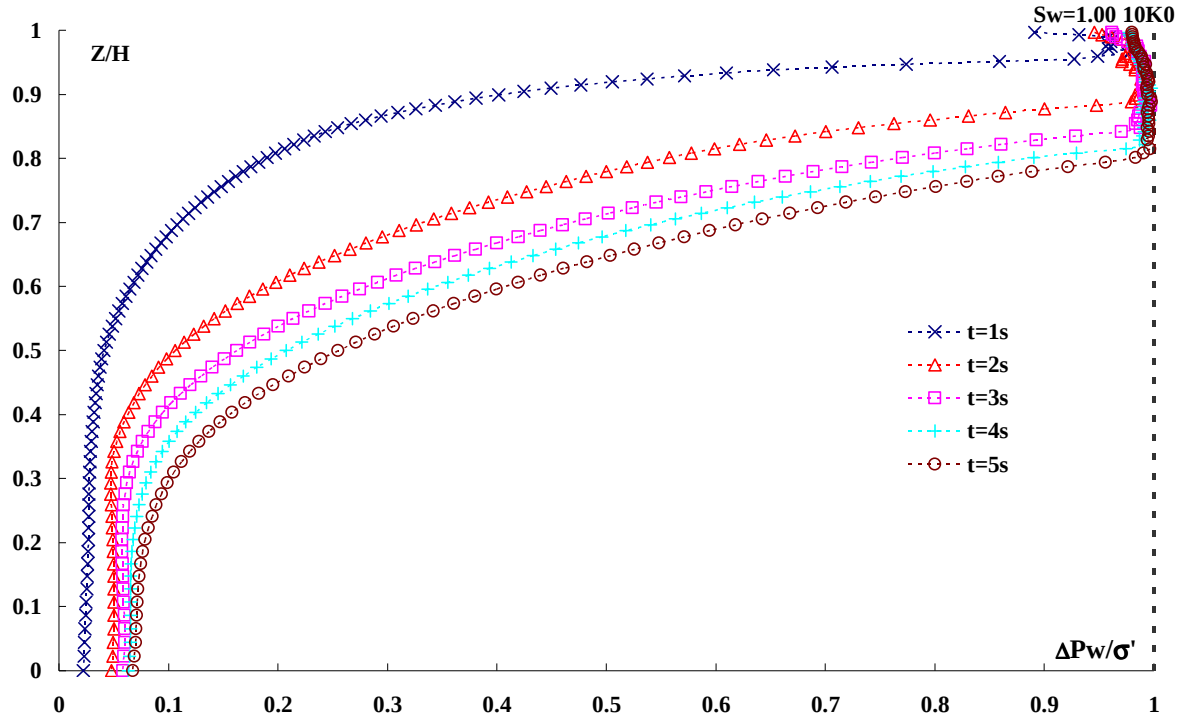

Figure 3.13 (a): Variation of the excess pore-water pressure S_w=100%, k=10K0 (Nevada sand I_d=0.4)

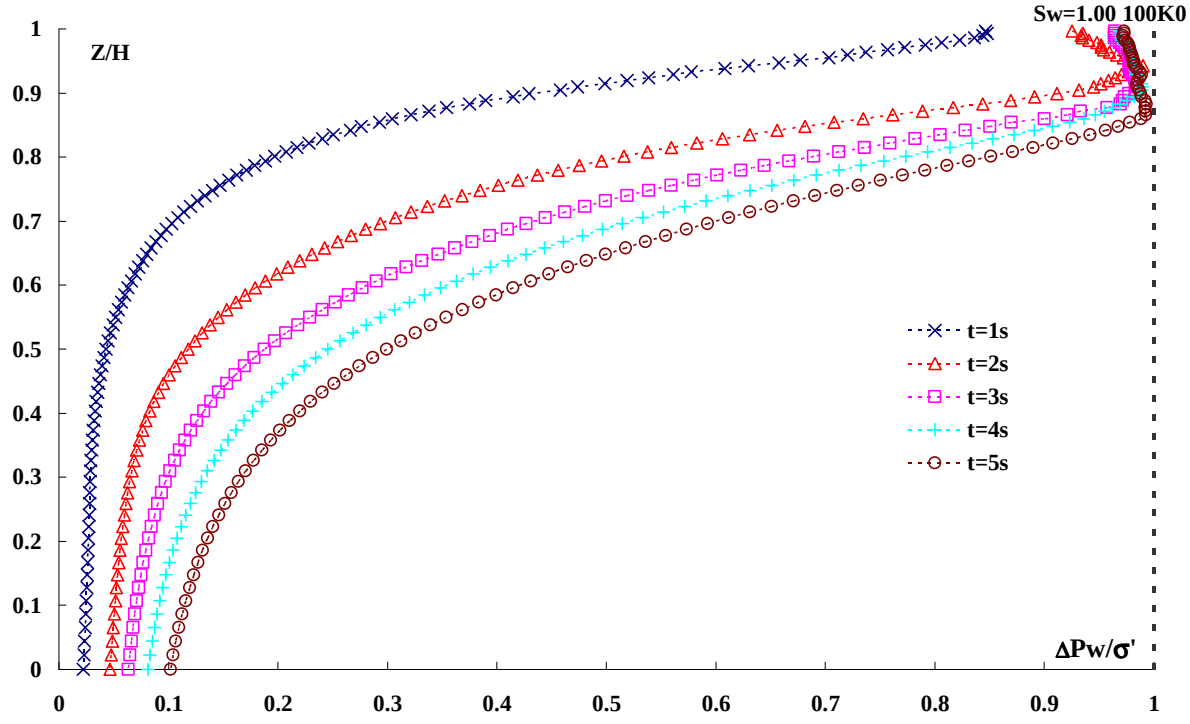

Figure 3.13 (b): Variation of the excess pore-water pressure S_w=100%, k=100K0 (Nevada sand I_d=0.4)

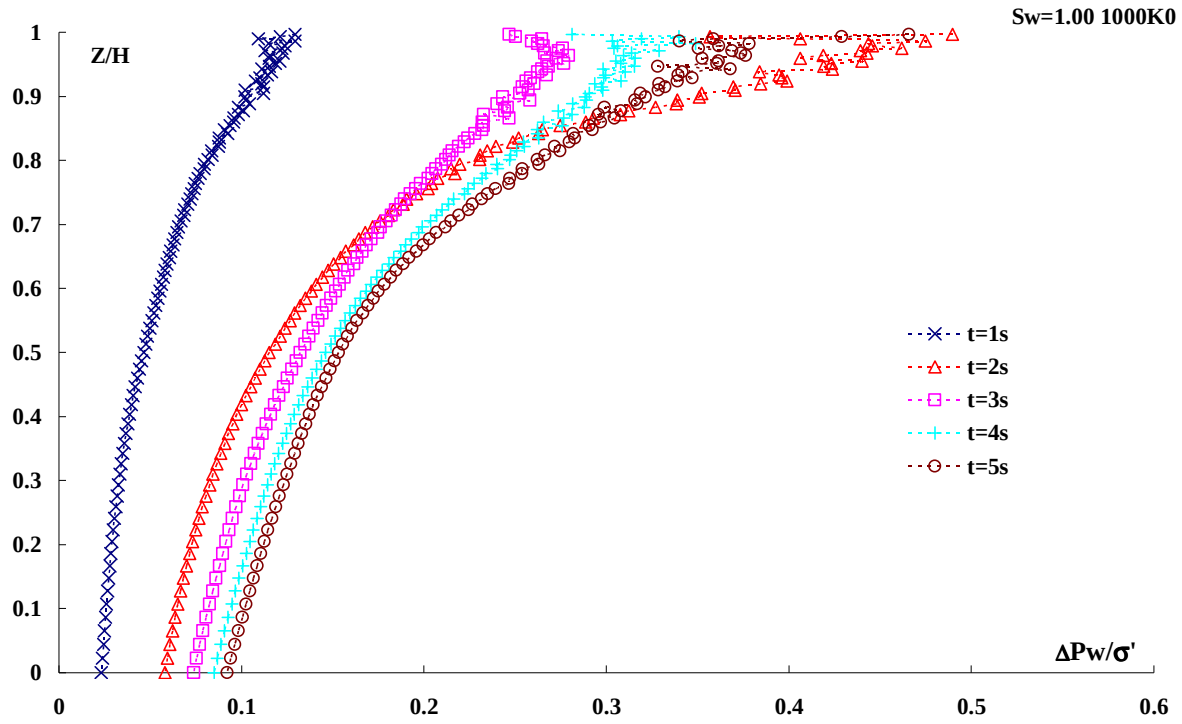

Figure 3.13 (c): Variation of the excess pore-water pressure S_w =100% , k=1000K0 (Nevada sand I_d =0.4)

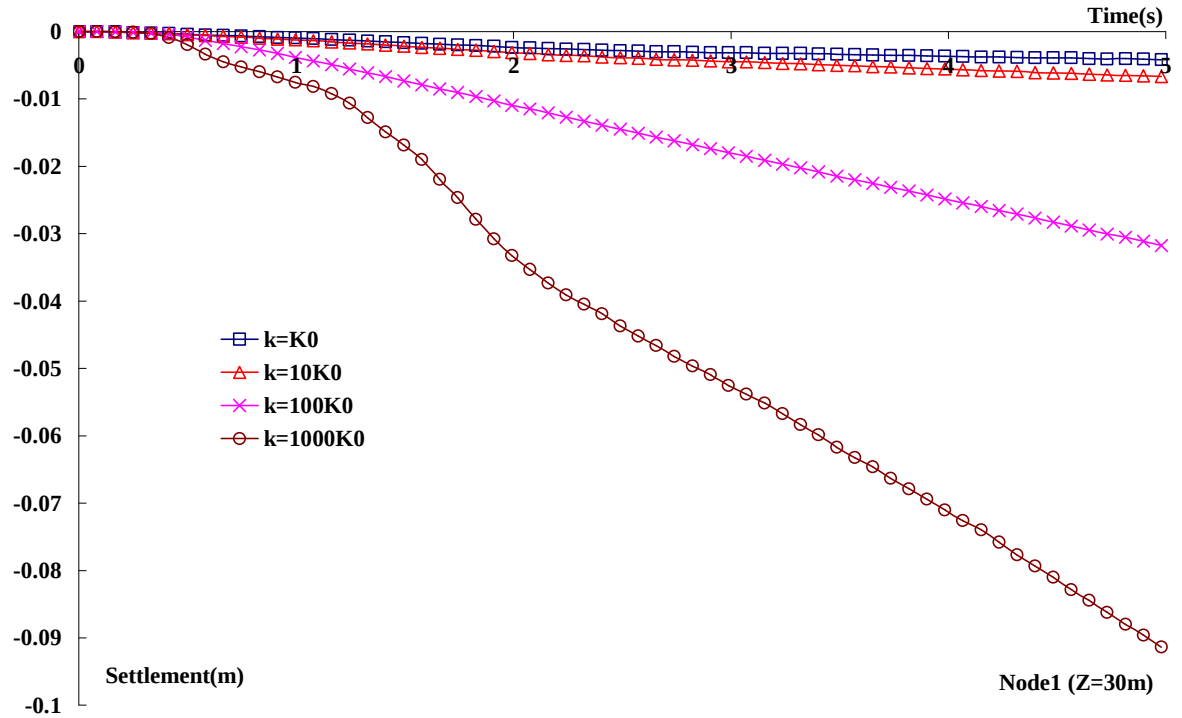

Figure 3.14: Influence of permeability on the settlement of the soil layer (fully saturated Nevada sand I_d =0.4)

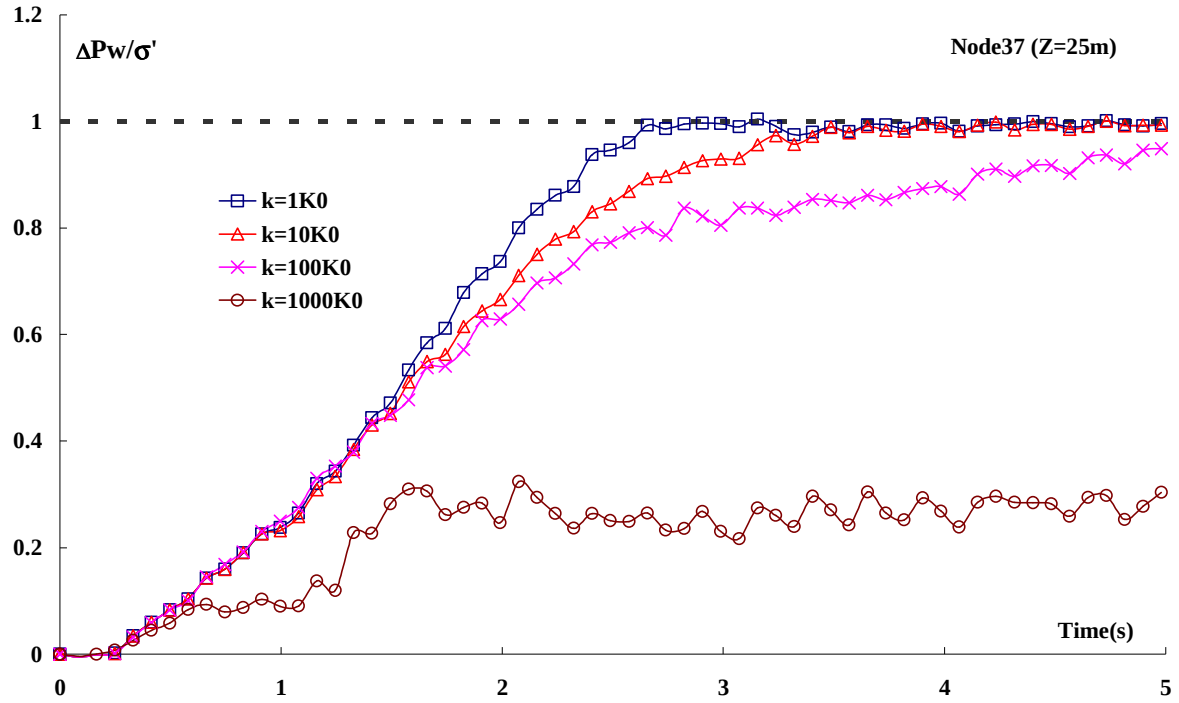

Figure 3.15: Influence of permeability on the generation of excess pore pressure (fully saturated Nevada sand I_d =0.4)

Figure 3.14 presents the settlement at the top of soil column for different values of permeability. Due to a greater value of the permeability, more pore-water flow out the column. As a result, greater settlement occurs. Generally, the in-situ observations of the liquefaction zone show that more important settlement is generated in liquefaction zone than that of non liquefied area. This is because the settlements observed are those after the dissipation of excess pore pressure. Before the dissipation of the excess pore pressure, the results in Figure 3.12 are reasonable.

Figure 3.15 presents the history of the normalised excess pore pressure in Node37 (Z=25m). It shows that the increase in the permeability leads to a decrease in the excess pore pressure generation rate.

(B) Unsaturated soil

The numerical simulation results for the soil layer with $S_w = 90\%$ are illustrated in Figures 3.16-3.18. Figure 3.16 gives the distribution of the maximum excess pore. It shows that, the increase in the soil permeability for partially saturated sand has lower influence on the generation of the excess pore pressure. The decrease in the permeability does not have a significant influence on settlement (Figure 3.17).

This section presents the influence of a decrease in the soil permeability for partially saturated case S_w=90%. The values of the permeability are k=1.0K0, 0.1K0, 0.01K0 and 0.001K0. Generally, under partially saturated condition, the influence of permeability is smaller than that

of the fully saturated case, as illustrated in Figure 1.12. Figure 3.19 gives the distribution of the maximum excess pore pressure. Figure 3.20 shows the generation of the excess pore pressure. It seems that, the variation of permeability for partially saturated sand soils has little influence on the generation of excess pore pressure, as well as on the settlement of soil layer (Figure 3.21). This is due to the high compressibility of the pore-fluid in partially saturated soils.

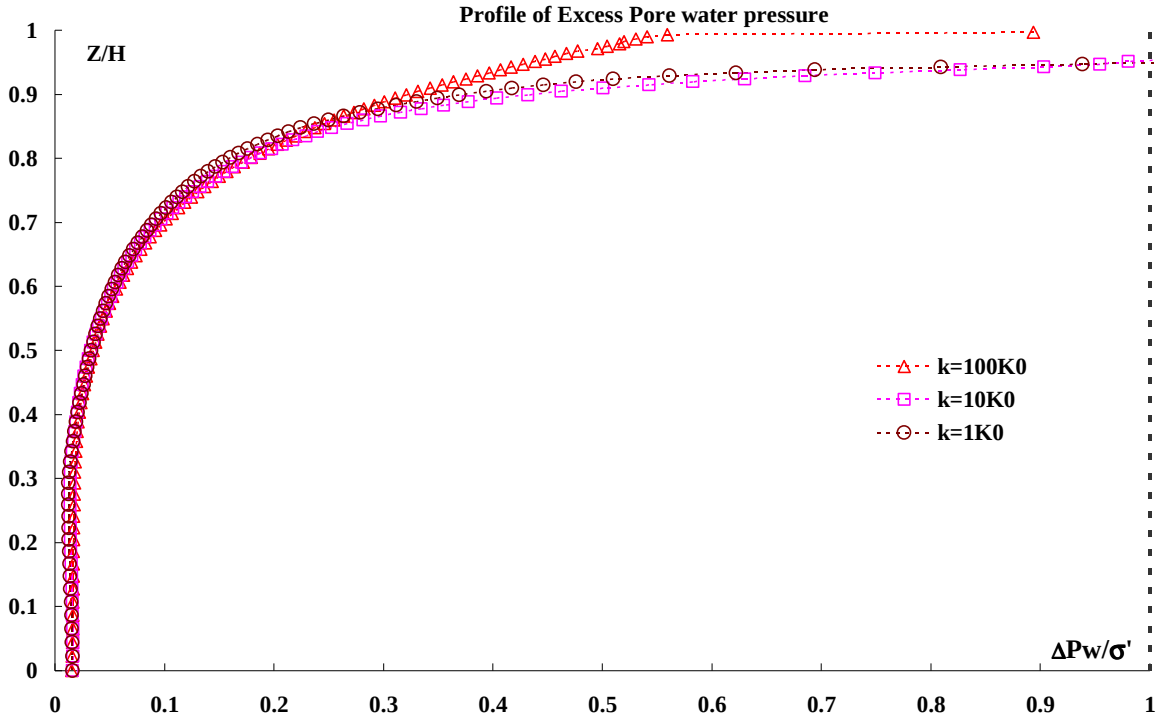

Figure 3.16: Influence of soil permeability on the maximum excess pore-water pressure distribution (Nevada sand I_d =0.4 S_w =90%)

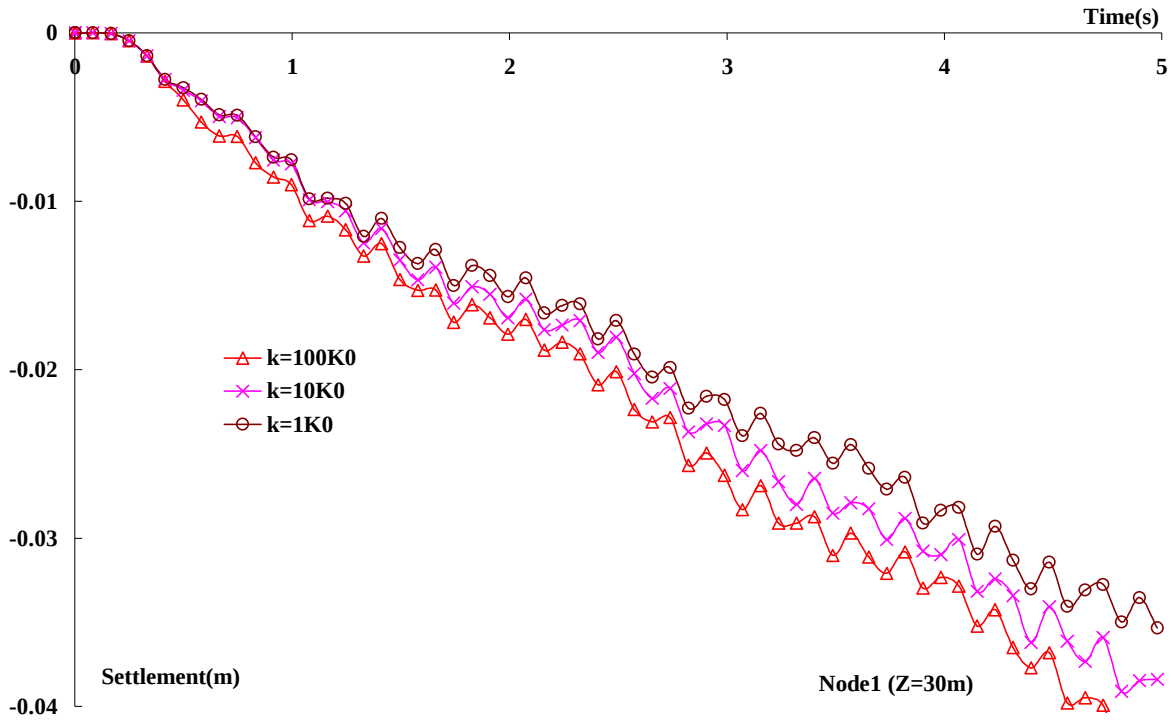

Figure 3.17: Influence of soil permeability on the settlement (Nevada sand I_d =0.4 S_w =90%)

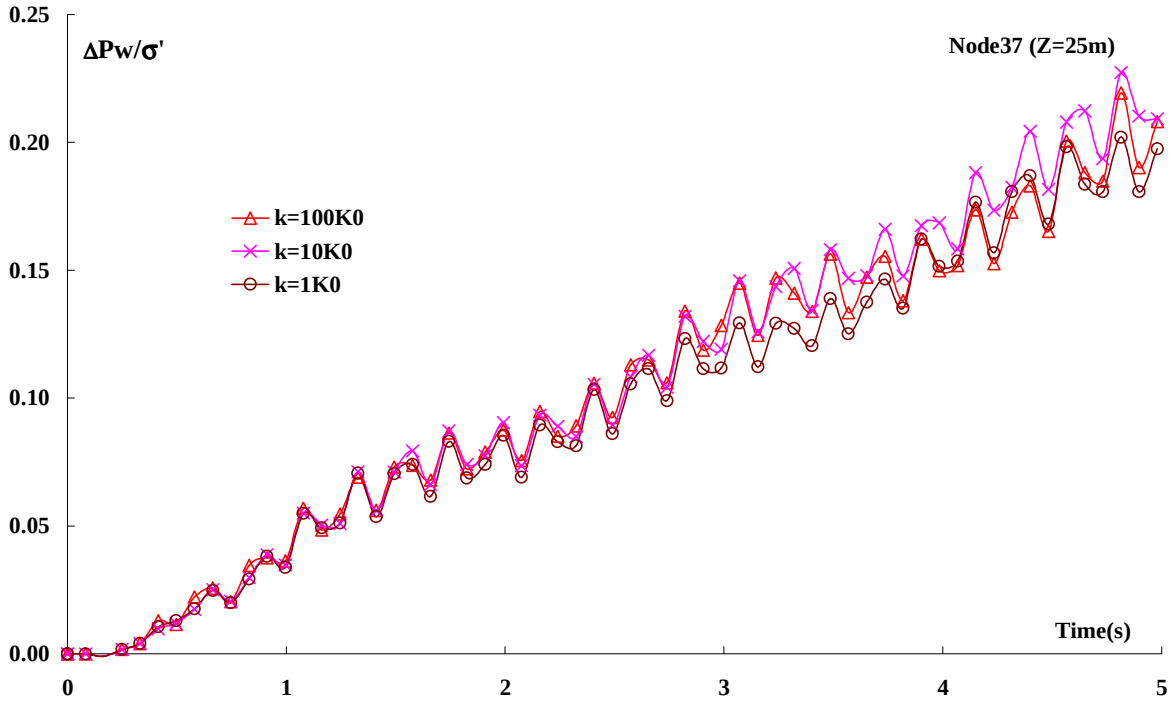

Figure 3.18: Influence of soil permeability on the excess pore pressure generation (Nevada sand I_d =0.4 S_w =90%)

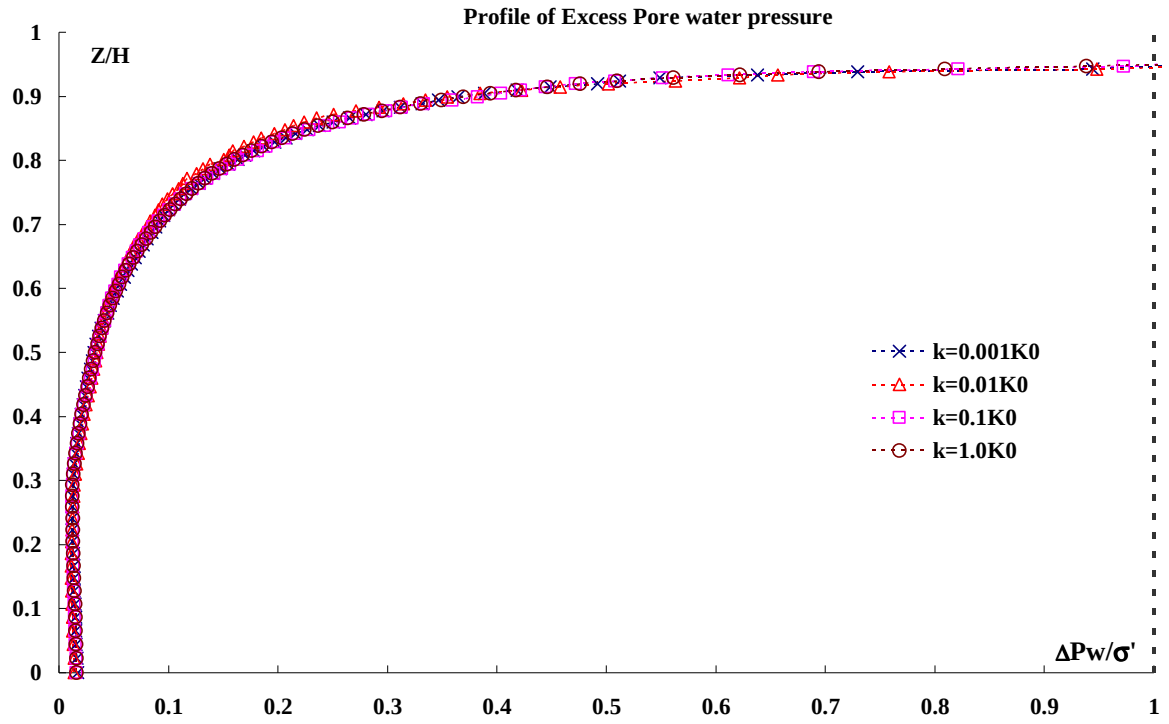

Figure 3.19: Influence of soil permeability on the maximum excess pore-water pressure distribution (Nevada sand I_d =0.4 S_w =90%)

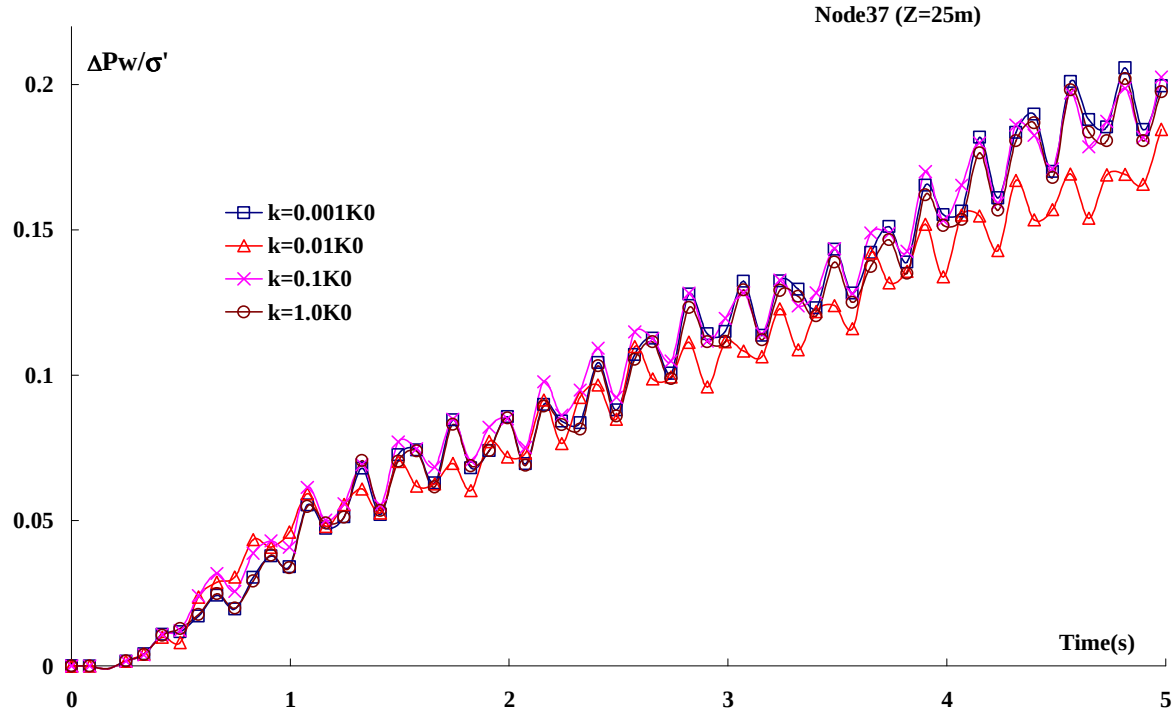

Figure 3.20: Influence of soil permeability on the excess pore-water pressure generation (Nevada sand I_d =0.4 S_w =90%)

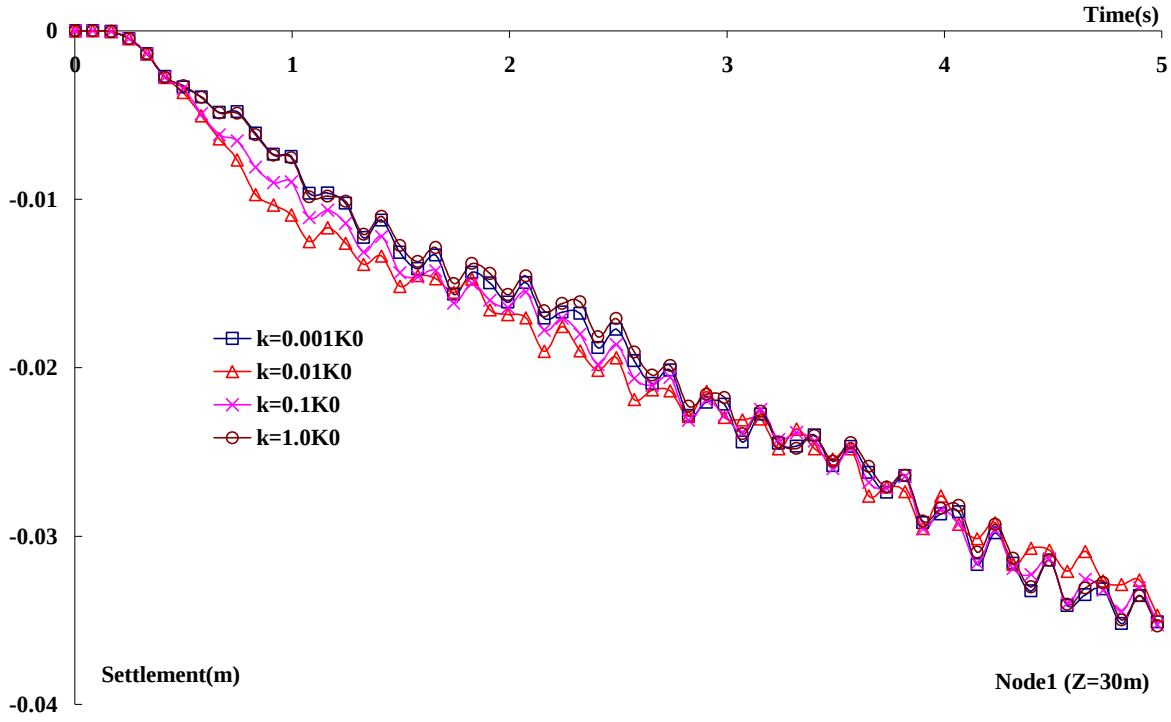

Figure 3.21: Influence of soil permeability on the settlement (Nevada sand I_d =0.4 S_w =90%)

3.5.3 Influence of the relative density

One of the main soil improvements against liquefaction concerns the soil densification. So the relative density is an important factor for the liquefaction of granular materials. In this section, the influence of relative density on the soil liquefaction will be analysed.

With the increase in relative density, the porosity, the void ratio and the permeability will decrease. As indicates in Table 3.3, for I_d =0.4, the porosity is 0.42, the void ratio is 0.736, and the permeability is 6.6×10^{-5} m/s; while for I_d =0.6, the porosity decreases to 0.4, and void ratio to 0.661, the permeability becomes 5.6×10^{-5} m/s. For higher relative density, the distribution of the pores is more favourable for entrapping air. We consider four cases including one fully saturated case and three unsaturated cases with the initial water saturations (S_w =99%, 95% and 90%). The numerical results are presented in Figures 3.22-3.24. Figure 3.22 gives the maximum excess pore pressure distributions. Figure 3.23 presents the settlement at the top of soil column. Figure 3.24 gives the history of the excess pore pressure at Node37 (Z=25m). Comparing these results to those of I_d =0.4, shows that the increase in the relative density leads to a decrease in the liquefaction zone. In fully saturated case, the liquefaction zone for I_d =0.4 concerns 20% of the layer, while for I_d =0.6, the liquefaction zone concerns only 7%; the liquefaction zone has been greatly reduced. The settlement at the top of the soil column decreases too. For unsaturated case with water saturation S_w = 90%, when I_d =0.4, the total settlement is equal to 0.035m, while for I_d =0.6, the final settlement is equal to 0.01m. The excess pore pressure generation rate decreases with the increase in the relative density. At

Node37 (Z=25m) for I_d=0.4, the liquefaction occurs, while for I_d=0.6, the ratio $\Delta p_w / \sigma_0'$ attains 0.38.

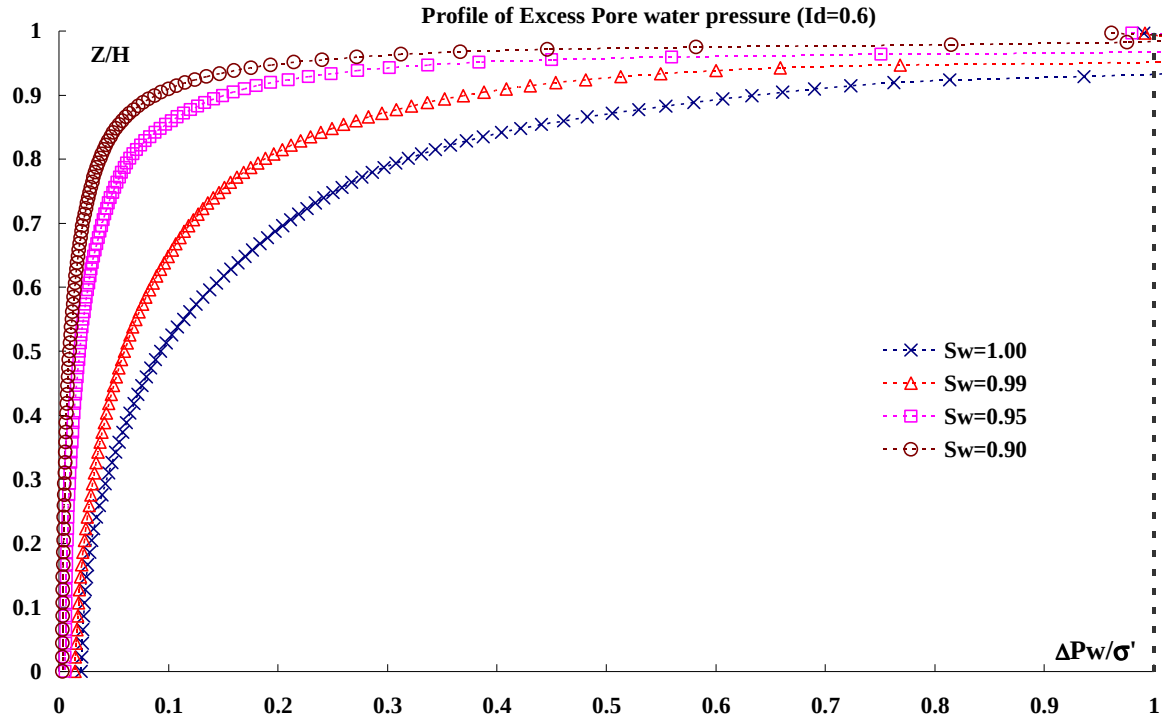

Figure 3.22: Influence of initial water saturation on the distribution of maximum excess pore-water pressure (Nevada sand I_d=0.6)

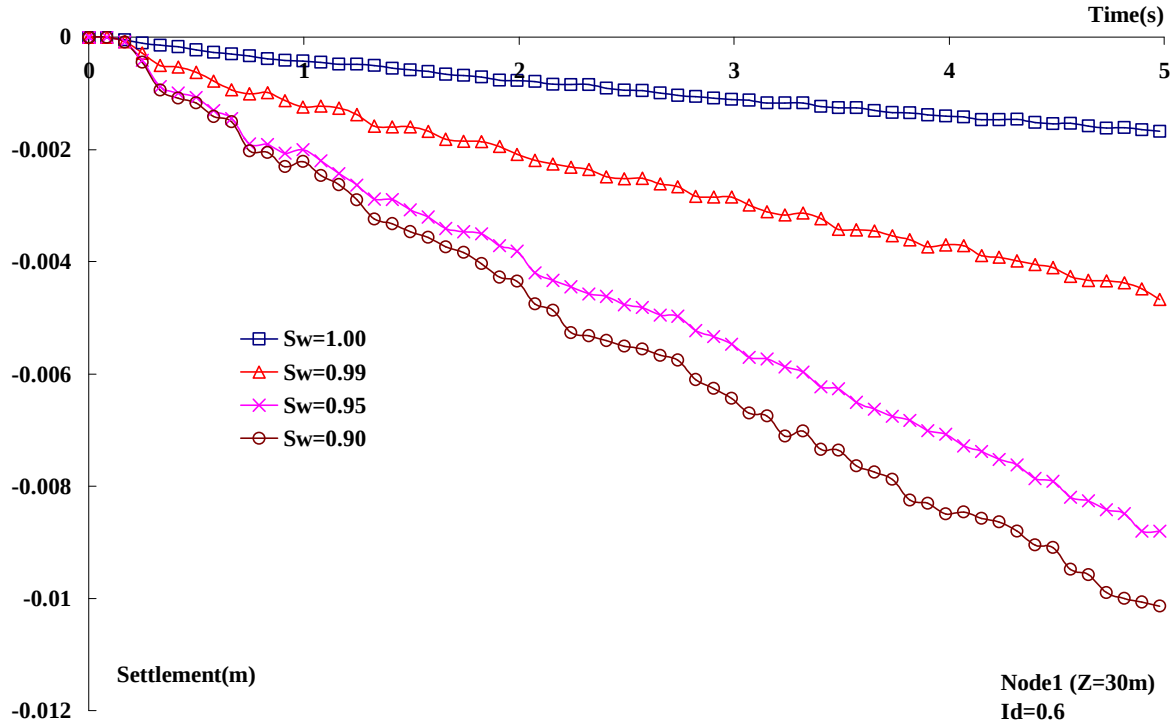

Figure 3.23: Influence of initial water saturation on the settlement (Nevada sand I_d=0.6)

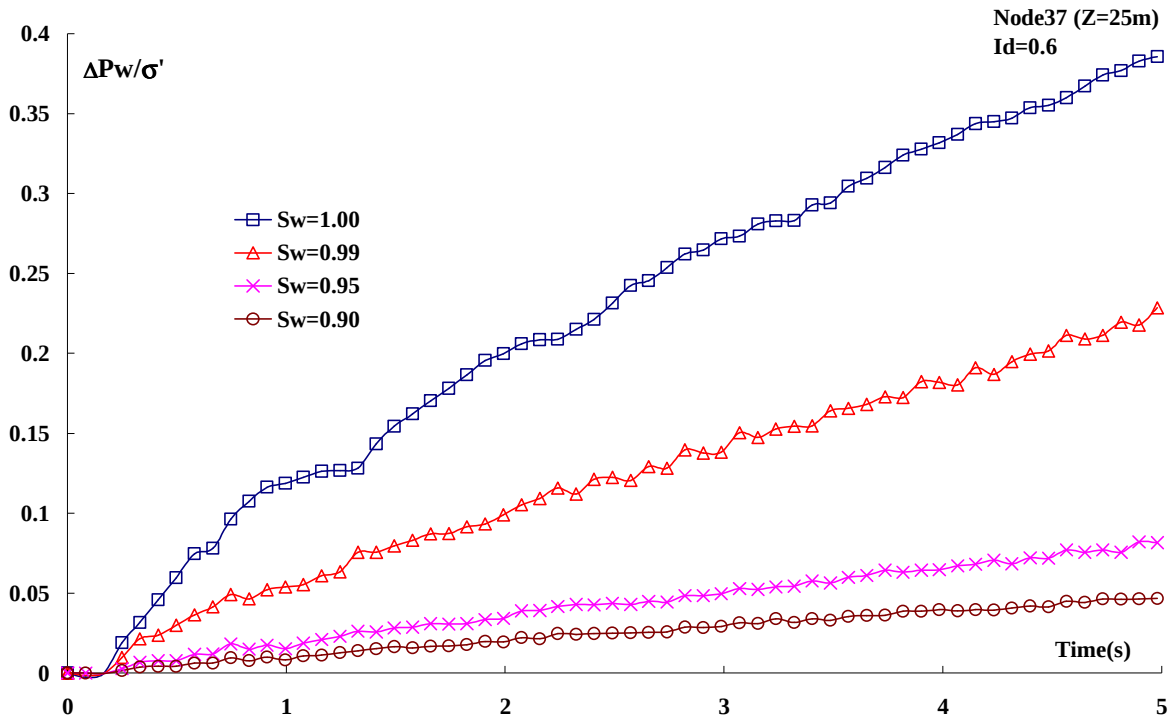

Figure 3.24: Influence of initial water saturation on the generation of the excess pore pressure (Nevada sand I_d =0.6)

3.6. Discussion on the tests of Yegian et al. (2007)

The water saturation has a great influence on the soil resistance to liquefaction. As illustrated by the examples in the section precedent. Some observations confirm the numerical results. However, few in-situ data can be found to verify this fact. In recent years, we realise that partial saturation could be an effective liquefaction mitigation methods. Some pioneers started experimental researches to simulate the in-situ dynamic response, such as Yegian et al. (2007). In the following, we present the tests and their analyse using the numerical method.

3.6.1 Introduction of experiment

The tests haven been conducted in Northeastern University in Boston (USA). A special flexible liquefaction box (Figure 3.25) was designed. A loose sand specimen in the box is subjected to a cyclic simple shear generated by a shaking table excitation at the bottom of the box. The liquefaction box is designed by considering strength, flexibility and workability, allowing: the preparation of loose saturated sand specimen; introduction of gas into the specimen; the measurement and detection of gas using cross-well radar. This apparatus allows conducting cyclic strain-controlled tests with pore-water pressure measurements to evaluate the effect of partial saturation on liquefaction potential.

The liquefaction box provided the ability to subject a soil specimen to controlled shear strains at different frequencies, induced by the shaking table. Figure 3.25 shows the dimensions and details of the box. The box walls and base are made of Plexiglas material. Two sides of the box are designed to rotate about their bottom edge and the other two sides are fixed to the base of the box, which in turn is fixed on the shaking table. The tops of the two movable sides are joined together at one end of an aluminium cross bar. The other end of the cross bar is fixed to a steel column in front of the shaking table. A special construction joint sealant is used as a flexible watertight joint between the Plexiglas sides. The sealant is a strong adhesive and acts as a flexible membrane allowing large deformations without rupture.

Fully saturated specimens are prepared by raining dry sand very slowly from a specific height (20 cm distances above the water level) into a predetermined amount of water placed in the liquefaction box. Tests are carried out with Ottawa sand, which is uniform sand with rounded particle shape. Since saturation could not be controlled accurately by measuring the B value as typically done in a triaxial cyclic test, the degree of water saturation is calculated using phase relationships. Partial saturation is induced by electrolysis or alternatively by drainage-recharge of pore-water.

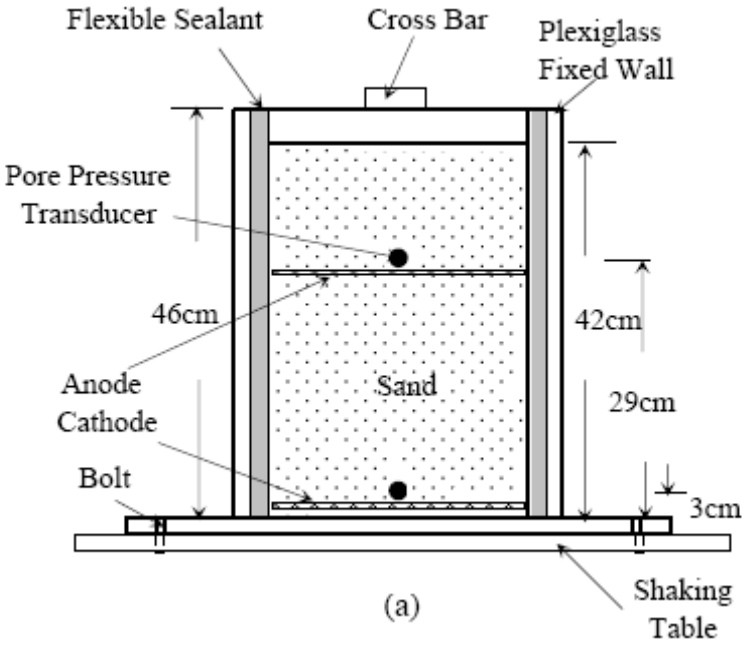

Figure 3.25 (a): Liquefaction box and setup for testing of specimens partially saturated through electrolysis (Yegian et al., 2007)

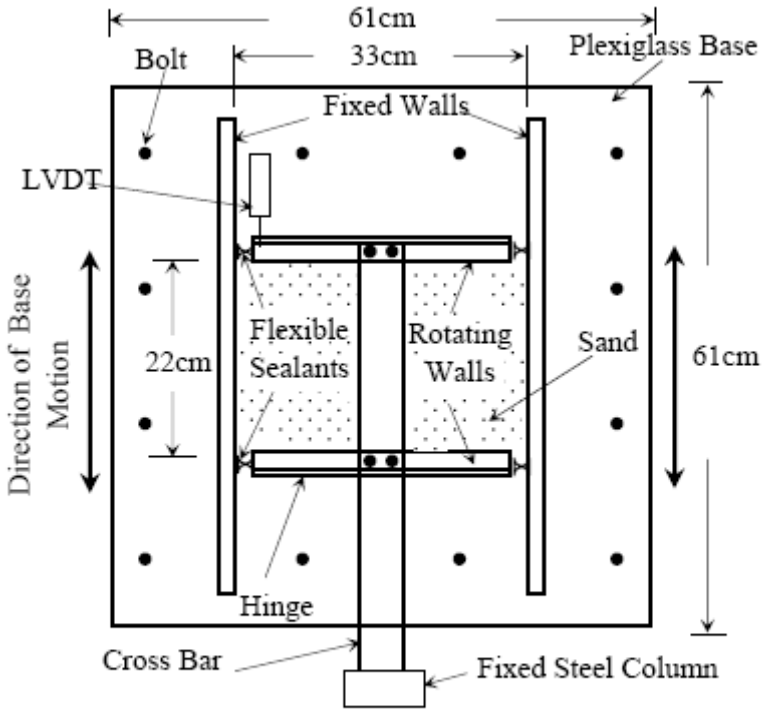

(b)

Figure 3.25 (b): Plan view of the liquefaction box (Yegian et al., 2007)

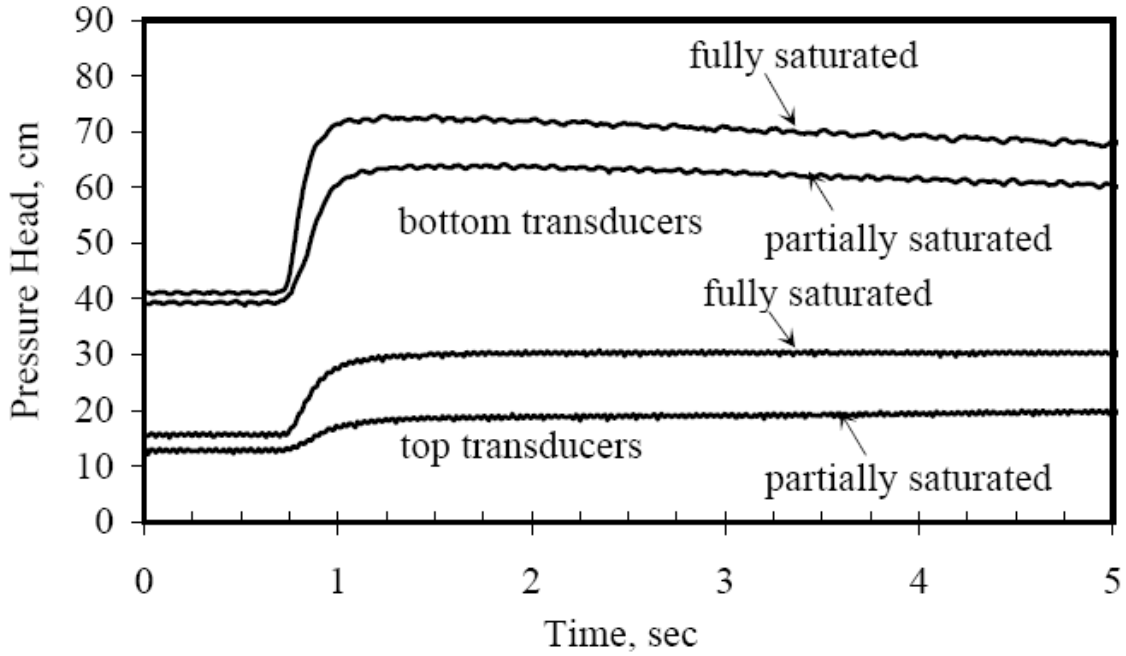

Figure 3.26 (a): Comparison of excess pore-water pressure generated in fully saturated Ottawa sand specimen, and partially saturated Ottawa sand specimen prepared through electrolysis (Sw=0.963) (Sample size: 21cm×33cm×42cm) (Yegian et al., 2007)

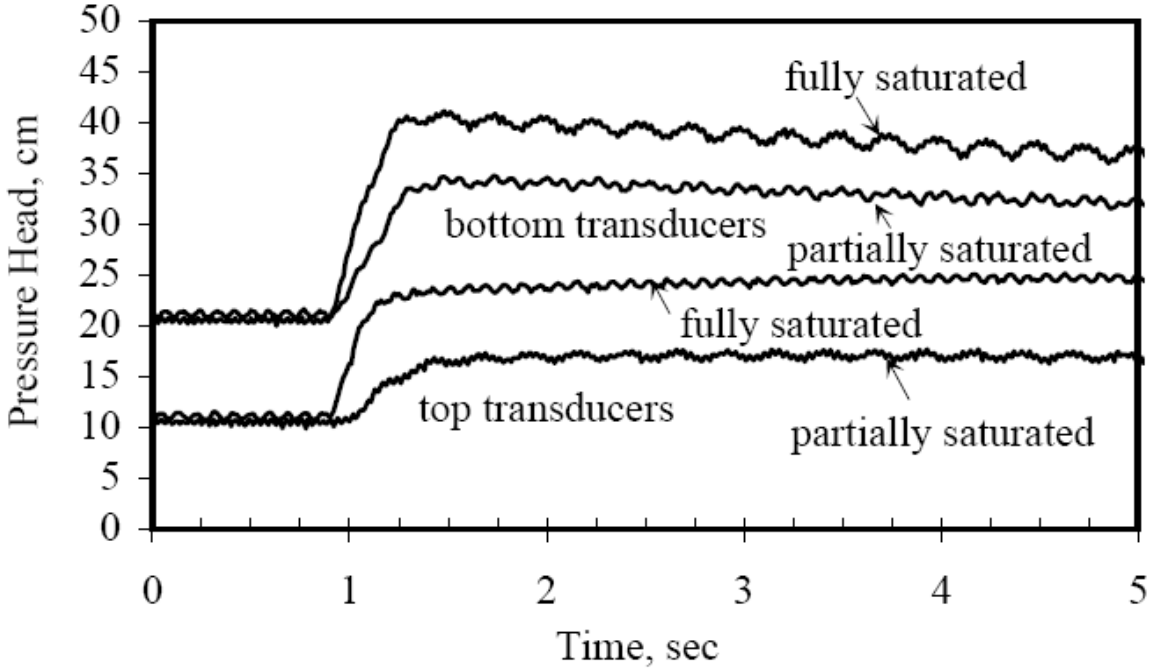

Figure 3.26 (b): Effect of entrapped air on the excess pore-water pressure generation in the partially saturated Ottawa sand specimen (Sw=0.963), prepared by drainage-recharge during shear strain controlled cyclic test (Sample size: 21cm×33cm×34cm) (Yegian et al., 2007)

3.6.2 Discussion

The experiments firstly simulate response of the in-situ response of partially saturated loose sand, and give us some valuable suggestions.

The results of the cyclic tests on fully saturated, partially saturated (induced by Electrolysis or Drainage-Recharge) are presented in Figure 3.26. The induced partially saturation will reduce the excess pore-water pressure generation rate. It can be observed that the slopes of the curves for fully saturated cases are sharper than that of unsaturated cases. This confirms the numerical simulation results illustrated in Figures 3.9, 3.10, 3.24.

The presence of gas in pore fluid reduces the rate of pore pressure generation, as shown by Martin et al. (1978), Yoshimi (1989), Xia and Hu (1991), Bouferra (2000) and Arab (2007). As a consequence, for nearly saturated case, the partially saturation will delay the liquefaction, but, if there is sufficient excitation, the liquefaction could occur. However, no liquefaction has been observed for partially saturated specimens, even for the saturation $S_w = 96.3\%$. The test results for partially saturated cases are doubtable. Similar to that of fully saturated cases, the pore pressure for partially saturated cases rapidly arrives at a peak value and then decrease. The peak value, however, is far away from liquefaction. This could be due to the drainage conditions. As indicated by the author "possible leakage may have occurred along the top transducer cable". This also confirms the influence of the permeability as discussed in section 3.61.

The settlements of specimens after test are reported; but without any comment. And among three cases, only two of them: that prepared by drainage-recharge and that of research on effect of sand type are presented. It seems that the settlement of fully saturated case is greater than that of partially saturated case. The settlement was measured after the dissipation of the excess pore pressure.

3.7. Conclusion

This chapter presented different applications of the proposed numerical model for unsaturated sandy soils together with a cyclic elasto-plastic constitutive equation to analysis of the influence of the water saturation, the permeability and the relative density on the soil liquefaction.

In the first section, the influence of water saturation is studied. Results show that the water saturation has an important influence on both monotonic and cyclic behaviour of sandy soils under undrained conditions. The decrease in the water saturation increases the compressibility of the pore fluid, and reduces the excess pore pressure generation rate. In addition, the analysis of free filed response of a liquefiable soil layer shows that, the decrease in water saturation mitigates the liquefaction. With the reduction in the initial water saturation, the excess pore pressure generation rate decreases. As a consequence, the liquefaction zone decreases.

The augmentation of the permeability increases the settlement and reduces the liquefaction risk for both fully saturated and partially saturated cases. However, the effect for unsaturated cases is less significant. For unsaturated case, the decrease in the permeability has low influence on the generation of the pore pressure and settlement. The increase in relative density increases the soil resistance to liquefaction. Finally, the experiments conducted by Yegian et al. (2007) confirm the results of the proposed model.

Conclusions

Liquefaction constitutes a major cause of damage induced by moderate or large earthquakes. Since the 1964 Niigata earthquake, intensive efforts have been made on the liquefaction researches. However, most liquefaction researches were based on fully saturated conditions. The experimental observations indicated that a little decrease in water saturation results in a significant increase in the liquefaction resistance. On the other hand, soils frequently encountered in the geotechnical engineering are unsaturated. The liquefiable soil layers located below the phreatic surface are not, as usual assumed, fully saturated but in near-fully saturated states. So it is necessary to study the liquefaction under partially saturated conditions.

This work includes the development of a numerical model for partially saturated sandy soils and its application to liquefaction. Based on experimental observations, some reasonable assumptions are taken: the pore-air pressure is equal to the pore-water pressure; the interaction between pore-air and pore-water is neglected; the pore-air flux is negligible. Together with the formulation of Coussy, a numerical model for partially saturated sandy soil is established. The proposed model has a similar form as that of fully saturated cases. The main difference lies in the Biot modulus, for the fully saturated soils, the Biot modulus is constant; while for the partially saturated cases, the Biot modulus depends on the pore-water pressure, the water saturation and the porosity. In fact, the proposed model can deal with both saturated and unsaturated problems. In place of the soil water characteristic curve, the idea gas law and the null pore-air flux assumption were used to determiner the water saturation in the constitutive equations. This can be applied to both drained and undrained conditions.

Terzaghis's 1-D consolidation problem is solved by the proposed model. A good agreement is obtained between the numerical and analytical results. Analyses of the bulk modulus and the Skempton coefficient confirm and verified the proposed model. The laboratory observations also confirm the results of the numerical model.

An elasto-plastic constitutive equation for granular material under both monotonic and cyclic loading conditions (MODSOL) is implanted in the proposed model to study the influence of water saturation on liquefaction. Numerical results show that the initial water saturation has a great influence on both monotonic and cyclic responses of loose sand. The decrease in water saturation leads to an increase in the liquefaction resistance. This result is due to the different excess pore pressure generation rates which are controlled by the initial water saturations (the compressibility of the water-air mixture).

Analysis of the free-field response of liquefiable sandy soil layer under dynamic loading shows that: the initial water saturation has a significant influence on the layer liquefaction resistance. The decrease in the initial water saturation can mitigate the liquefaction. With the decrease in water saturation, the initial liquefaction will be delayed and the liquefaction zone will be reduced. When the water saturation is lower than certain value, the liquefaction can not occur. However, the settlements at the top of layer before the dissipation of the excess pore pressure will increase with the decrease in water saturation.

The influences of the soil permeability and the relative density on soil liquefaction are presented. The permeability has a significant influence on the free filed response. The increase in the permeability leads to a decrease in liquefaction potential, and to an increase in the settlement at the top of soil layer. However, the influence of permeability in partially saturated sandy soils is less significant than that for fully saturated cases. The increase in the relative density reduces the liquefaction potential, and as well as the settlement of the soil layer.

Reference

Abaci S., Edwards J. S., 1992, Whittaker B. N., Relative permeability measurements for two phase flow in unconsolidated sands, Mine Water and the environment, Vol. 11, No. 2, pp. 11-26.

Alonso E. E., Gens A., Hight D. W., 1987, Special problem soils, General Rep. Proc., 9th European Conference on Soil Mechanics and Foundation Engineering, Dublin, pp.1087–1146.

Alonso E. E., Gens A., Josa A., 1990, A constitutive model for partially saturated soils, Geotechnique, Vol. 40, No. 3, pp. 405-430.

Arab A., 2007, Comportement des sols sous chargement monotone et cyclique, Thèse de doctorat, Université des Sciences et Technologies d'Oran.

Arulmoli K., Muraleetharan K. K., Hossain M. M., Fruth L. S., 1992, VELACS Verification of liquefaction analyses by centrifuge studies laboratory testing program soil data report.

Bian H. B., Shahrour I., 2007, A numerical model for dynamic response of unsaturated sands, 4th International Conference on Earthquake Geotechnical Engineering, June 25-28.

Biot M. A., 1941, General theory of three dimensional consolidation, Journal of application physic, Vol. 12, pp. 155-164.

Biot M. A., 1962, Mechanics of deformation and acoustic propagation in porous dissipation media, J. Acoust. Soc. of America, Vol. 34, pp. 1254-1264.

Biot M. A., 1956, Theory of propagation of elastic waves in a fluid saturated porous solid, Journal of application physic, Vol. 28, pp. 168-191.

Bird Juliet F., Bommer Julian J., 2004, Earthquake losses due to ground failure, Engineering geology, Vol. 75, No. 2, pp. 147-179.

Bishop A. W., Blight G. E., 1963, Some aspects of effective stress in saturated and unsaturated soils, Geotechnique, Vol. 13, pp. 177-197.

Bishop A. W., 1959, The principle of effective stress, Teknisk Ukeblad 39, 859–863.

Bouferra R., 2000, Etude en laboratoire de la liquéfaction des sols, Thèse de doctorat, Université des Sciences et Technologies de Lille.

Brennan A. J., Madabhushi S. P. G., 2006, Liquefaction remediation by vertical drains with varying penetration depths, Soil dynamics and earthquake engineering, Vol. 26, pp. 469-475.

Chaney R. C., 1978, Saturation effects on the cyclic strength of sands, Earthquake engineering and soil dynamics, ASCE, Vol. 1, pp. 342-358.

Chehade W., 1991, Méthodologie pour la validation des modèles des géomatériaux : Application aux modèles élastoplastiques des sols, Thèse de doctorat, Université des Sciences et Technologies.

Coussy O., 1991, Mécanique des milieux poreux.

Coussy O., 2004, Poro mechanics, John-Wiley.

Dafalias Y. F., 1986, Bounding surface plasticity I: mathematical formulation and hypoplasticity. Journal of Engineering Mechanics, ASCE 112 (9), pp. 966–987.

Dunn S. L., Vun P. L., Chan A. H. C., 2006, Damgaard J. S., Numerical modeling of wave-induced liquefaction around pipelines, Journal of Waterway, Port, Coastal and Ocean Engineering, Vol. 132, No. 4, pp. 276-288.

Elgamal A., Yang Z., Parra E., 2003, Modeling of cyclic mobility in saturated cohesionless soils, International journal of plasticity, Vol. 19, pp. 883-905.

Elgamal et al., 2007, A review of lager-scale testing facilities in geotechnical earthquake engineering, Earthquake geotechnical engineering, Edited by Kyriazis D. Pitilaks, Springer.

Finn W. D. L., Lee K. W., Martin G. R., 1977, An effective stress model for liquefaction. J. Geotechnical Engineering Division, ASCE 103, pp.513–533.

Fredlund D. G., 1977, Morgenstern N. R., Stress state variables for unsaturated soils, ABB Rev, Vol. 103 No. 5, pp. 447-466.

Fredlund D. G., 1993, Rahardjo H., Soil mechanics for unsaturated soils, John-Wiley.

Fredlund D. G., 2006, Unsaturated Soil Mechanics in Engineering Practice, Journal of Geotechnical and Geoenvironmental Engineering ASCE, Vol. 132, No. 3, pp. 286-321.

Fredlund D. G., 1994, Xing A., Equations for the soil-water characteristic curve, Canadian Geotechnical Journal, Vol. 31, No. 3, pp. 521-532.

Gatmiri B., Delage P., Cerrolaza M., 1998, UDAM: A powerful finite element software for the analysis of unsaturated porous media, Advances in engineering software, Vol. 29, No. 1, pp. 29-34.

Goulding R. B., 2006, Tensile strength, shear strength and effective stress for unsaturated sand, Dissertation of University of Missouri-Columbia.

Harada N., Towhata I., Takatsu T., Tsunoda S., Sesov V., 2006, Development of new drain method for protection of existing pile foundations from liquefaction effects, Soil dynamics and earthquake engineering, Vol. 26, pp. 297-312.

Ishihara K., Tsukamoto Y., 2004a, Cyclic strength of imperfectly saturated sands and analysis of liquefaction, Proc. Japan Acad., 80, Ser. B, pp.372-391.

Ishihara K., Tsukamoto Y., Kamada K., 2004b, Undrained behaviour of near-saturated sand in cyclic and monotonic loading, Cyclic behaviour of soils and liquefaction phenomena, Triantafyllidis, pp.27-39.

Jafari-Mehrabadi A., Abdi M. A., 2007, Popescu Radu, Analysis of liquefaction susceptibility of nearly saturated sands, International journal for numerical and analytical methods in geomechanics, Vol. 31, No. 5, pp. 691-714.

Jia Y., 2006, Contribution à la modélisation thermo-hydro-mécanuqye des roches partiellement saturées: application au stockage des déchets radioactifs, Thèse de doctorat, Université des Sciences et Technologies de Lille.

Kamata T., Tsukamoto Y., Tatsuoka F., Ishihara K., 2007, Possibility of undrained flow in suction-developed unsaturated sandy soils in triaxial tests, 4th International Conference on Earthquake Geotechnical Engineering, June 25-28.

Khalili N., Geiser F., Blight G. E., 2004, Effective stress in unsaturated soils: review with new evidence, International journal of geomechanics, ASCE, Vol. 4, No. 2.

Khalili N., Loret B., 2001, An elasto-plastic model for nonisothermal analysis of flow and deformation in unsaturated soils: Formulation. International Journal of Solids and Structure, Vol. 38, pp. 8305–8330.

Khoshnoudian F., 1999, Etude du comportement des tunnels sous chargement sismique, Thèse de doctorat, Ecole Central de Lille.

Khoshravan A. A., 1995, Problèmes de sols satures sous chargement dynamique : Modèle cyclique pour les sols et validation sur des essais en centrifugeuse, Thèse de doctorat, Université des Sciences et Technologies de Lille.

Kim T., 2001, Moisture-induced tensile strength and cohesion in sand, Ph. D. dissertation, University of Colorado at Boulder.

Kokusho T., 2000, Correlation of pore-pressure B-value with P-wave velocity and Poisson's ratio for imperfectly saturated sand or gravel, Soils and Foundations, Vol. 40, No. 4, pp. 95-102.

Kokusho T., Matsumoto M., 1999, Nonlinear site amplification in vertical array records during Hyogo-ken Nanbu earthquake, Soils and Foundations, Special Issue, No. 2, pp. 1-9.

Lewis R. W., Schrefler B. A., 1998, The finite element method in the static and dynamic deformation and consolidation of porous media, John-Wiley.

Loret B., Khalili N., 2000, A three-Phase model for unsaturated soils, International Journal for Numerical and Analytical Methods in Geomechanics, Vol. 24, pp. 893-927.

Loret B., Khalili N., 2002, An effective stress elastic-plastic model for unsaturated porous media, Mechanics of Materials, Vol. 34, pp. 97-116.

Lu N., Wu B., Tan C. P., 2007, Tensile strength characteristics of unsaturated sands, Journal of Geotechnical and Geoenvironmental Engineering.

Luckner L., van Genutchen M., Nielsen D. R., 1989, A consistent set of parametric models for the two-phase flow of immiscible fluids in the subsurface, Water Resource Research, Vol. 25, No. 10, pp. 2187-2193.

Martin G. R., Finn W. D. L., Seed H. B., 1978, Effects of system compliance on liquefaction testes, Journal of the geotechnical engineering division, Vol. 104, No. GT4.

Martin G. R., Finn W. D. L., Seed H. B., 1975, Fundamentals of liquefaction under cyclic loading, J. Geotech., Division ASCE, Vol. 101, pp. 423-438.

Matsushi Y., Matsukura Y., 2006, Cohesion of unsaturated residual soils as a function of volumetric water content, Bull Eng Geol Env, Vol. 65, pp. 449-455.

Nagao K., Azegami Y., Yamada S., Suemasa N., Katada T., 2007, A Micro-bubble injection method for a countermeasure against liquefaction, 4th International Conference on Earthquake Geotechnical Engineering, June 25-28.

Okamura M., Ishihara M., Tamura K., 2006, Degree of saturation and liquefaction resistances of sand improved with sand compaction pile, Journal of geotechnical and Geoenvironmental engineering, ASCE, Vol. 132, No. 2, pp. 258-264.

Okamura M., Soga Y., 2006, Effects of fluid compressibility on liquefaction resistance of partially saturated sand, Soils and Foundations, Vol.46, No.5, pp. 659-700.

Ousta R., Shahrour I., 2001, Three-dimensional analysis of the seismic behaviour of micropiles used in the reinforcement of saturated soils, Int. J. for Numerical and Analytical Methods in Geomechanics, No 25, pp. 183-196.

Ousta R., 1998, Etude du comportement sismique des micropieux, Thèse de doctorat, Université des Sciences et Technologies de Lille.

Pastor M., Zienkiewicz O.C., 1986, A generalized plasticity hierarchical model for sand under monotonic and cyclic loading. In: Pande, G.N., Van Impe, W.F. (Eds.), Proceedings, 2nd International Conference on Numerical Models in Geomechanics. M. Jackson and Son, pp. 131–150.

Pastor M., Zienkiewicz O. C., Chan A. H. C., 1990, Generalized plasticity and the modeling of soil behaviour, International journal for numerical and analytical methods in geomechanics, 14, 151-190.

Pietruszczak S., Pande G. N., 1996, Constitutive relations for partially saturated soils containing gas inclusions, Journal of geotechnical engineering, Vol. 122, No. 1, pp. 50-58.

Sawada S., Tsukamoto Y., Ishihara K., 2006, Residual deformation characteristics of partially saturated sandy soils subjected to seismic excitation, Soil dynamics and earthquake engineering, Vol. 26, pp. 175-182.

Shahrour I., Chehade W., 1992, Development of a constitutive elastoplastic model for soils, 11th international congress on rheology, Bruxelles, Edition P. Moldenaers and R. Keuning, Elsevier.

Sheng Z. J., 1999, Theoretical soil mechanics, China Waterpower Press.

Singh R., Roy D., Jain S. K., 2005, Analysis of earth dams affected by the 2001 Bhuj Earthquake, Engineering Geology, Vol. 80, pp. 282-291.

Sumer B. M., Truelsen C., Fredsoe J., 2006, Liquefaction around pipelines under waves, Journal of Waterway, Port, Coastal and Ocean Engineering, Vol. 132, No. 4, pp. 266-275.

Terzaghi K., 1936, The shearing resistance of saturated soils and the angle between the planes of shear, Proceedings of the 1st International Conference on Soil Mechanics and Foundation Engineering, Vol. 1, 54–56.

Tsukamoto Y., Ishihara K., Nakazawa H., Kamada K., Huang Y., 2002, Resistance of partly saturated sand to liquefaction with reference to longitudinal and shear wave velocities, Soils and Founds, Vol. 42, No. 6, pp 93-104.

Tsukamoto Y., Kamata T., Tatsuoka F., Ishihara K., 2007, Undrained flow characteristics of partially saturated sandy soils in triaxial tests, 4th International Conference on Earthquake Geotechnical Engineering, June 25-28.

Wang H. F., 2000, Theory of linear poroelasticity with application to geomechanics and hydrogeology.

Wroth C. P., Houlsby G. T., 1985, Soil mechanics: property characterization and analysis procedure, Proceeding 11th ICSMEF.

Xia H., Hu T., 1991, Effects of saturation and back pressure on sand liquefaction. Journal of Geotechnical Engineering, Vol. 117, No. 9, pp. 1347–1362.

Yang D. Q., Sheng Z. J., 1992, Study on generalized consolidation theory of unsaturated soils, the 7th International conference on Expansive soils, Dallas, USA, Vol. 1, pp. 158-162.

Yang J., 2002, Liquefaction resistance of sand in relation to P-wave velocity, Géotechnique, Vol. 52, No. 4, pp. 295-298.

Yang J., Savidis S., Sato T., Li X. S., 2003, Influence of vertical acceleration on soil liquefaction: New findings and implications, Proceeding Soil and rock America 2003, Cambridge, Mass, Vol.1.

Yang J., 2006, Frequency dependent amplification of unsaturated surface soil layer, Journal of geotechnical and geoenvironmental engineering, Vol. 132, No.4, pp. 526-531.

Yang J., 2001, Sato Tadanobu, Analytical study of saturation effects on seismic vertical amplification of a soil layer, Géotechnique, Vol. 51, No. 2, pp. 161-165.

Yasuda S., 2007, Remediation methods against liquefaction which can be applied to existing structures, Earthquake geotechnical engineering, Edited by Kyriazis D. P., Springer.

Yegian M. K., Eseller-Bayat E., Alshawabkeh A., Ali S., 2007, Induced-Partial saturation for liquefaction mitigation: Experimental investigation, Journal of geotechnical and geoenvironmental engineering, ASCE, Vol. 133, No. 4, pp. 372-380.

Yoshimi Y., Tanaka K., Tokimatsu K., 1989, Liquefaction resistance of a partially saturated sand, Soils and foundations, vol. 29, No. 3, pp. 157-162.

Zienkiewicz O. C., Chan A. H. C., Pastor M., Schrefler B. A., Shiomi T., 1999, Computational Geomechanics with special reference to earthquake engineering, John-Wiley.

Zienkiewicz O. C., Chang C. T., Bettess P., 1980, Drained, undrained, consolidating and dynamic behaviour assumptions in soil, Géotechnique 30, No. 4, 385-395.

Zienkiewicz O. C., Pande G. N., 1977, Some useful forms of isotropic yield surfaces for soil and rock mechanics, in finite elements in geomechanics, edited by G. Gallagher.

Zienkiewicz O. C., Shiomi T., 1984, Dynamic behaviour of saturated porous media; the generalized Biot formulation and its numerical solution, International journal for numerical and analytical methods in geomechanics, Vol. 8, pp. 71-96.